

**Investigating Genome Editing Techniques
in Parasite Immunotherapy: Pioneering the
Development of a Viable Attenuated
Cryptosporidium parvum strain for
Prophylactic Vaccination**

Jackson Feijia Chen

Division of Experimental Medicine, Faculty of Medicine

McGill University, Montreal

November 2024

A thesis submitted to McGill University in Partial Fulfillment of the Requirements
of the Degree of Master of Science

© Jackson Chen, 2024

Detailed Table of Contents

BRIEF ABSTRACT	5
RÉSUMÉ BREF	6
ACKNOWLEDGEMENTS	8
CONTRIBUTION OF AUTHORS	10
ABBREVIATIONS	11
LIST OF FIGURES AND TABLES	16
INTRODUCTION	18
BACKGROUND AND EXPERIMENTAL RATIONALE.....	18
RESEARCH HYPOTHESIS.....	19
RESEARCH OBJECTIVES	19
SIGNIFICANCE	19
LITERATURE REVIEW	20
BACKGROUND OF CRYPTO	20
Global Impact of Diarrheal Diseases	20
Historical Context and Notable Outbreaks	20
DISEASE TRANSMISSION AND EPIDEMIOLOGY	21
Molecular Analysis and Species Prevalence.....	22
CLINICAL MANIFESTATIONS AND COMPLICATIONS	23
DIAGNOSTICS METHODS FOR CRYPTO.....	23
Microscopic Examination.....	24
Serological Methods	24
Molecular Methods	25
IMMUNE RESPONSES AGAINST CRYPTOSPORIDIUM	25
Innate Immune Responses	25
Adaptive Immunity: Cellular Immune Responses.....	26
Adaptive Immunity: Humoral Immune Responses.....	27
VACCINE RESEARCH AND DEVELOPMENT	27
DNA-based Vaccines	27
Attenuated <i>Salmonella</i> Vaccines.....	28
Recombinant Antigen Vaccines	28
The Role of Adjuvants	29
Live Attenuated Vaccines.....	29

CRISPR-CAS SYSTEMS	29
Mechanisms and Applications	30
Type II CRISPR-Cas9 Systems	30
CRISPR-Cas Applications in Parasites	30
ROLES OF CYSTEINE PROTEASES	31
Cysteine Proteases in Protozoa	31
Cysteine Proteases in Helminths.....	32
Cysteine Proteases in Other Infectious Diseases	32
METHODOLOGY.....	33
BIOINFORMATICS ANALYSIS FOR TARGET SELECTION OF CP1	33
Candidate Antigen Selection Inclusion Criteria.....	33
T-cell Epitope Prediction and Scoring Analysis.....	34
B-Cell Epitope Prediction and Scoring.....	35
Combinatory T and B Cell Epitope Scoring Analysis	35
C. PARVUM IOWA OOCYST INFECTION AND PURIFICATION	35
Infection Protocol of IFN γ R-KO Mice via Oral Gavage.....	35
Extraction and Purification of Oocysts from Intestines	36
Extraction and Purification of Oocysts from Stool.....	37
Verification of Integrity of Extracted <i>C. parvum</i> Oocysts	37
Freeze-and Thaw Lysis Protocol of Oocysts.....	38
DNA Extraction and Quantification.....	38
CONSTRUCTION OF CP1 AND TK KNOCKOUT REPAIR CASSETTES	39
Creation of TK- and CP1-specific Repair Cassettes	39
Inclusion of Missing <i>C. parvum</i> enolase gene 3'UTR.....	41
PCR Optimization Using Overlap Fusion PCR Assembly	41
Verification and Concentration of Repair Cassette Templates.....	42
Sanger Sequencing Analysis	42
Ligation into pJet Blunt Cloning Vector	42
Transformation into Dh5 α <i>Escherichia (E.) coli</i> Cells	43
Restriction Enzyme Double Digestion Verification.....	43
Mass Production of Repair Cassette Templates	44
Ethanol Precipitation for DNA Concentration.....	44
DESIGN, SELECTION, AND SYNTHESIS OF SGRNA CANDIDATES	45
<i>In silico</i> Selection of gRNA Candidates with EuPaGDT.....	45
Template Design of Selected CP1- and TK-specific gRNA Design Constructs	46
<i>In vitro</i> Transcription of gDNA Candidates.....	46

Recombinant SpCas9 Enzyme Production	46
<i>in vitro</i> DNA Cleavage Assay Assembly and Analysis	47
INTEGRATION AND TESTING OF CRISPR-CAS9 PLASMIDS	47
Ligation of Select sgRNA Sequences into the hSpCas9 Plasmid	47
Transformation of the Plasmid into DH5 α <i>E. coli</i>	48
PCR and Sequencing to Confirm Integrity of Ligated sgRNA	48
QPCR OPTIMIZATION FOR QUANTIFICATION OF SPOROZOITES	49
Specificity of 18S rDNA and Hsp70 gene primers for PCR	49
qPCR Optimization with the Confirmed Targets	49
EXCYSTATION AND ELECTROPORATION OF C. PARVUM SPOROZOITES.....	50
Purification and Preparation of Infectious Oocysts	50
Preparation of Sporozoites for Oocyst Excystation	50
Electroporation of Sporozoites with AMAXA 4D Nucleofector	50
IN VITRO INFECTION AND VERIFICATION OF C. PARVUM INFECTION	51
Preparation of HCT-8 Cells for Infection (Days 0 – 2).....	51
Infection of HCT-8 Cells with Electroporated Sporozoites (Day 3).....	51
Nanoluciferase Detection Quantification (Day 5)	52
Cell Harvesting, DNA Extraction, and PCR Verification (Day 5).....	52
<i>RESEARCH FINDINGS</i>.....	53
CP1 Demonstrated Superior Immunogenicity and Antigenicity Compared to Other Antigen Candidates From T- and B-Cell Epitope Analysis	53
Successful Construction of Revised CP1RCFL and TKRCFL	53
Verification and Analysis of CP1RCFL and TKRCFL Ligated Plasmids.....	54
In Vitro Characterization of Compatible CP1- and TK-sgRNA Candidates.....	54
Optimizing RNP:Template Ratios and Off-Target Binding	55
Successful Ligation of CP1sg2-1326 and TKsg2-132 into hSpCas9 Plasmid.....	55
High Specificity of 18S rDNA-based qPCR Curve for Sporozoite Quantification	56
Insignificant Reporter Detection for Preliminary <i>in vivo</i> Nucleofection.....	56
<i>FIGURES AND TABLES</i>	57
<i>DISCUSSION</i>	75
<i>FINAL CONCLUSIONS AND SUMMARY</i>.....	86
<i>APPENDIX</i>.....	88
<i>REFERENCES</i>.....	90

Brief Abstract

Cryptosporidiosis, caused by *Cryptosporidium* spp., is a significant parasitic enteric disease affecting humans and animals in low- and middle-income countries and developed nations. Severe health complications and mortality rates are exceptionally high in immunocompromised populations. Treatment options are severely limited, and no vaccine is available. This research incorporates the latest advances of CRISPR-Cas9 technology to disrupt the pathogenicity of *C. parvum* by targeting and knocking out the Cryptopain-1 (CP1) gene, a crucial virulence factor expressed during the invasive parasite stages critical for host cell invasion and nutrient acquisition. The goal is to create a stable attenuated strain for vaccine development and drug research screening.

Active SpCas9-sgRNA ribonucleoprotein (RNP) complexes were designed to target the CP1 gene in *C. parvum* sporozoites. The high immunogenicity and antigenicity properties of CP1 were confirmed with a comprehensive and meticulous bioinformatics analysis compared to other potent targets expressed on the cell surface of *C. parvum* sporozoites and merozoites. These targets included *C. parvum* glycoprotein 2 (Cpgp2), *C. parvum* glycoprotein 15/45 (Cpgp15/45), *C. parvum* glycoprotein 900 (Cpgp900), and circumsporozoite-like glycoprotein (CSL). Repair cassette templates were designed for homologous recombination and guide RNAs with high on-target activity and minimal off-target effects, which were selected using advanced bioinformatics tools. *In vivo*, electroporation nucleofection assays with a Lonza Amaxa 4D nucleofector transfected previously excysted *C. parvum* sporozoites with active SpCas9-sgRNA RNP complexes were evaluated using the human ileocecal carcinoma (HCT-8) model transfectable cell line. Molecular assays demonstrated the high specificity of the *de novo* constructed repair templates, and selected guide RNAs for CP1 showed high specificity and efficiency without any off-target binding potential.

Future studies will evaluate the long-term efficacy, safety, and scalability of the CP1 knockout approach for vaccine production and its applicability to other *Cryptosporidium* species and parasites. The successful development of an attenuated strain through CRISPR-Cas9 technology could significantly advance cryptosporidiosis research and contribute to the development of effective treatments and vaccines. This could motivate us all to work towards reducing the global burden of this disease, inspiring a collective effort to combat cryptosporidiosis.

Résumé Bref

La cryptosporidiose, causée par *Cryptosporidium* spp., est une maladie entérique parasitaire significative affectant les humains et les animaux dans les pays à revenu faible et intermédiaire ainsi que dans les nations développées. Les complications de santé graves et les taux de mortalité sont exceptionnellement élevés chez les populations immunodéprimées. Les options de traitement sont très limitées et aucun vaccin n'est disponible. Cette recherche intègre les dernières avancées de la technologie CRISPR-Cas9 pour perturber la pathogénicité de *C. parvum* en ciblant et en éliminant le gène Cryptopain-1 (CP1), un facteur de virulence crucial exprimé pendant les stades invasifs du parasite, essentiels pour l'invasion des cellules hôtes et l'acquisition de nutriments. L'objectif est de créer une souche atténuée stable pour le développement de vaccins et le dépistage de la recherche sur les médicaments.

Des complexes ribonucléoprotéiques (RNP) SpCas9-sgRNA actifs ont été conçus pour cibler le gène CP1 dans les sporozoïtes de *C. parvum*. Les propriétés immunogènes et antigéniques élevées de CP1 ont été confirmées par une analyse bioinformatique complète et méticuleuse, comparée à d'autres cibles potentiellement puissantes exprimées à la surface cellulaire des sporozoïtes et des mérozoïtes de *C. parvum*. Ces cibles comprenaient la glycoprotéine 2 de *C. parvum* (Cpgp2), la glycoprotéine 15/45 de *C. parvum* (Cpgp15/45), la glycoprotéine 900 de *C. parvum* (Cpgp900) et la glycoprotéine de type circumsporozoïte (CSL). Des modèles de cassettes de réparation ont été conçus pour la recombinaison homologue et des ARN guides avec une activité ciblée élevée et des effets hors cible minimaux ont été sélectionnés à l'aide d'outils bioinformatiques avancés.

In vivo, des essais de nucléofection par électroporation avec un nucléofecteur Lonza Amaxa 4D ont transfecté des sporozoïtes de *C. parvum* précédemment excystés avec des complexes RNP actifs SpCas9-sgRNA, évalués à l'aide de la lignée cellulaire transfectable du modèle de carcinome iléocœcal humain (HCT-8). Les essais moléculaires ont démontré la haute spécificité des modèles de réparation nouvellement construits, et les ARN guides sélectionnés pour CP1 ont montré une spécificité et une efficacité élevées sans potentiel de liaison hors cible.

Les études futures évalueront l'efficacité, la sécurité et l'évolutivité à long terme de l'approche d'élimination de CP1 pour la production de vaccins et son applicabilité à d'autres espèces de *Cryptosporidium* et parasites. Le développement réussi d'une souche atténuée grâce à

la technologie CRISPR-Cas9 pourrait considérablement faire progresser la recherche sur la cryptosporidiose et contribuer au développement de traitements et de vaccins efficaces. Cela pourrait nous motiver tous à travailler pour réduire le fardeau mondial de cette maladie, inspirant un effort collectif pour combattre la cryptosporidiose.

Acknowledgements

I want to express my deepest gratitude to my supervisor, Dr. Momar Ndao, for his unwavering support, mentorship, and expertise in parasitology. His guidance and technical knowledge have taught me the importance of curiosity and lifelong learning. His assistance in grant writing, fatherly support, and dedication to my growth as a researcher and person have been instrumental. Dr. Ndao's influence on my personal and professional development is profound, and his role in this research is significant. Thank you for always being there to provide encouragement and wisdom and fostering an environment where I could thrive academically and personally. Your persistence, kindness, and patience made this journey enjoyable and fulfilling.

I am immensely grateful to Makan for introducing me to the world of proteomics and metabolomics technology. His mentorship on my first project, identifying novel protein biomarkers in BALB/c mouse testicles for Chagas disease, was pivotal in my early research career. Maxime's guidance on sonication and standard operating procedural (SOP) formulation was crucial in my development as a researcher. James's assistance during my fourth-year undergraduate honours research project on Taqman-based RT-qPCR for filaria diagnosis was invaluable. His mentorship in optimizing the quadruplex detection machine for lymphatic filariasis was instrumental in my success. Their support and encouragement have been a constant source of motivation and have significantly influenced the direction and outcomes of this research.

I would also like to thank Samarth, Fabio, and Nathalie from the NRCP. Your unwavering support in finding and ordering reagents and guiding me through the early stages of PCR machines was invaluable. Lily Yang, your mentorship on the CRISPR-Cas project, including *in vivo* infection with C57/BL6 IFN γ R KO mice and genomic DNA extraction, was pivotal in my research. Your patience and willingness to share your knowledge have been incredibly inspiring. Thanks to Karine for your expertise on *Cryptosporidium*, especially *C. parvum* purification, identification techniques, and proper animal handling procedures. Your support and care were greatly appreciated, and your positivity brightened even on the most challenging days. Thank you to the training staff at the RI-MUHC animal facility, including Annie and Lydia, for their guidance on handling, anesthesia, and bleeding techniques for mice and rats. Your expertise and kindness have been invaluable. I am grateful to Adam, Iris, Kaitlin, Gio, Collin, Selena, and Fatima from the Brian Ward lab for their support and friendship during my undergraduate years. Kaitlin, thank you

for providing luciferase plasmids, and Adam for the mCherry plasmids. Karine, thank you for the RT-qPCR reagents. Your generosity and camaraderie have made the lab a wonderful place to work. Thanks to the MIMM413 TA crew, including Cal, Adam, Dhilan, Kayla, Laura, and Lindsay, for the late-night study sessions and boba sessions. Your friendship and support have been a source of joy and strength. Rohan and Melanie from the NRC, your guidance on Cas9 purification and detection was invaluable. Thank you for your patience and for always being willing to help.

Thank you to Tristan and Ivan from Dr. Tremblay's lab for teaching me mammalian electroporation and transfection techniques. Your expertise and willingness to share your knowledge have been greatly appreciated. Thanks to the Marcel Behr lab for guidance on using the fluorescent detector machine. Special thanks to Dr. Orthwein's lab for allowing us to borrow their AMAXA 4D nucleofector and coordinating logistics. Martin and Omar from the NRC, thank you for collaborating on the NRC Ideation New Beginnings Project grant. Your support and collaboration have been crucial to the success of this project.

Thank you to Soumaya for helping with intestine purification and cultivating *C. parvum* oocysts. Your dedication and hard work have been truly inspiring—special thanks to Mancy and Camilla for their work on bioinformatics, RNA extraction, and DNA amplification. Your expertise and support have been invaluable. I sincerely thank Dr. Brian Ward and Jason for their challenging questions and guidance. Your insights and encouragement have pushed me to strive for excellence. Thanks to Fabio, Iris, and Jason for teaching me how to run a western blot and use the imaging room. Thank you to the immunohistochemistry platform at the RI-MUHC for preparing and staining slide samples. Your expertise and support have been crucial to my research. Finally, I thank Dr. Andrew Mouland, Dr. Michel Tremblay, and Dr. Christopher Prada for their guidance and support throughout my research journey. Your wisdom and encouragement have been invaluable.

And lastly, thank you to the rest of the Ndao/Ward lab. I've had a wonderful time being a part of this giant (yet slowly dwindling) family, and I am endlessly grateful to everyone for their support, friendship, and the countless memories we've shared. Your contributions have made this journey unforgettable, and I look forward to many more adventures together.

Contribution of Authors

I, Jackson Chen, the primary junior researcher and M.Sc. graduate student at McGill University, authored this thesis. My unique contributions include writing all chapters and sections outlined in this thesis, including the introduction, literature review, methods and materials, research findings, discussion, conclusions, and future directions. The research presented in this thesis was conducted under the supervision and guidance of Dr. Momar Ndao, the principal investigator and supervisor. Dr. Danuta Radzioch, the leading academic advisor from the Division of Experimental Medicine, along with Dr. Michel Tremblay and Dr. Christopher Fernandez Prada, the two committee members, provided additional support and feedback throughout the research process. While I was responsible for all the writing portions of each section outlined in this thesis, these were reviewed and revised by Dr. Ndao to ensure accuracy and clarity.

Abbreviations

- 18S rDNA: 18S ribosomal DNA
- AGE: Agarose gel electrophoresis
- ApE: A Plasmid Editor
- AsCas12a: *Acidaminococcus* sp. Cas12a
- BALB/c: Inbred strain of laboratory mice
- B cells: Bone marrow-derived (B) lymphocytes
- BL6: C57BL/6, a common inbred strain of laboratory mice
- Bp: Base-pair
- BSA: Bovine serum albumin
- *C. parvum*: *Cryptosporidium parvum*
- CCL2: C-C Motif Chemokine Ligand 2
- CD4+: Cluster of differentiation 4, T4 cells
- CD8+: Cluster of differentiation 8, T-killer cells
- CIP: Calf intestinal alkaline phosphatase
- Clan CA: Caspase activation
- COWP: *C. parvum* oocyst wall protein
- CpG: Cytosine-phosphate-Guanine
- CpGT1/2: *C. parvum* putative glucose transporter 1/2
- CP: Cysteine protease
- CP1: Cryptopain-1
- CP1-3'EnoUFLK3: CP1 repair cassette construct, fragment #3
- CP1EnoNN2: CP1 repair cassette construct, fragment #2
- CP15'FLK1: CP1 repair cassette construct, fragment #1
- CP1RCFL: CP1 full-length repair cassette construct
- Cpgp2, 900: *C. parvum* glycoprotein 2, 900
- Cpgp15/45: *C. parvum* glycoprotein 15/45
- CRISPR-Cas9: Clustered regularly interspaced short palindromic repeats and CRISPR-associated protein 9
- crRNA: CRISPR RNA

- Crypto: Cryptosporidiosis
- CSL: Circumsporozoite-like glycoprotein
- Ct value: Cycle threshold value
- CTLs: Cytotoxic T-Lymphocytes
- CXCL10: C-X-C Motif Chemokine Ligand 10
- DALYs: Disability-adjusted life years
- ddH₂O: distilled, deionized water
- DHFR: Dihydrofolate reductase
- DMSO: Dimethyl sulfoxide
- DNA: Deoxyribonucleic acid
- Dpi: Days post-infection
- DSB: Double-stranded breaks
- DTT: Dithiothreitol
- *E. coli*: *Escherichia coli*
- EDTA: Ethylenediaminetetraacetic acid
- EIA: Enzyme immunoassay
- ELISA: Enzyme-linked immunosorbent assay
- EnoP: *C. parvum* enolase promoter
- EuPaGDT: Eukaryotic Pathogen gRNA Design Tool
- FBS: Fetal bovine serum
- FDA: Food and Drug Administration
- FnCas12a: *Francisella novicida* cas12a
- GALT: Gut-associated lymphoid tissue
- GM-CSF: Granulocyte-macrophage colony-stimulating factor
- HBC: Hyperimmune bovine colostrum
- HBSS: Hank's balanced salt solution
- HCT-8 cells: Human ileocecal carcinoma cells
- HDR: Homology-directed repair
- HF: High fidelity
- His: Histidine

- HIV/AIDS: Human immunodeficiency virus/Acquired immunodeficiency syndrome
- HNH: Histidine-asparagine-histidine
- HRP: horseradish peroxidase
- Hsp70: Heat shock protein 70
- IEDB: Immune epitope database
- IEC: Intestinal epithelial cell
- IFN γ R: Interferon-gamma receptor
- IgM/A/D/G: Immunoglobulin M/A/D/G
- IL-1 β //2/4/12/18/21/31/33: Interleukin- 1 beta/2/4/12/18/21/31/33
- ILC: Innate lymphoid cell
- IMPDH: Inosine monophosphate dehydrogenase
- iNOS: Inducible nitric oxide synthase
- IC assay: Immunochromatographic assay
- IPTG: Isopropyl β -D-1-thiogalactopyranoside
- KO: Knockout
- K11777: N-methyl piperazine-Phe-homoPhe-vinyl sulfone phenyl
- Kbp (Mbp): Kilo base-pair (Mega base-pair)
- KCl: Potassium chloride
- KH₂PO₄: Potassium dihydrogen phosphate
- LB: Luria-Bertani
- LbCas12a: *Lachnospiracae bacterium* Cas12a
- LMICs: low- and middle-income countries
- MAS-PCR: Multiple allele specific-polymerase chain reaction
- MCS: Multiple cloning site
- MgCl₂: Magnesium chloride
- MHC: Major histocompatibility complex
- MPro: Main protease
- NaCl: Sodium chloride
- NaHCO₃: Sodium bicarbonate
- NeoR: Neomycin resistance gene

- NEB: New England Biolabs
- NHEJ: Non-homologous end joining
- Ni-NTA: Nickel-nitrilotriacetic acid
- NK cell: Natural killer cell
- Nluc: Nanoluciferase
- NO: Nitric oxide
- NOD mice: Non-obese diabetic mice
- NRC: National Research Council of Canada
- NSG mice: NOD-SCID (Non-obese diabetic/Severe combined immunodeficiency) mice
- Nts: Nucleotides
- ODN: Oligonucleotides
- PAM: Protospacer Adjacent Motif
- PBS: Phosphate-buffered saline
- P2A peptide: Porcine Teschovirus-1 2A peptide
- PRR: Pattern recognition receptors
- Proteinase K: *Tritirachium album* serine proteinase K
- PVDF: polyvinylidene fluoride
- PVA: Polyvinyl alcohol
- qPCR: quantitative polymerase chain reaction
- RFLP: Restriction fragment length polymorphism
- RLU: Relative luminescence units
- RNA: Ribonucleic acid
- RNase A: Ribonuclease A
- RNP: Ribonucleoprotein
- RPM: Rotations per minute
- RPMI media: Roswell Park Memorial Institute media
- RT-PCR: Real-time polymerase chain reaction
- RT-qPCR: Reverse transcriptase quantitative polymerase chain reaction
- RuvC: Crossover junction endodeoxyribonuclease RuvC
- SaCas9: *Staphylococcus aureus* Cas9

- SCID: Severe combined immunodeficiency
- SDS-PAGE: sodium dodecyl sulphate polyacrylamide gel electrophoresis
- SEM: Standard error of the mean
- sgRNA: single guide RNA
- shRNA: short-hairpin RNA
- SOP: Standard operating procedure
- SpCas9: *Streptococcus pyogenes* Cas9
- TAE: Tris-acetic acid-EDTA
- TBE: Tris-borate-EDTA
- TBST buffer: Tris-buffered saline with Tween-20 buffer
- TCID₅₀: Tissue Culture Infectious Dose 50
- T cells: Thymus-derived (T) lymphocytes
- TE buffer: Tris-EDTA buffer
- TGF- β : Transforming growth factor-beta
- Th1/2/17: T helper 1/2/17
- TK: Thymidine kinase
- TK-3'EnoUFLK3: TK repair cassette construct, fragment #3
- TK5'FLK1: TK repair cassette construct, fragment #1
- TKEnoNN2: TK repair cassette construct, fragment #2
- TKRCFL: TK full-length repair cassette
- TLR: Toll-like receptors
- T_m: Melting temperature
- TNF- α : Tumour necrosis factor-alpha
- tracrRNA: Trans-activating CRISPR RNA
- TRAP: Thrombospondin-related adhesive protein
- UTR: Untranslated region
- USD: U.S.A. dollars
- UV light: Ultraviolet light
- WHO: World Health Organization
- ZN: Ziehl-Neelsen

1. Complete List of Figures and Tables

Figures

<i>Figure 1: Complete Graphical Timeline for C. parvum CPI-KO Vaccine Development.....</i>	<i>57</i>
<i>Figure 2: CRISPR-Cas9 Mediated Genetic Knockout Strategy for Excysted C. parvum Sporozoites</i>	<i>58</i>
<i>Figure 3: Immunogenicity and Antigenicity Bioinformatics Screening of C. parvum Surface Glycoproteins and Enzymes</i>	<i>58</i>
<i>Figure 4: In Silico Prediction and Scoring of T-cell and B-cell Immune Epitopes</i>	<i>59</i>
<i>Figure 5: Overlap Fusion Assembly PCR Process for Amplifying CPI- and TK-specific Repair Cassettes</i>	<i>59</i>
<i>Figure 6: Stepwise PCR Amplification of Fragments and Full-length Repair Cassette Constructs</i>	<i>60</i>
<i>Figure 7: Verification of Extracted pJet1.2 Blunt Cloning Plasmids from Transformed DH5α E. coli cells Containing Ligated CPI- or TK-specific Repair Cassettes.....</i>	<i>61</i>
<i>Figure 8: In Silico Analysis, Design, and Verification of Single Guide RNAs for CPI and TK Gene Knockouts</i>	<i>62</i>
<i>Figure 9: Selection and Optimization of CPI- and TK-sgRNA Candidates by Measuring in Vitro DNA Cleavage Efficacy</i>	<i>63</i>
<i>Figure 10: Verification of Non-off Template Binding Specificity for CP1sg2, CP1sg3, TKsg2, and TKsg3 Candidates.....</i>	<i>64</i>
<i>Figure 11: Verification of CP1sgRNA2-1326 and TKsgRNA2-132 Integration into hSpCas9 Plasmid by Nested PCR</i>	<i>65</i>
<i>Figure 12: Validation of Cp 18S rDNA Binding Specificity to C. parvum IOWA DNA.....</i>	<i>66</i>
<i>Figure 13: Quantification of C. parvum DNA using Cp18s rDNA qPCR Standard Curve.....</i>	<i>67</i>
<i>Figure 14: Optimization of Transient Sporozoite Nucleofection with the Full-Length Nluc-NeoR Plasmid Vector</i>	<i>68</i>

Tables

Table 1: Comprehensive Evaluation of Antigen Targets with Raw Epitope Prediction Scores69

Table 2: Features and Sequences for all Key Components Within CP1- and TK-specific Repair Cassettes70

Table 3: Features and Sequences for all Key PCR Fragments and Primers for CP1RCFL and TKRCFL Constructs.....71

Table 4: Selected Guide RNA Sequences and Their Proximity to Flanking Homology Regions...72

Table 5: Primers Used for Amplification of Each CP1- or TK- Guide RNA Candidate73

Table 6: Precise Cleavage Bands and Molecular Sizes for the in Vitro DNA Cleavage Assay74

2. Introduction

2.1 Background and Experimental Rationale

Cryptosporidium spp., primarily *Cryptosporidium parvum* and *Cryptosporidium hominis*, are apicomplexan protozoan parasites causing gastroenteric cryptosporidiosis (Crypto) outbreaks globally in humans¹⁻³. High morbidity is reported among millions of young children under five and immunocompromised individuals in low and middle-income countries (LMICs), resulting in chronic severe malnutrition, growth stunting, and developmental cognitive defects³⁻⁵. In developed countries, large-scale waterborne outbreaks have been recorded in the USA, the UK, Canada, Australia, and Japan due to *C. parvum* oocyst resistance to conventional water purification strategies⁶⁻⁸. The largest waterborne outbreak, affecting up to 500,000 people, occurred in Milwaukee, Wisconsin, costing 97 million USD in direct costs and causing significant mortality in high-risk populations^{9,10}. In Canada, outbreaks have significantly impacted Indigenous communities in Nunavik, Quebec, and Nunavut territory, as well as in Ontario, British Columbia, and Saskatchewan due to limited access to clean water and healthcare¹¹⁻¹⁸. Currently, no vaccines are available, and the only U.S. FDA-approved treatment, nitazoxanide, is ineffective for the most vulnerable populations, including the elderly, young children, HIV/AIDS patients, and organ transplant recipients^{2,5,19-23}. Crypto poses a significant public health and economic burden in Canada and worldwide, with an estimated annual cost of 1.2 billion USD²⁴.

This project focuses on *C. parvum* due to its ubiquitous host infectability across humans, livestock, pets, birds, and wildlife and its ease of genetic tractability^{1,23,25-28}.

Advances in Clustered Regularly Interspaced Short Palindromic Repeats (CRISPR)-CRISPR-associated (Cas)-mediated genome editing and model culture systems have enabled a better understanding of the parasite's ontogeny and host-pathogen interactions^{16,29-35}. A promising development is the cysteine protease inhibitor, N-methyl piperazine-Phe-homoPhe-vinyl sulfone phenyl (K11777), which has shown efficacy in rescuing C57BL/6 Interferon-gamma receptor knockout (IFN γ R-KO) mice from lethal *C. parvum* infection by inhibiting the Cryptopain-1 (CP1) protein^{36,37}. This project aims to generate an attenuated strain of *C. parvum* by deleting CP1 using CRISPR-Cas9 (6.1-Fig. 1). CP1 is crucial for parasite maturation, nutrient acquisition, and host immune invasion³⁶⁻³⁸. By disrupting essential genes, we aim to create a viable attenuated strain

with impaired replicative growth and virulence but retained viability and immunogenicity for mass production and prophylactic vaccination (6.2-Fig. 2). This strategy is supported by the success of live-attenuated vaccines based on other related protozoan parasites³⁹⁻⁴². Assessing CP1 as a potential target of K11777 and evaluating the efficacy of a CP1 knockout (CP1-KO) *C. parvum* as a live-attenuated vaccine candidate may provide insights into parasitology and molecular biology, facilitating reproducible studies on CRISPR-Cas-mediated attenuation of related parasites.

2.2 Research Hypothesis

Deleting CP1 will reduce *C. parvum*'s replication and virulence while ensuring viability and immunogenicity. Vaccinating mice with CP1-KO *C. parvum* will elicit a robust immune response, leading to lower parasite levels and increased survival after challenge with the virulent wild-type strain.

2.3 Research Objectives

1. Develop a tool for studying parasite biology and host-parasite interactions (6.2-Fig. 2).
2. Validate genome editing in the compact genome of *C. parvum* using CRISPR-Cas.
3. Create an attenuated strain by disrupting critical genes, ensuring sustained production and immunogenicity.
4. Monitor oocyst output and explore pathways contributing to potential virulence resurgence.
5. Evaluate attenuated oocysts as a potential live attenuated vaccine candidate.

2.4 Significance

The potential success of this research may significantly impact Crypto prevention and treatment, presenting a positive development in addressing this disease. Previous studies have shown the feasibility of using CRISPR-Cas9 for gene editing in *C. parvum*.^{16,27,30,43-47} Developing a genetically attenuated strain of *C. parvum* targeting a critical virulence factor is crucial in providing new tools for combating Crypto. The findings from this research could lead to the first effective vaccine against Crypto, significantly reducing the global burden of the disease and improving health outcomes for high-risk human populations.^{17,48,49}

3. Literature Review

3.1 Background of Crypto

3.1.1 Global Impact of Diarrheal Diseases

Diarrheal-associated diseases, caused by various pathogens, including viruses, bacteria, and parasites, are among the top five causes of death globally and the fourth leading cause in children under five years of age, resulting in approximately 800,000 deaths annually^{3,25,50,51}. Since 2017, over 6 billion cases and 1.5 million deaths have been reported worldwide in 195 countries and territories^{2,22}, making diarrheal disease the second most common health disorder after upper respiratory infections. It is also the fifth leading cause of death year-round^{2,49,52}. Among the primary causative agents of diarrheal-associated morbidities and mortalities, *Cryptosporidium* spp. are intestinal apicomplexan parasites causing acute gastroenteritis, particularly in pediatric populations. These parasites are zoonotic and can infect a wide range of vertebrates. Infection can occur with as few as ten oocysts in healthy individuals and potentially even a single oocyst in immunocompromised persons^{1,5,53}. There is no effective vaccine for Crypto, and the only FDA-approved treatment, nitazoxanide, is limited in efficacy, especially in Human Immunodeficiency Virus-infected or Acquired Immunodeficiency Syndrome-affected (HIV/AIDS) patients^{19,54-57}. Of the 26 recognized *Cryptosporidium* species, *C. parvum* and *C. hominis* are responsible for about 90% of human infections, leading to an estimated annual loss of 12 million disability-adjusted life years (DALYs)^{2,52}. Other species, such as *C. meleagridis*, *C. felis*, *C. canis*, *C. suis*, *C. muris*, and *C. andersoni*, also infect humans. Seven of the 40 validated ‘genotypes,’ including the *C. hominis* monkey genotype and the *C. parvum* mouse genotype, have also been identified as human pathogens but may only cause transient infection^{58,59}.

3.1.2 Historical Context and Notable Outbreaks

The first human cases of Crypto were reported in 1976^{60,61}. The disease gained significant attention during the AIDS epidemic due to its severe impact on immunocompromised patients. One of the most significant outbreaks occurred in Milwaukee, Wisconsin, in 1993, affecting approximately 403,000 people⁹. Symptoms included watery and mucoid diarrhea, lasting a median of 9 days in healthy individuals and over 14 days in immunocompromised individuals. The

outbreak resulted in around 4,400 hospitalizations and approximately 100 deaths, primarily among the elderly and immunosuppressed⁷. The economic impact was substantial, with costs estimated at 96.2 million USD, including 64.6 million USD in productivity losses and 31.7 million USD in medical expenses^{10,62,63}. In Canada, between 1974 and 2001, *Cryptosporidium* was identified as the third most associated pathogen in waterborne outbreaks^{11,17,64}. Notable examples include the 1996 Cranbrook outbreak in British Columbia, where 2,000 people were initially infected, spreading to 10,000-15,000 more in Kelowna⁶⁵. The 2001 North Battleford outbreak in Saskatchewan resulted in 1,907 confirmed cases due to equipment failures at the water filtration plant⁶⁶. In the USA, an estimated 748,000 cases occur annually, with an annual cost of 45.8 million USD in hospitalizations^{24,67,68}. In Quebec, Crypto became a notifiable disease in 2003, with reported cases increasing in recent years, particularly in the Indigenous region of Nunavik^{13,15}. These increases were attributed to the higher sensitivity of PCR testing compared to previous methods^{11,12,14}. More recently, in the UK, a significant outbreak occurred in 2024 in the Brixham area, with 100 confirmed cases and over 100 additional reported symptoms linked to contaminated water⁶⁹. The outbreak led to a boil water notice affecting approximately 40,000 residents⁶⁹. Another unprecedented outbreak in 2023 saw cases spike threefold above usual rates, with 2,411 laboratory-confirmed cases reported from mid-August to early October^{70,71}. This surge was linked to travel and swimming, particularly in Spain and other Mediterranean countries^{70,71}.

3.2 Disease Transmission and Epidemiology

Cryptosporidium spp. transmission is similar to giardiasis, caused by *Giardia duodenalis*, and is common in humans, livestock, and wildlife⁷²⁻⁷⁵. Oocysts are released in large quantities from infected hosts and spread through direct or indirect transmission. The infectious dose varies by strain, ranging from 9 to 2066 oocysts²³. Direct transmission occurs via the fecal-oral route, including animal-to-animal, animal-to-human (zoonotic), human-to-animal, and human-to-human (anthroponotic) pathways. *C. hominis* is strictly anthroponotic, while *C. parvum* is zoonotic, infecting cattle, sheep, and goats²³. Zoonotic transmission often involves farmers, veterinarians, and others in contact with infected animals⁷⁶. Respiratory transmission has also been reported in mammals, including humans. Recent studies have also identified the potential for *Cryptosporidium* spp. to be transmitted through contaminated fresh produce, highlighting the importance of food safety measures in preventing outbreaks^{12,77}. In developed nations, waterborne transmission is

prevalent among those in contact with contaminated water sources^{25,78}. Drinking and recreational water, such as swimming pools and lakes, have led to multiple large-scale outbreaks in the past 25 years, particularly in Australia, New Zealand, and Europe^{8,79}. Estuarine and coastal waters are significant risk factors, with shellfish acting as vectors for infectious oocysts. A survey in the USA found *Cryptosporidium* spp. in 55% of surface waters and 17% of drinking water supplies^{7,18}.

C. hominis and *C. parvum* infections have been reported in over 90 countries, causing approximately 50.8% of waterborne parasitic diseases²³. In developing countries, approximately 7.2% of the population experiences *Cryptosporidium* infection at least once in their lifetime, compared to 2.5% in industrialized countries. Prevalence rates are higher in Asia, Australia, Africa, and Central and South America than in Europe and North America⁸. *Cryptosporidium* is the most common cause of diarrheal illness in developing countries' children under two years of age, second only to rotavirus². The repercussions of large-scale waterborne outbreaks have led to increased monitoring and intervention of water supplies, improved water treatment and testing standards, and greater demand for public health permits and wildlife regulation in recreational areas^{17,25}.

3.2.1 Molecular Analysis and Species Prevalence

Molecular analysis of approximately 3,600 stool samples from immunocompromised and immunocompetent individuals revealed that *C. hominis* was the most prevalent species (~54%), followed by *C. parvum* (~35%), *C. meleagridis* (~6%), *C. felis* (~3%), and *C. canis* (~3%). This highlights the widespread nature of *Cryptosporidium* spp. and the importance of understanding species-specific transmission dynamics. The infectious dose of *Cryptosporidium* varies by strain, with the dose required to infect 50% of subjects (ID₅₀) estimated to be approximately 10-83 oocysts for *C. hominis* and 132 oocysts for *C. parvum* in immunocompetent adults⁶⁷. This low infectious dose underscores the parasite's high transmissibility and the need for stringent control measures, especially in vulnerable populations. *Cryptosporidium* spp. pose significant risks in both environmental and occupational settings. Livestock farming for cattle, goats, sheep, pigs, horses, and deer has been implicated in human infections through ecological contamination^{80,81}. Farmers, veterinarians, veterinary students, researchers, and technicians are at higher risk due to their close contact with infected animals^{81,82}. Respiratory transmission, though less common, has been reported in mammals, including humans, further complicating control efforts⁸³.

3.3 Clinical Manifestations and Complications

Crypto severity ranges from asymptomatic oocyst shedding to severe, life-threatening disease. Symptoms typically appear within 14 days of ingesting oocysts, with a mean onset of 5-7 days⁶⁷. In a study of 50 immunocompetent volunteers, symptoms ranged from 2 to 26 dpi, presenting as acute gastroenteritis characterized by watery diarrhea, abdominal pain, nausea, vomiting, and low-grade fever⁸³. The duration and intensity of symptoms can vary, with some experiencing prolonged illness. Disease outcome and onset depend on the infection site, parasitic characteristics (e.g., species/genotype, age of oocysts), and host factors (e.g., age, nutritional status, immunocompetency, previous exposure)^{3,84}. Most healthy individuals experience transient, self-limiting symptoms lasting up to three weeks¹⁰. However, *Cryptosporidium* spp. can persist longer than other enteric pathogens, leading to hospitalization and, in rare cases, death⁴⁸. Invasive small intestine infections often cause epithelial damage, disrupting absorption and barrier functions. This can lead to villous atrophy, blunting, crypt cell hyperplasia, and chronic inflammation, characterized by mononuclear cell infiltration of lymphocytes, histiocytes, and eosinophils in the lamina propria⁸⁵. Disruption of the microvillous border results in the loss of membrane-bound digestive enzymes and reduced absorption of fluids, electrolytes, and nutrients, leading to severe dehydration^{18,86}. In severe cases, patients may experience malnutrition, weight loss, and failure to thrive, particularly in children. Complications can extend beyond the gastrointestinal tract. Extraintestinal manifestations, although rare, include respiratory Crypto, which can cause coughing and dyspnea⁶⁰. In immunocompromised individuals⁸³, the parasite can disseminate to other organs, leading to pancreatitis, cholecystitis, and hepatitis^{17,48,87}. These complications further exacerbate the patient's condition and complicate treatment efforts.

3.4 Diagnostics Methods for Crypto

Cryptosporidium was identified as a “neglected pathogen” by the WHO’s Neglected Diseases Initiative in 2004^{3,22}. It is common in developing nations and nearly universal in impoverished areas, where it is frequently underdiagnosed due to climate changes, poverty, and lack of access to diagnostic tools and primary healthcare services. Even in developed countries like the USA, it is estimated that only 1% of cases are diagnosed and reported, making accurate diagnosis crucial for disease control and the development of novel, effective cures⁴.

3.4.1 Microscopic Examination

Microscopic examination can be performed using wet mount preparation or by staining smears with modified acid-fast or fluorescent stains. *Cryptosporidium* can be detected in both preserved and unpreserved stool samples. Samples should be preserved in 10% formalin, sodium acetate formalin, or polyvinyl alcohol (PVA) if there is a delay in processing⁸⁸. However, some staining techniques may not be compatible with PVA-preserved samples⁸⁹. Formalin-preserved samples may not be ideal for molecular diagnosis, even though oocysts can be identified using light or phase-contrast microscopy. The sensitivity of microscopy can be enhanced by reducing debris through oocyst concentration methods like centrifugation, Sheather's sucrose flotation, saturated salt flotation, and the Allen and Ridley formol-ether method^{88,89}. The modified formol-ether method is widely used due to its higher sensitivity. In cases of high clinical and epidemiological suspicion with repeated negative results, immunomagnetic separation is a time-consuming and expensive but effective option⁹⁰.

Various staining techniques have been developed to overcome the small size of *Cryptosporidium* oocysts⁹¹. Romanowsky stains, such as Giemsa and Jenner's, were among the first used for identifying oocysts⁸⁹. These techniques generate a wide range of hues, allowing the differentiation of cellular components. Stained oocysts appear semi-translucent with a narrow clear halo and stain blue to azure, with red or purple eosinophilic granules visible as dots. However, these techniques need more sensitivity and specificity. The acid-fast Ziehl-Neelsen (ZN) stain, introduced in 1981 and later modified, became widely used, with oocysts appearing as red spherules against a pale green background⁸⁹. Safranin-methylene blue and the fluorogenic stain auramine-phenol are alternatives, but auramine-phenol is considered the gold standard due to its high sensitivity and specificity. Smears stained with auramine-phenol or ZN stain allow for subsequent DNA extraction for speciation⁹².

3.4.2 Serological Methods

Serological methods are highly effective for screening large numbers of samples, especially in epidemiological surveys. These techniques detect antigens or antibodies with high sensitivity and specificity. Antigen detection, helpful in diagnosing acute infections, involves antibodies labelled with fluorescent or enzyme reporters. Monoclonal antibodies (mAbs) against the oocyst

wall antigen can precisely detect oocysts^{44,47,93}. Commercially available assays for antigen detection include enzyme immunoassay (EIA), enzyme-linked immunosorbent assay (ELISA), and immunochromatographic (IC) assays. ELISA offers high specificity and quick processing of many samples, while the IC assay provides rapid results but with lower sensitivity^{67,94}. Detecting antibodies to *Cryptosporidium*-specific antigens in serum, saliva, or fecal samples is an indirect and valuable method for seroepidemiological surveys, indicating infection or exposure⁸⁹.

3.4.3 Molecular Methods

For decades, conventional and immunological methods were the primary diagnostics for *Crypto*⁹⁵. These methods are time-consuming, require skilled microscopists, and are prone to false-positive and false-negative results. The invention of molecular techniques, especially polymerase chain reaction (PCR), has revolutionized diagnostic laboratories. PCR-based methods are more sensitive, detect as few as 1 to 106 oocysts are less time-consuming, and allow differentiation of viable and non-viable oocysts⁵⁹. They can also identify species, genotypes, and subtypes, crucial for detecting *Cryptosporidium* prevalence and transmission routes²³. These methods include PCR-restriction fragment length polymorphism (PCR-RFLP), multiplex allele-specific-PCR (MAS-PCR), and quantitative real-time PCR (qRT-PCR)⁹⁵. Species can be identified using specific gene targets such as 18S ribosomal DNA (18S rDNA), thrombospondin-related adhesive protein (TRAP) C1, *Cryptosporidium* oocyst wall protein (COWP), Heat shock protein (Hsp)70, and dihydrofolate reductase (DHFR) genes^{83,88}.

3.5 Immune Responses against *Cryptosporidium*

3.5.1 Innate Immune Responses

The innate immune response is crucial for controlling *C. parvum* infection. After ingestion, *Cryptosporidium* oocysts release sporozoites in the intestine lumen, which migrate to intestinal epithelial cells (IECs), the first barrier and primary target for the sporozoites⁹⁶. Chemokines released by infected IECs attract dendritic cells, promoting chemotaxis^{67,77}. Inflammatory monocytes secrete tumour necrosis factor-alpha (TNF- α) and interleukin-1 beta (IL-1 β), increasing intestinal permeability^{1,17,97}. Nitric oxide (NO), produced independently of interferon-gamma (IFN- γ), is essential for clearing the infection⁹⁸. Inhibiting inducible nitric oxide synthase (iNOS)

increases parasitism and oocyst shedding^{17,99}, as iNOS-derived NO disrupts the parasite's metabolic processes and inhibits its replication within host cells subject to arginine availability¹⁰⁰.

Mucosal immunity, involving antigen-presenting cells like macrophages and dendritic cells, is vital for clearing *Cryptosporidium*^{99,101}. Natural killer (NK) cells and IFN- γ are vital players²⁷. During the acute phase, sporozoites induce IL-12 production by macrophages and dendritic cells, activating NK cells along with IL-18 and TNF- α ^{27,102}. IFN- γ produced by NK cells and macrophages inhibits parasite invasion and intracellular development^{27,44}. NK cells can also kill infected IECs by inducing programmed cell death. The presence of NK cells significantly helps contain the infection, as evidenced by the susceptibility of IFN γ R-KO mice to *Cryptosporidium* infection^{103,104}. Severe combined immunodeficiency (SCID)-IFN γ KO and IL-12pKO mice are highly susceptible, and anti-IL-12 treatment exacerbates Crypto in newborn SCID mice¹⁰⁴⁻¹⁰⁶.

Innate lymphoid cells (ILCs) also play a crucial role in early immune responses to *Cryptosporidium*. The infection triggers the release of IL-18 from IECs and IL-12 production by dendritic cells, which collectively stimulate ILC production of IFN- γ ¹⁰⁶⁻¹⁰⁸. This innate IFN- γ is required for early parasite control and acts directly on infected IECs to restrict parasite growth¹⁰⁶. Additionally, ILCs contribute to the production of other cytokines that enhance the recruitment and activation of various immune cells at the infection site¹⁰⁶.

3.5.2 Adaptive Immunity: Cellular Immune Responses

Adaptive immune responses are necessary for resolving *Cryptosporidium* infections. The gut-associated lymphoid tissue (GALT) in the intestine is the primary defense against gastrointestinal pathogens^{18,75}. T-cell responses, especially CD4+ T cells, are critical for mounting adequate immune responses¹⁰⁹. In AIDS patients, *Cryptosporidium* infection is common when CD4+ T cell counts are below 100 cells/ μ L¹⁷. T helper 17 (Th17) cells play a crucial role in early infection stages, producing IL-17 to support innate immunity^{107,110}. Increased levels of Th17 cytokines, such as IL-17, IL-6, TNF- α , TGF- β , and IL-23, are found in the GALT and spleen of immunosuppressed mice infected with *C. parvum*^{111,112}.

The promotion of cell-mediated immune responses and killing of infected cells is partly due to IL-12 and IFN- γ secretion by macrophages and dendritic cells¹¹³. IFN- γ induces

differentiation of naive CD4+ T cells into Th1 cells, which secrete IFN- γ and promote cytotoxic T cell differentiation¹¹⁴. CD8+ T cells also contribute to parasite clearance by producing IFN- γ and potentially lysing infected IECs²⁷. However, they are not the primary actors in adaptive responses against *Cryptosporidium*¹⁰⁸. Studies show that CD4+ T cells are more critical for protection, with CD8+ T cells playing a supportive role^{99,114}. Innate and adaptive immune responses are essential for controlling and resolving *Cryptosporidium* infections¹⁰⁸.

3.5.3 Adaptive Immunity: Humoral Immune Responses

While cell-mediated immune responses are well-documented, the significance of humoral immune responses remains less clear¹⁰⁸. B-cells produce secretory IgA, and systemic antibodies specific to *Cryptosporidium* spp., including serum IgM, IgA, and IgG, are generated after infection^{17,115}. However, these antibodies are generally insufficient to prevent and control the disease⁴⁵. As *Cryptosporidium* spp. are intracellular pathogens, it is believed that antibody responses may be directed against the extracellular invasive stages of the parasite¹⁷. This response disrupts the parasite's attachment or entry into the host's intestinal epithelial cells¹⁷. Despite this, antibodies may still play a supportive role in protection. It remains unclear whether antibody responses represent a redundant or non-essential mechanism or are markers of other underlying immune responses¹⁰⁸. Hyperimmune bovine colostrum (HBC) has shown significant prophylactic and therapeutic effects, with studies indicating that administering HBC or antibodies can protect newborn animals against infection^{82,100}. The potential of antibodies to prevent Crypto in humans needs to be better characterized, but insights from veterinary medicine offer valuable lessons.

3.6 Vaccine Research and Development

3.6.1 DNA-based Vaccines

Plasmid vector-based immunization techniques have stimulated antigen-specific B and T cell responses in various infection models. The first DNA vaccine expressing the Cpgp15/60 gene, a sporozoite surface antigen, was administered into the mammary glands of cows¹¹⁶. The resulting sera and colostrum provided a protective response in infected cell culture assays and immunosuppressed mice¹¹⁷. Intranasal Cpgp15 DNA vaccination led to a specific and long-lasting production of anti-Cpgp15 IgA antibodies in intestinal secretions and specific IgG in the sera of

mice, persisting for up to one year after the initial vaccination¹¹⁸. Wang et al. demonstrated that immunization with Cpgp15/60 elicited a high IgG antibody response and conferred partial protection against *Cryptosporidium* challenge in mice¹¹⁹. Mice immunized with Cpgp23-DNA exhibited partial protection against *C. parvum* infection, with over a 60% reduction in oocyst shedding after the challenge¹²⁰. Another study found that administering a DNA vaccine encoding Cpgp15 and Cpgp23 induced Th1 immune responses and increased resistance to infection¹¹⁴.

3.6.2 Attenuated *Salmonella* Vaccines

Attenuated *Salmonella* vaccines, with their ability to induce both cell-mediated and humoral responses, elicit systemic and local immunity, and ease of administration, present a versatile tool in immunization strategies^{40,121}. These vaccines have successfully delivered heterologous antigens for various organisms, including intestinal parasites like *Toxoplasma gondii* and *Eimeria tenella*¹²². The attenuated *Salmonella enterica* serovar *Typhimurium* strain SL3261 was initially employed as an antigen delivery system for the oral immunization of mice against two *C. parvum* antigens, Cpgp23 and Cpgp40¹²¹. Thirty-five days post-immunization, specific serum IgG antibodies against Cpgp23 or Cpgp40 were detected using ELISA^{100,123}. Additionally, serum IgA and mucosal IgA antibodies were found in 30% of the mice immunized with Cpgp23¹⁰⁰. Furthermore, prime-boosting with Cpgp23 and Cpgp40 DNA vaccine vectors followed by *Salmonella* immunization significantly enhanced antibody responses to both antigens¹²¹.

3.6.3 Recombinant Antigen Vaccines

Recent studies have demonstrated that the Cpgp15 recombinant antigen effectively eliminates *C. parvum* infection in cattle and can help avoid false-negative results in animal farms¹⁰⁰. CP15 and CSL peptides stimulate antibody production and neutralize parasite entry *in vitro*. Recombinant proteins Cpgp15 and Cpgp23 extend the prepatent period, reduce oocyst shedding, and lead to significant antibody and Th1 cytokine production and increased numbers of CD4+ cells^{118,124,125}. However, they provide only partial protection against *C. parvum* challenge. Additionally, recombinant antigens such as profilin and *Cryptosporidium* apyrase have shown promise in inducing specific and potent humoral and cellular immune responses¹¹⁴.

3.6.4 The Role of Adjuvants

The use of adjuvants can enhance the effectiveness of suboptimal vaccines. Some adjuvants utilize toll-like receptor (TLR) ligands, such as oligodeoxynucleotides (ODNs), which can stimulate the immune system through TLRs or genes for cytokines like interleukin-12 (IL-12) or granulocyte-macrophage colony-stimulating factor (GM-CSF), which boost immune signals when expressed. In one study, intraperitoneal and oral pretreatment with the oligodeoxynucleotide CpG ODN 1668 led to a significant initial upregulation of cytokines and CD69 mRNA in the intestine, reducing parasite load through a TLR9-dependent mechanism. Additionally, cytokines such as IL-18 and IL-12 can enhance the immune response by inducing a Th1 response. For instance, co-immunization with a multivalent DNA vaccine and the pMEM12R plasmid encoding IL-12 further enhanced immune responses compared to the multivalent DNA *Cryptosporidium* vaccine alone

3.6.5 Live Attenuated Vaccines

Live-attenuated vaccines have historically been shown to elicit long-lasting memory immune responses^{40,41,126}. Gamma irradiation can attenuate oocysts or sporozoites, but excessive treatment can kill the parasite, while insufficient radiation allows the parasite to develop fully, leading to *Crypto*¹⁰³. A study demonstrated that calves exposed to irradiated oocysts experienced reduced parasite reproduction and developed partial resistance to reinfection¹⁰⁰. Recent advancements have explored using CRISPR/Cas9 gene editing to create specific knockout and knock-in tagged strains of *C. parvum*^{28,93,127}. These genetically modified strains aim to reduce virulence while maintaining the ability to elicit a protective immune response^{45,93,127}.

3.7 CRISPR-Cas Systems

3.7.1 Mechanisms and Applications

The CRISPR–Cas system is an adaptive immune mechanism in most bacteria and archaea. It protects them from infection by phages, viruses, and other foreign genetic elements by incorporating viral DNA into the bacterial host's chromosomes³¹. It consists of CRISPR repeat-spacer arrays, transcribed into CRISPR RNA (crRNA) and trans-activating CRISPR RNA (tracrRNA), along with Cas genes encode Cas proteins with endonuclease activity³⁴. When foreign genetic elements invade prokaryotes, Cas proteins cut the foreign DNA into short fragments, then

integrate into the CRISPR array as new spacers^{128,129}. Upon subsequent invasions by the same genetic elements, crRNA quickly recognizes and pairs with the foreign DNA, guiding Cas proteins to cleave the target sequences, thereby protecting the host¹³⁰.

Scientists have harnessed this system to directly reprogram endonucleases to specific genes, making CRISPR a powerful genome editing technique that allows for precise, sequence-specific modifications of DNA or RNA^{34,131}. This highly reprogrammable technology has been successfully applied in agriculture, therapeutics, combating infectious agents, the food industry, and bioenergy¹³². CRISPR-Cas systems are categorized into two main classes: Class 1 and Class 2. These classes are divided into six types, labelled I through VI, and several subtypes¹³³. Class 1 systems (Types I, III, and IV) feature complexes with multiple effector Cas proteins, whereas a single effector protein characterizes Class 2 systems (Types II, V, and VI)¹³⁴.

3.7.2 Type II CRISPR-Cas9 Systems

The Type II CRISPR-Cas9 system, derived from *Streptococcus pyogenes* (SpCas9), is among the most well-studied and widely utilized CRISPR-Cas systems¹³³. This system comprises the RNA-guided Cas9 endonuclease and a single-guide RNA (sgRNA). The Cas9 protein features two nuclease domains, HNH and RuvC, each responsible for cleaving one strand of the target double-stranded DNA^{129,135}. The sgRNA is a streamlined fusion of crRNA and tracrRNA, which, together with the Cas9 protein, forms a ribonucleoprotein complex capable of binding and cutting specific DNA targets³⁴. A protospacer adjacent motif (PAM) sequence is essential for the Cas9 protein to bind to the target DNA¹³⁶. During genome editing, Cas9 exclusively cuts double-stranded DNA, creating double-strand breaks (DSBs) that are subsequently repaired by DNA repair mechanisms: homology-directed repair (HDR) and nonhomologous end joining (NHEJ)³⁰.

3.7.3 CRISPR-Cas Applications in Parasites

CRISPR/Cas technology, a versatile tool for genome editing, species-specific diagnosis, drug resistance research, and gene drive strategies, is making significant strides in the field. It enables the production of transgenic malaria parasites, such as *Plasmodium* lines expressing Cas9, chimeric *Plasmodium* lines, knockdown and knockout transgenic parasites, and parasites

expressing alternative alleles¹³⁷⁻¹³⁹. Additionally, it can create mutant strains of *Anopheles* mosquitoes, including male-only populations, wingless mosquitoes, and knock-out/knock-in mutants^{39,139}. Developing a CRISPR/Cas-based diagnostic kit that identifies *Plasmodium* species or drug-resistance markers in malaria settings is a game-changer^{39,140}. This kit promises to revolutionize disease diagnosis with its affordability and rapid detection. Furthermore, advancements in genome modifications using scalable CRISPR/Cas technologies address current limitations in culturing, maintaining, and analyzing these attenuated parasites¹⁴¹. This capability to investigate parasite genome functions opens new avenues for understanding the pathogenesis of malaria^{142,143}. CRISPR-Cas also detects *Toxoplasma gondii*, *Schistosoma haematobium*, and other parasites in blood, urine, or feces¹³³. This CRISPR-based assay offers several significant advantages over traditional methods, such as similar sensitivity and specificity, straightforward observation of reaction outcomes, stable and easy transportation conditions, and minimal reliance on specialized equipment^{34,133,143,144}.

3.8 Roles of Cysteine Proteases

3.8.1 Cysteine Proteases in Protozoa

The clan CA (papain-like) family of cysteine proteases (CPs) is crucial for many protozoan parasites, including apicomplexans and kinetoplastids^{38,145,146}. CPs facilitate cell invasion, nutritive degradation of host proteins, and the modification of parasite proteins during life cycle transitions^{38,146,147}. The *C. parvum* genome contains genes encoding 20 clan CA cathepsin L-like proteases^{148,149}. Among these, five genes code for cryptopains, cathepsin L-like proteases^{93,150}. However, only cryptopain-1 (CP1) has been biochemically analyzed¹⁵¹. Upon secretion, CPs can affect host tissues and immune responses beyond the site of parasite colonization, thereby increasing the pathogen's virulence. The small molecular inhibitor compound K11777 was found to arrest the growth of *C. parvum* in human intestinal cell lines and also rescued susceptible C57BL/6 interferon- γ receptor knockout mice from lethal infection³⁶. This potent anti-*Cryptosporidium* activity is believed to result from K11777 inhibiting the active site of CP1³⁶. This highlights the potential of targeting CP1 for therapeutic interventions against Crypto¹⁵².

Orthologous cathepsin L-like proteases are validated as potential therapeutic targets in extensive *in vitro* and *in vivo* studies with *Plasmodium falciparum* and *Trypanosoma cruzi*^{137,153,154}.

In *P. falciparum*, CPs are involved in hemoglobin degradation, a critical process for the parasite's survival within red blood cells^{139,154}. Inhibitors targeting these proteases have shown significant antimalarial activity¹⁵⁵. For instance, CP falciparum-2 is essential for hemoglobin hydrolysis, and its inhibition leads to the parasite's death¹⁵⁴⁻¹⁵⁶. Similarly, in *T. cruzi*, the etiological agent of Chagas Disease, CPs play essential roles in host cell invasion, immune evasion, and regulating autophagy, mainly for survival under nutrient-limiting conditions^{144,157,158}. The protease cruzipain is a major virulence factor, facilitating the parasite's ability to infect host cells and evade the immune system^{153,159}. Small-molecule inhibitors targeting these enzymes have effectively reduced parasite load and improved survival in infected animal models^{37,160-162}.

3.8.2 Cysteine Proteases in Helminths

CPs are vital in the biology and pathogenesis of helminths. These enzymes are essential for the degradation of host hemoglobin, the principal source of amino acids for many parasitic helminths^{163,164}. For instance, in the liver fluke *Fasciola hepatica*, cathepsin L-like proteases are involved in tissue invasion and nutrient acquisition¹⁶⁵. These proteases degrade host proteins, facilitating the parasite's migration through host tissues and aiding in nutrient absorption¹⁶⁶. In the nematode *Haemonchus contortus*, CPs facilitate the degradation of host blood proteins, assisting in the parasite's survival and pathogenicity¹⁶⁴. Targeting these proteases with specific inhibitors has shown promise in controlling helminth infections by targeting their digestive enzymes^{167,168}.

3.8.3 Cysteine Proteases in Other Infectious Diseases

Furthermore, CPs are also found in various infectious agents, including viruses, bacteria, and fungi^{169,170}. These enzymes play pivotal roles in the pathogenesis of these organisms by facilitating processes such as cell invasion, immune evasion, and nutrient acquisition^{169,170}. For example, in the case of the SARS-CoV-2 virus, the main protease (Mpro) is a CP essential for viral replication¹⁷¹. Inhibitors targeting Mpro have shown potential as antiviral therapies^{171,172}. Similarly, in bacterial pathogens like *Staphylococcus aureus*, CPs contribute to virulence by degrading host tissues and evading immune responses^{173,174}. These proteases are also involved in the pathogenesis of fungal infections, where they aid in tissue invasion and immune evasion, thereby facilitating persistent, recurring infections^{169,170}.

4. Methodology

4.1 Bioinformatics Analysis for Target Selection of CP1

CP1's role as a vital immunogen, expressed during the sporozoites, merozoites, and type II meront stages of *C. parvum* development, was established through comprehensive bioinformatics *in silico* analysis using various online databases and 3D modelling tools. This analysis benchmarked CP1 against ten other highly expressed surface glycoproteins, including Cpgp2, Cpgp900, Cpgp23, Cpgp15/45, and circumsporozoite-like glycoprotein (CSL) (6.3-Fig. 3). Enzymes like Thymidine kinase (TK) and IMP dehydrogenase (IMPDH), central to pyrimidine and purine synthesis pathways during parasite replication, respectively, were included for a thorough T and B cell epitope evaluation due to their active roles in parasite survival and intracellular replication (6.4-Fig 4).

4.1.1 Candidate Antigen Selection Inclusion Criteria

The target antigens were selected based on their immunogenicity, antigenicity, conservation across various isolates, and roles in the parasite's life cycle (6.3-Fig. 3)^{25,148,175-177}.

- **Cryptopain-1 (CP1: cgd6_4880):** A cysteine protease and potent immunogen actively expressed in the sporozoites, merozoites, and type II meront stages. CP1 appears involved in protein processing, host cell invasion, and nutrient uptake^{36,37,178}.
- **Cpgp2 (AY71868)** is a surface antigen involved in the initial attachment of sporozoites to host intestinal epithelial cells (IECs). It is highly immunogenic and conserved among isolates, facilitating invasion¹¹⁹.
- **Cpgp23 (U34390):** Expressed on both sporozoites and merozoites, Cpgp23 is highly immunogenic and conserved¹⁷⁹. It can induce protective immunity in animal models and interact with host cell surface glycosaminoglycans, which may facilitate invasion^{179,180}.
- **Cpgp900 (cgd7_4020)** is another surface antigen that aids initial attachment and invasion¹⁸¹. It is highly immunogenic and conserved among different isolates^{181,182}.
- **Cpgp15/45 (AF1141166):** A complex of two glycoproteins covalently linked by a disulphide bond¹¹⁶. They are expressed on both sporozoites and merozoites and are involved in the

invasion and egress of the parasite from host cells^{116,183,184}. Cpgp15/45 can induce protective immunity in animal models and has been proposed as a potential vaccine candidate¹⁸⁵.

- **Circumsporozoite-like glycoprotein (CSL: CM000431):** This surface antigen shares structural and functional similarities with the circumsporozoite protein of *Plasmodium spp.*, the malaria parasite¹⁸⁶. CSL is expressed on the sporozoites and merozoites of *C. parvum* and can bind to heparin and heparan sulphate on the host cell surface¹⁸⁶. CSL can elicit protective immunity in animal models and has been suggested as a vaccine target^{187,188}.
- **Thymidine kinase (TK: AY466379):** An enzyme responsible for the phosphorylation process of making DNA synthesis precursors^{30,189}. TK is required for the parasite's growth and replication, with a distinct structure and substrate specificity from the human enzyme^{28,190}. TK inhibitors, such as acyclovir and ganciclovir, have been shown to inhibit *C. parvum* growth *in vitro* and *in vivo*^{28,177,190-193}.
- **IMP dehydrogenase (IMPDH):** This purine biosynthetic enzyme is essential for RNA and DNA synthesis for the parasite's survival and replication²⁸. It also has a different structure and regulation from the human enzyme^{194,195}. IMPDH inhibitors, such as mycophenolic acid and tiazofurin, have been shown to inhibit *C. parvum* growth *in vitro* and *in vivo*¹⁹⁵⁻¹⁹⁷.
- **CSL Adjacent Proteins 1 and 2:** These hypothetical proteins were included in the bioinformatics analysis due to their tight proximity to the CSL coding sequence within *C. parvum* chromosome 6 and potential similar functions^{148,150}. Although their exact roles are unknown, their evolutionary conservation and possible involvement in host cell attachment and invasion warranted their inclusion in the analysis¹⁴⁸.

4.1.2 T-cell Epitope Prediction and Scoring Analysis

The binding affinity of T cell epitopes to MHC Class I molecules was assessed using the Immune Epitope Database (IEDB) for both murine and human models to ensure cross-reactivity and translatability, as they are critical to presenting antigenic epitopes to cytotoxic T cells. The evaluation criteria included antigenicity, allergenicity, cross-reactivity, and stability (6.4-Fig 4). **Antigenicity** was evaluated using VaxiJen v.3.0¹⁹⁸, which predicts the probability of a protein being an antigen based on its physicochemical properties. **Allergenicity** was assessed using AllerTOP v.2.0¹⁹⁹, which predicts the potential of a protein to cause allergic reactions. **Cross-reactivity** was determined using ToxiPred v2.0²⁰⁰, which evaluates all epitopes' potential toxicity

and cross-reactivity within a relevant model host. **Stability** was assessed using ProtParam - ExPASy²⁰¹, which evaluates the stability of the epitopes in the biological environment.

Epitopes were scored from 0 to 13 across each criterion, with higher scores indicating better potential (6.15-Table 1). Each candidate's potentially allergenic epitopes or cross-reactive epitopes were given a score of zero to avoid any potentially adverse reactions in a mammalian host. Potentially longer epitopes of longer than thirteen amino acids long were excluded from the analysis due to a high degree of sequence similarity within known toxic antigens to human hosts, thus increasing the risk of cross-reactivity and adverse immune responses²⁰². The average scores from each predicting database were calculated to evaluate each epitope's potential (9.1-Table 7).

4.1.3 B-Cell Epitope Prediction and Scoring

The binding affinity of B cell epitopes to MHC Class II molecules was assessed using the IEDB database for both murine and human models. The evaluation criteria included antigenicity and hydrophilicity, which were evaluated using the IEDB database and antigenic peptide prediction tools. Hydrophilic peptides are more likely to be exposed on the surface of the antigen and recognized by B cells. Epitopes were again scored from 0 to 13 across each criterion, with higher scores indicating better potential (6.15-Table 1). The average scores from each predicting database were calculated to evaluate each epitope's potential comprehensively (9.2-Table 8).

4.1.4 Combinatory T and B Cell Epitope Scoring Analysis

The best T- and B-cell epitope prediction scores from each analysis were combined, and the top three candidates were selected for further evaluation and verification (6.15-Table 1). This integration allowed for identifying top targets based on their potential to elicit both cellular and humoral immunity against *C. parvum* and verifying the high immunogenicity potential of CP1.

4.2 *C. parvum* IOWA Oocyst Infection and Purification

4.2.1 Infection Protocol of IFN γ R-KO Mice via Oral Gavage

The infection protocol involved administering a precise dose of infectious 4,000 *C. parvum* IOWA II oocysts suspended in 100 μ L of PBS to each in-housed and bred C57/BL6 IFN γ R-KO

mouse²⁰³ that were cared for in the animal facility of the RI-MUHC. Previously purified infectious oocysts were housed in potassium dichromate at 4°C in viable 1.7 mL Eppendorf tubes. These oocysts were counted using a disposable hemocytometer at 40x magnification with a light microscope. The oocysts were washed several times with distilled and deionized (dd)H₂O to remove the potassium dichromate solution entirely and spun at 4°C at 10,000 x g using a bench-top centrifuge. After washing, the oocysts were counted again with the hemocytometer to ensure the oocyst pellet remained in the tube. The oocysts were then aliquoted to 4,000 per 100 µL of PBS per mouse using one mL laboratory-certified syringe needles and stored in an ice bucket until infection. Male or female mice, all greater than eight weeks of age, were pre-treated with an 8% NaHCO₃ solution to neutralize stomach acid, enhancing the survival of the oocysts through the gastrointestinal tract^{28,189}. The mCherry TK-tagged genetically modified mouse-adapted *C. parvum* IOWA II strain (shortened as TK-mCherry IOWA *C. parvum*) was graciously donated by Dr. Boris Striepen's lab at the University of Pennsylvania to serve as a confocal imaging control group^{43,44,47}. Post-infection, the animals were housed in CL-2 units due to the parasite infection and observed closely for clinical signs, including diarrhea, lethargy, dehydration, and any unexpected weight fluctuations. The mice were monitored at least once daily and were euthanized at day twelve post-infection (12dpi)^{36,204} to ensure humane treatment and compliance with safe animal use protocols.

4.2.2 Extraction and Purification of Oocysts from Intestines

Following the humane isofluorane-CO₂ euthanasia and physical dislocation, the intestines of infected mice are harvested for oocyst extraction and purification. The intestines are placed in sterile 50 mL plastic containers containing 25 mL 0.04% Tween-20/PBS, and 50 mg of Sputasol (a mixture of 0.1 g Dithiothreitol (DTT), 0.78 g sodium chloride (NaCl), 0.02 g potassium chloride (KCl), 0.112 g disodium hydrogen phosphate (Na₂HPO₄), and 0.02 g potassium dihydrogen phosphate (KH₂PO₄) to create an active working solution of 7.5 mL, pH of 7.4) is added to each sample. The samples are homogenized using autoclaved probes, which are subsequently washed in beakers containing bleach, ethanol, and water successively. A magnet is added to each container, and the samples are incubated on stirrer plates for 1.5 hours in a cold room. The intestine solutions are then transferred into 50 mL Falcon tubes and centrifuged at 2,500 x g for 10 minutes at 4°C.

The supernatant is discarded, and the pellet is resuspended in 8 mL of 0.04% Tween-20/ddH₂O and 4 mL of diethyl ether. The mixture is carefully vortexed for 20-30 seconds and centrifuged at 2,500 x g for 10 minutes at 4°C. The supernatant, containing fat in the ether layer, is meticulously removed. The oocyst-containing pellet is washed with 20 mL of cold ddH₂O, centrifuged, and the supernatant is removed. The pellet is then resuspended in 20 mL of cold saturated NaCl solution, vortexed, and overlaid with 5 mL of cold ddH₂O. After centrifugation at 2,500 x g for 10 minutes at 4°C, 1 mL of the interphase is collected four times into two Eppendorf tubes pre-filled with 1 mL of water each. The samples are centrifuged at 13,200 x g for 30 minutes with precision, the supernatant is removed, and the oocysts from the same mouse are pooled together into one tube. The volume is adjusted to 1 mL of Phosphate-buffered saline (PBS) for short-term storage or potassium dichromate for long-term storage, and the oocysts are counted and stored at 4°C.^{203,205}.

4.2.3 Extraction and Purification of Oocysts from Stool

Stool samples were collected daily from infected mice and stored at 4°C. The samples were homogenized in PBS and filtered through a 70 µm cell strainer to remove large debris. The filtered stool homogenate was subjected to NaCl/ddH₂O gradient centrifugation to separate the oocysts from the fecal debris. The oocysts were collected from the interface, washed with PBS, and stored in potassium dichromate solution at 4°C. To ensure the efficient recovery of oocysts, the stool samples were mixed with an equal volume of 0.04% Tween20/ddH₂O and vortexed with precision for 30 seconds. The mixture was centrifuged at 2,500 x g with precision for 10 minutes at 4°C, and the supernatant was discarded. The pellet was resuspended in 10 mL of cold ddH₂O and centrifuged at 2,500 x g for 10 minutes at 4°C. The supernatant was removed, and the pellet was resuspended in 10 mL of cold saturated NaCl solution, vortexed with precision, and overlaid with 5 mL of cold ddH₂O. After centrifugation at 2,500 x g for 10 minutes at 4°C, the oocysts were collected from the interphase, washed with PBS, and stored in potassium dichromate solution at 4°C.

4.2.4 Verification of Integrity of Extracted *C. parvum* Oocysts

The integrity of the extracted oocysts was verified using phase-contrast microscopy. A small aliquot of the purified oocysts was placed on a microscope slide and examined under a phase-contrast microscope at 400x magnification. Intact oocysts should appear as spherical, refractile

bodies, while lysed or damaged oocysts should appear irregular and non-refractile^{100,205}The percentage of intact oocysts against the total number of oocysts counted was calculated to assess the quality of the extraction and purification process.

4.2.5 Freeze-and Thaw Lysis Protocol of Oocysts

A freeze-thaw lysis protocol was employed to lyse the *C. parvum* oocysts and release genomic DNA. Purified oocysts were resuspended in 200 μ L lysis buffer (10 mM Tris-HCl, 1 mM EDTA, 0.5% SDS, pH 8.0). The suspension was subjected to ten cycles of freezing at -80°C with liquid nitrogen for one minute and thawing at 80°C for one minute each. This process disrupted the oocyst wall, releasing genomic DNA into the lysis buffer using the Qiagen QiAMP DNA mini kit (Qiagen, Germantown, USA), per the manufacturer's instructions. The lysate was then centrifuged at 12,000 x g for 10 minutes to remove debris, and the genomic DNA supernatant was collected. To ensure complete lysis, the lysate was treated with ThermoFischer proteinase K (20 μ g/mL) (ThermoFischer, Eugene, USA) and incubated at 56°C for 1 hour, followed by an additional centrifugation step at 12,000 x g for 10 minutes.

4.2.6 DNA Extraction and Quantification

Genomic DNA was extracted from the lysate using the Qiagen DNA Miniprep kit (Qiagen, Germantown, USA) according to the manufacturer's instructions for the extraction protocol from blood samples. The extracted DNA was eluted in 50 μ L of the provided kit's elution buffer and stored at -20°C until further use. The concentration and purity of the extracted DNA were assessed using a Nanodrop spectrophotometer. The DNA concentration was measured at 260 nm, and the purity was determined by calculating the A260/A280 ratio. DNA samples with an A260/A280 ratio between 1.8 and 2.0 were considered pure and suitable for downstream applications. Additionally, the integrity of the extracted DNA was verified by 1.7% Tris-Acetic Acid-EDTA [Ethylenediamine tetraacetic acid] (TAE) agarose gel electrophoresis analyzed on the Bio-Rad EZ gel doc machine at 100V for 40 minutes (Bio-Rad, San Francisco, USA). Imaging gel samples using 1 μ L ThermoFischer SYBR Safe DNA gel stain (ThermoFischer Scientific, Eugene, USA) indicated that intact genomic DNA should appear as a single high-molecular-weight band, verified with the ThermoFischer GeneRuler 1kpb+ DNA ladder (ThermoFischer Scientific, Eugene, USA).

4.3 Construction of CP1 and TK Knockout Repair Cassettes

4.3.1 Creation of TK- and CP1-specific Repair Cassettes

Creating the CP1 (cgd6_4880) and TK (AY466379.1) knockout reporter repair cassettes involved designing specific repair cassettes for each target gene (CP1RCFL and TKRCFL). These repair cassettes were designed to contain the highly transcriptionally active *C. parvum* enolase gene promoter and the fused coding sequence of the Nanoluciferase-Neomycin (Nluc-NeoR) reporter gene, flanked by 50 – 1000 base pairs (bp) extended homology untranslated regions flanking the target site to facilitate homologous recombination. Due to the ease of PCR amplification, we opted for 50-bps specific 3' and 5' UTRs, the minimum length required for proper HDR within the parasite nucleus^{16,30,189}. After targeted double-stranded break repair, HDR is necessary since *C. parvum* lacks the critical enzymatic machinery for the error-prone NHEJ DNA repair pathway^{16,114,148,203,205}. Similarly, the fusion repair cassette template was designed to be a nucleofection positive for the TK gene due to its successful genetic tagging and knockout modifications from 2015 and subsequent reporter experiments¹⁶. The exact sequences of each component of the repair cassette template are outlined in section 6.16-Table 2 and listed as follows:

- *C. parvum* enolase promoter sequence (CpEnoPro) [363bps]: 5'-
TGGGGAAACTAAATATACTGAAATTCGGTAGATTCTATATCTCACGGGACAGCTTT
TCACACACACTTAGTTCTATATTGCGTCATAACTTTTGTTTTTTTTTGTGCACTTTT
TTTCTCTTATATTCAAGTAAGTGGTTTAGATTCTCTAAGGGCGGGAATATGAATTAG
TGGCAATTCAAAGGATTTAAACGATCAGGCGCCTGCACACCAAACCTCTAATTCGT
ACACAGCATGCCCGAGGTTATAGATATAGATACTGCGAAATTATTTTCATTGTTTCA
GTTAAGAAATAATAAAATATTTTATTATAGTTATTTTCCAAATTTATTTGAGATTTTGT
TATTGAAGTTTAGCCGTCGAC-3'
- Nanoluciferase gene coding sequence (Nluc) [519bps]: 5'-
ATGGTCTTCACACTCGAAGATTTTCGTTGGGGACTGGCGACAGACAGCCGGCTACA
ACCTGGACCAAGTCCTTGAACAGGGAGGTGTGTCCAGTTTGTTCAGAATCTCGG
GGTGTCCGTAACCTCCGATCCAAAGGATTGTCCTGAGCGGTGAAAATGGGCTGAAG
ATCGACATCCATGTCATCATCCCGTATGAAGGTCTGAGCGGCGACCAAATGGGCCA
GATCGAAAAAATTTTAAAGGTGGTGTACCCTGTGGATGATCATCACTTTAAGGTGA
TCCTGCACTATGGCACACTGGTAATCGACGGGGTTACGCCGAACATGATCGACTAT

TTCGGACGGCCGTATGAAGGCATCGCCGTGTTTCGACGGCAAAAAGATCACTGTAA
CAGGGACCCTGTGGAACGGCAACAAAATTATCGACGAGCGCCTGATCAACCCCG
ACGGCTCCCTGCTGTTCCGAGTAACCATCAACGGAGTGACCGGCTGGCGGCTGTG
CGAACGCATTCTGGCGGCTAGC-3'

- Neomycin gene coding sequence (NeoR) [803bps]: 5'-
ATGATTGAACAAGATGGTTTACACGCTGGTTCTCCCGCCGCTTGGGTTCGAAAGAC
TTTTCGGTTATGACTGGGCTCAACAAACCATCGGTTGCTCTGATGCCGCCGTCTTC
CGTCTTTCTGCTCAAGGTCGTCCTGTTCTTTTCGTC AAGACCGACCTTTCTGGTGC
CCTTAATGAACTTCAAGATGAAGCTGCCCGTCTTTCTTGGCTTGCCACCACCGGTG
TTCCTTGCGCTGCTGTCCTTGACGTTGTC ACTGAAGCCGGTAGAGACTGGCTTCTT
TTAGGTGAAGTCCCCGGTCAAGATCTTCTTTCTTCTCACCTTGCTCCTGCCGAAAA
AGTTTCTATCATGGCTGATGCTATGCGTCGCTTTCATACCCTTGATCCCGCTACCTG
CCCTTTCGACCACCAAGCCAAACATCGTATCGAACGTGCTCGTACTCGTATGGAA
GCCGGTCTTGTCGATCAAGATGATCTTGACGAAGAACATCAAGGTCTTGCCCCTG
CCGAACTTTTCGCCAGACTTAAGGCCCGTATGCCCGACGGTGAAGATCTTGTCGT
CACCCATGGTGATGCCTGCTTACCCAATATCATGGTTGAAAATGGTCGTTTTTCTG
GTTTCATCGACTGTGGTCGTCTTGGTGTCGCCGACCGTTATCAAGATATTGCCTTA
GCTACCCGTGATATTGCTGAAGAACTGGTGGTGAATGGGCTGACCGTTTCCTTGT
CCTTTACGGTATCGCCGCTCCCGATTCTCAACGTATCGCCTTCTATCGTCTTCTTGA
CGAATTCTTCTGATTAATTA-3'
- CP1 5'UTR flanking homology sequence (CpCP15UTR) [74bps]: 5'-
GATGACATGACAAGATATTCAAAAAAATTTGATGATTATATGTTGAAGTTAATTGAA
CTAAAAAGTAATTAAGT-3'
- CP1 3'UTR flanking homology sequence (CpCP13UTR) [50bps]:
5'-GCATTTCAAGTGTGTTGACTAAGTAATTCTAATATATTTCAAGCATTCTCAGA-3'
- TK 5'UTR flanking homology sequence (CpTK5UTR) [76bps]: 5'-
CCATCTAACACAAAGAATTCAACAATTTACCTAATAAATACTTTAAAGCAATAATAT
CACTCATACTACTGCAAA-3'
- TK 3'UTR flanking homology sequence (CpTK3UTR) [50bps]:
5'-GCAAAATTTGGCGCAGCTATGGCGCCTCTTGAAAGTGCCTAAAAAGGAGT-3'

4.3.2 Inclusion of Missing *C. parvum* enolase gene 3'UTR

To enhance the stability and expression of the inserted genes, we included the 3' untranslated region (UTR) of the *C. parvum* enolase gene (cgd5_1960) in the repair cassette templates (6.16-Table 2). This region was missing from the original Nluc-NeoR fusion reporter encoded plasmid template that the Boris Striepen lab provided, as confirmed by Sanger sequencing with Genome Quebec. The enolase 3'UTR (5'-GTTCGTGGCGTGTAGGATAGTATCGATTAAGTTTTTCTTTTATCTTAATT-3') plays a crucial role in mRNA stability and translation efficiency²⁰⁶. By incorporating this element, we aimed to ensure robust expression of the transfected parasite's selectable marker and reporter genes.

4.3.3 PCR Optimization Using Overlap Fusion PCR Assembly

Both repair cassette constructs were amplified using a four-step overlap fusion PCR process, allowing seamless assembly of multiple DNA fragments *de novo* (6.5-Fig. 5). This method was chosen for its efficiency and precision in producing the desired constructs, similar to Gibson Assembly. Each part of the repair cassette template for CP1 and TK was designed separately in three DNA strands, numbered PCR fragments 1 – 3, using the New England Biolabs (NEB) High-Fidelity (HF) Phusion DNA polymerase PCR kit (NEB, Ipswich, USA). Each template strand contained at least 20 nucleotides overlapping regions with the subsequent strand for seamless assembly without mutations or sequence errors.

All PCR reactions were prepared and analyzed at 20 μ L total reactions, then scaled up to 50 μ L per reaction to maximize template amounts once confirmed to contain the correct band size and sequence analyzed from agarose gel electrophoresis (6.6-Fig. 6). All PCR reactions were performed on a Bio-Rad PCR Machine (Bio-Rad, San Francisco, USA) with custom settings and 1 μ L Dimethyl Sulfoxide (DMSO) included. PCR conditions were optimized to ensure high-fidelity amplification and minimal non-specific products. Critical parameters were systematically varied to achieve optimal results, including 1) annealing temperature was determined using the **NEB Tm Calculator** (Tm = melting temperature); 2) extension time was set to the maximum of 30 seconds per kilo base-pair of DNA template (30s/1kbp); 3) final extension time was set to the maximum of 8 – 10 minutes; 4) magnesium chloride (MgCl₂) concentration was set at the default concentration with the included Phusion 5X HF Buffer; 5) primer concentrations were optimized

to 0.45 μM ; and 6) template DNA amounts ranged from 1 – 5 μL per reaction, ensuring that <250 μg was present. Primer pairs for each PCR reaction were designed using the **Primer3 Input** web design tool and verified using **Multiple Primer Analyzer | Thermo Fisher Scientific - CA** to avoid self- or cross-dimerization activity, set at the default output sensitivity value of ‘3’. The key features, identifiers sequencing data, and sequence lengths of each PCR fragment and primer pair for both repair cassette templates are outlined in section 6.17-Table 3.

4.3.4 Verification and Concentration of Repair Cassette Templates

Following PCR amplification, the repair cassette templates were verified by 1.7% Tris-TAE agarose gel electrophoresis ran on the Bio-Rad EZ gel doc machine (Bio-Rad, San Francisco, USA) and imaged with 1 μL ThermoFischer SYBR Safe DNA gel stain (ThermoFisher Scientific, Eugene, USA), 1.7% agarose gel electrophoresis to confirm the presence of the expected bands and imaged with 1 μL ThermoFischer SYBR Safe DNA gel stain (ThermoFisher Scientific, Eugene, USA) (6.6-Fig. 6). The correct-sized bands were excised from the gel and purified using the NEB Monarch agarose gel extraction kit (NEB, Ipswich, USA). The concentration of the purified templates was determined using a Nanodrop spectrophotometer to ensure sufficient quantities for downstream applications.

4.3.5 Sanger Sequencing Analysis

CP1RCFL and TKRCFL PCR products were subjected to Sanger sequencing to confirm the accuracy of the sequences. This step was crucial to ensure no mutations were introduced during the PCR amplification process. Genome Quebec performed the sequencing, and the results were analyzed using the A Plasmid Editor (ApE) free Windows software to verify the integrity of the repair cassette templates and ensure no sequence errors were made before moving forward.

4.3.6 Ligation into pJet Blunt Cloning Vector

Confirmed CP1RCFL and TKRCFL sequence templates were then ligated into the pJet1.2 blunt cloning vector within the multiple cloning site (MCS) using the ThermoFisher CloneJet PCR Cloning Kit (ThermoFisher Scientific, Eugene, USA). This vector was chosen for its high cloning

efficiency and compatibility with blunt-ended PCR products. The ligation reactions were set up using the provided T4 DNA ligase within the cloning kit, and the conditions were optimized to maximize the yield of recombinant plasmids. Reactions were set up following manufacturing recommendations by performing a 3:1, 4:1, and 5:1 cloning vector (2974 bps) to repair cassette template reactions by molarity using the [NEBioCalculator](#) web tool. The blunt cloning ligation reaction was followed since the NEB HF Phusion DNA polymerase (NEB, Ipswich, USA) performed blunt template cleavage in the previous PCR reactions. The pQE30 plasmid that came with the pJet cloning vector kit was used as a positive control by adding 5 μ L of the positive control plasmid directly to transform competent Dh5 α *E. coli* cells. In contrast, water was a negative control for ligation and transformation.

4.3.7 Transformation into Dh5 α *Escherichia (E.) coli* Cells

Eppendorf tubes containing 25 μ L of Dh5 α high competency *E. coli* cells (ThermoFisher Scientific, Eugene, USA) were thawed on ice for 10 minutes. To each tube, 3 μ L of the ligation products (CP1RCFL and TKRCFL) were added and gently mixed by flicking. The mixtures were incubated on ice for 30 minutes, followed by heat shock at 42°C for 45 seconds, and then placed back on ice for 5 minutes. Subsequently, 100 μ L of Luria-Bertani (LB) broth was added, and the tubes were incubated at 37°C with shaking at 280 rotations per minute (RPM) for one hour. The cultures were then plated on LB-agar plates containing 50 μ g/mL ampicillin and incubated overnight at 37°C. Individual colonies were selected and screened for insert integration by colony PCR. Successfully transformed colonies were used to inoculate 6 mL of LB broth with 50 μ g/mL ampicillin and grown overnight at 37°C with shaking at 280 RPM. Plasmid extractions were performed the following day using the ThermoFisher GeneJet Plasmid Miniprep Kit (ThermoFisher Scientific, Eugene, USA), according to the manufacturer's protocol. Purified plasmids were stored at -20°C.

4.3.8 Restriction Enzyme Double Digestion Verification

To confirm the integrity and orientation of the repair cassette inserts within the pJet cloning vector, purified plasmids from prospective positive colonies were subjected to double digestion with XbaI and XhoI enzymes purchased from NEB (NEB, Ipswich, USA), which flank the 5' and

3' insert sites of the vector, respectively. The reaction mixture included one μg of plasmid DNA, 1 μL each of XbaI and XhoI enzymes (10 units each), and 5 μL of 10X NEB rCutSmart Buffer (NEB, Ipswich, USA, with PCR-grade nuclease-free water added to a final volume of 50 μL per digestion reaction. The mixture was incubated at 37°C for 1 hour and then heat-inactivated at 65°C for 15 minutes using the Bio-Rad PCR Machine (Bio-Rad, San Francisco, USA). The digestion products were analyzed using agarose gel electrophoresis. A 2% agarose gel was prepared, and 5 μL of the digestion reaction, mixed with 1 μL of 6X DNA gel loading dye, was loaded into the gel wells. Additionally, 1 μL of undigested plasmids containing the CP1RCFL and TKRCFL inserts were included as a negative control. The gel was run at 100V for 40 minutes in 1X TAE buffer. DNA bands were visualized using SYBR Safe staining and analyzed with ImageJ software. The expected band sizes were compared to the ThermoFisher GeneRuler 1 kbp+ DNA ladder (ThermoFisher Scientific, Eugene, USA) to verify the repair cassette inserts' sequence presence and correct orientation.

4.3.9 Mass Production of Repair Cassette Templates

For large-scale production, confirmed CP1RCFL- and TKRCFL-inserted plasmids were extracted using the Qiagen Plasmid Maxiprep kit (Qiagen, Germantown, USA). This process involved culturing the transformed *E. coli* cells in large volumes (≥ 1000 mL) of LB broth supplemented with 50 $\mu\text{g}/\mu\text{L}$ ampicillin, followed by plasmid extraction using the Qiagen maxiprep protocol, per the manufacturer's instructions. The extracted plasmids were then concentrated using a super-sized centrifuge to obtain high yields and stored at 20°C.

4.3.10 Ethanol Precipitation for DNA Concentration

Linearized CP1RCFL and TKRCFL were concentrated using ethanol precipitation to obtain high-quality, concentrated DNA for subsequent electroporation into *C. parvum* oocysts. For the ethanol precipitation, 3M Sodium acetate, pH 5.2, was prepared by dissolving 408.3 g sodium acetate trihydrate in ~ 800 ml H_2O , adjusting the pH with glacial acetic acid, and bringing the final volume to 1 L. Cold 100% ethanol and 70% ethanol (both stored at -20°C) were used. DNA samples were transferred to 1.7 mL Eppendorf tubes, and if the sample volume was less than 200 μL , ddH₂O was added to reach 200 μL . Sodium acetate was added at one-tenth the sample volume,

followed by 2.5 times the sample volume of 100% ethanol. The mixture was incubated at -20°C for at least one hour. After incubation, the samples were centrifuged at $14,000\times g$ for 15 minutes at 4°C . The supernatant was removed, and the pellet was washed with $200\ \mu\text{l}$ of cold 70% ethanol, followed by centrifugation for 10 minutes at 4°C . The supernatant was removed, and the residual ethanol was evaporated. The DNA pellets were resuspended in Tris-EDTA (TE) buffer, pH 8.0, and quantified to ensure a minimum $3\ \mu\text{g}/\mu\text{L}$ concentration for trial nucleofection reactions.

4.4 Design, Selection, and Synthesis of sgRNA Candidates

4.4.1 *In silico* Selection of gRNA Candidates with EuPaGDT

For CRISPR guide engineering with the SpCas9 enzyme, known for its high cleavage efficiency and specificity^{31,189,207-209}. The Eukaryotic Pathogen sgRNA Web Design Tool (EuPaGDT) was used to select optimal sgRNA candidates for *silico*. SpCas9 requires a PAM sequence 5'-NGG-3' at the 3' end of the guide RNA sequence for DNA recognition and cleavage.^{35,93,210-215} Four gRNA candidates for each gene target (CP1 and TK) were selected to maximize the likelihood of successful gene disruption by targeting different loci within the 3' or 5' flanking regions, enhancing SpCas9-DNA binding, cleavage and recombination efficiency^{136,207}.

The selection criteria included:

- 1) **High-reported CRISPR efficiency score:** Based on the guide RNA's predicted efficiency in inducing double-strand breaks.
- 2) **High GC content (40 – 60%):** Enhances binding affinities and cleavage efficiencies.
- 3) **Absence of off-target binding within the *C. parvum* genome:** Ensures specificity to avoid unintended gene edits.
- 4) **No binding within related *Cryptosporidium* parasites, including *C. andersoni*, *C. muris*, *C. bovis*, and *C. hominis*.**
- 5) **No binding within other similar apicomplexan parasites, including *Plasmodium falciparum*, *Toxoplasma gondii*, and *Eimeria tenella*.**
- 6) **Proximity to either the 5' or 3' untranslated regions (UTRs):** Guides near these regions are more likely to disrupt gene function effectively.

The exact sequences for the four guide RNAs selected for CP1 and TK, along with their proximity to either the 5' or 3' target untranslated regions, are listed in section 6.18-Table 4.

4.4.2 Template Design of Selected CP1- and TK-specific gRNA Design Constructs

Primers were designed to span the T7 promoter sequence plus two ending guanine nucleotides to initiate *in vitro* transcription (6.8-Fig. 8A-B). Each CP1/TK guide RNA candidate has a different, forward primer that includes the T7 promoter sequence (5'-TAATACGACTACTA TAG -3') and the 20-nucleotide (nt) long guide RNA sequence. In contrast, they all share the same consensus reverse primer that spans the tracrRNA sequence (5'-GTTTTAGAGCTAGAA ATAGCAAGTTAAAATAAGGCTAGTCCGTTATCAACTTGAAAAAGTGGCACCGAGTCG GTGCTTTT-3'), using the provided human codon-optimized (h)SpCas9-gRNA plasmid by the Boris Striepen lab as the DNA template (6.19-Table 5). PCRs were amplified following the NEB HF Phusion DNA polymerase kit (NEB, Ipswich, USA). For the PCR cycling parameters, refer to Chapter 4 Methodology, section 4.3.3 [PCR Optimization Using Overlap Fusion PCR Assembly](#).

4.4.3 *In vitro* Transcription of gDNA Candidates

Following amplification of each gRNA template (refer to Chapter 4 Methodology, section 4.2.6 [DNA Extraction and Quantification](#)), an eight-to-ten-hour long *in vitro* transcription reaction was conducted using the ThermoFisher T7 MEGAscript Transcription Kit (Thermo Fischer Scientific, Eugene, USA), followed by RNA Purification with the ThermoFisher MEGAclear RNA Purification kit (ThermoFisher Scientific, Eugene, USA) per the manufacturer's instructions. To confirm successful transcription, denaturing agarose gel analysis was performed using TBE (Tris, Boric Acid, EDTA). The steps included preparing a 2% denaturing TBE agarose gel, loading the RNA samples with RNA loading buffer, running the gel at 100V for 1 hour in 1X TBE buffer with ethidium bromide, and visualizing the RNA bands under UV light with SYBR Safe RNA gel stain.

4.4.4 Recombinant SpCas9 Enzyme Production

As part of an ongoing collaboration, the National Research Council (NRC) provided the entire process, including the design, amplification, ligation, transformation, expression,

purification, and quantification of active purified recombinant SpCas9 enzymes for the subsequent *in vitro* screening assays in this chapter.

4.4.5 *in vitro* DNA Cleavage Assay Assembly and Analysis

To assess the DNA cleavage efficiency of the SpCas9-sgRNA complexes, the recombinant SpCas9 protein was first assembled with each purified sgRNA candidate *in vitro* at room temperature for 10 minutes to activate the RNP complex. The target DNA template, containing both the sgRNA binding site and PAM sequence, was then added to the RNP complex to initiate *in vitro* DNA cleavage and double-stranded breaks. CP1gene Fwd primer: 5'-AAATTTGATGATTATATGTTGAAGTTAATTGAAC-3'. CP1gene Rev primer: 5'-TCTGAGAATGCTGAAATA TATTAGAATTAC-3'. TKgene Fwd primer: 5'-TAAAGCAATAATATCACTCATACCTAC-3'. TKgene Rev primer: 5'-ACTCCTTTTTAGGCACTTTCAAGA-3'. The reaction was assembled at room temperature in the following order: 20 μ L of nuclease-free water, 3 μ L of 10X Cas9 NEBuffer3.1 (NEB, Ipswich, USA), 3 μ L of 300 nM sgRNA (30 nM final), 1 μ L of 1 μ M SpCas9 Nuclease, *S. pyogenes* (30 nM final), and 3 μ L of 30 nM substrate DNA (3 nM final), making a total reaction volume of 30 μ L. The mixture was gently mixed and pulse-spun in a microfuge, then incubated at 37°C for 1 hour. After incubation, 1 μ L of Proteinase K was added to the reaction and incubated at 37°C for 10 minutes to release the cleaved DNA template from the SpCas9 catalytic binding site. Before analysis, 1 μ L of RNase A was added to the reaction and incubated at 65°C for 30 minutes to digest free-floating sgRNA. The mixture was then loaded onto a 2% TAE agarose gel, ran for 100V for 50 minutes and imaged under UV light with SYBR Safe. The efficiency of target DNA cleavage was analyzed against the template DNA in the second well using ImageJ gel densitometry. The exact size of the predicted cleavage fragments was calculated based on the cleavage site 3 bps upstream of the PAM sequence, with each gRNA fragment pattern listed in section 6.20-Table 6, and Microsoft Excel calculated the DNA cleavage efficiency score.

4.5 Integration and Testing of CRISPR-Cas9 Plasmids

4.5.1 Ligation of Select sgRNA Sequences into the hSpCas9 Plasmid

To prepare and ligate the selected CP1sg2-1326 and TKsg2-132 sgRNA sequences into the no-guide hSpCas9 plasmid (provided by the Boris Striepen lab) for plasmid-based electroporation

analysis^{30,189}, 10 mL of LB with kanamycin (50 µg/mL) was inoculated with competent Dh5α *E. coli* containing the hSpCas9 plasmid and incubated overnight at 37°C. The plasmid was isolated and purified using the ThermoFisher GeneJet Plasmid Miniprep Kit (ThermoFisher Scientific, Eugene, USA), then digested with NEB BbsI restriction enzyme at 37°C (NEB, Ipswich, USA). Digestion was confirmed on a 2% TAE agarose gel, and the linearized DNA was purified and dephosphorylated with NEB Calf Intestinal Alkaline Phosphatase (CIP) at 37°C for 1 hour (NEB, Ipswich, USA), then diluted to 50 ng/µL. For the guide RNA insert preparation, 6.5 µL ultra-pure water, 1 µL 100 µM Forward Guide primer, 1 µL 100 µM Reverse Guide Oligo, 1 µL T4 DNA Ligase Reaction Buffer, and 0.5 µL T4 Polynucleotide Kinase (T4PNK) enzyme combined. The mixture was incubated at 37°C for 30 minutes, then at 95°C for 5 minutes, decreasing by 5°C each cycle for 14 cycles, and held at 4°C. The guide RNA insert was diluted at 1:200 and 1:500. For the ligation, 6.5 µL ultra-pure water, 50 ng hSpCas9 plasmid, 1 µL diluted Guide RNA insert, 1 µL NEB T4 DNA Ligase Reaction Buffer (NEB, Ipswich, USA) and 0.5 µL T4 DNA Ligase were combined and incubated at room temperature for 1–3 hours. The ligation efficiency was improved using a higher concentration of T4 DNA ligase and extending the extension time to 16 hours (overnight) at 4°C^{16,30}.

4.5.2 Transformation of the Plasmid into DH5α *E. coli*

For protocol specifics, refer to Chapter 4 Methodology, section 4.3.7 [Transformation into Dh5α *Escherichia \(E.\) coli* Cells](#).

4.5.3 PCR and Sequencing to Confirm Integrity of Ligated sgRNA

To screen for positive clones, 5–10 colonies were picked and inoculated in 3 ml LB with kanamycin (50 µg/ml) and incubated overnight at 37°C. A small amount of bacterial culture (2 µL) from each colony was used to perform PCR, using the Reverse Guide Oligo and the Forward Screening Primer (5'-CTTTACTATTTATTCCGCTTCCACATGC-3'). The PCR products were analyzed on 2% TAE agarose gel, where a ~200 bp product visualized using SYBR Safe indicated correct ligation. Positive bacterial cultures were then mini-prepped with the ThermoFischer GeneJet Miniprep kit (ThermoFischer Scientific, Eugene, USA) and sequenced with Genome Quebec using the forward screening primer to confirm the presence of the correct sgRNA insert.

4.6 qPCR Optimization for Quantification of Sporozoites

4.6.1 Specificity of 18S rDNA and Hsp70 gene primers for PCR

To confirm target specificity, the 18S ribosomal DNA (18S rDNA) gene (AF164102.1) and the heat shock protein 70 (Hsp70) gene (U69698.2) were selected. PCR was performed using the Promega GoTaq DNA Polymerase kit (Promega, Madison, USA), containing 1X GoTaq Green Master Mix, 0.5 μM of each forward and reverse primer, and 2 μL of oocyst genomic template DNA, with nuclease-free water added to a final volume of 25 μL (6.12-Fig. 12). The sequencing primers used were 18S rDNAFwd (5'-CATGGATAACCGTGGTAAT-3') and 18s rDNARev (5'-TACCCTACCGTCTAAAGCTG-3') for the 18S rDNA gene, with an expected product size of 178 bp. In comparison, the Hsp70Fwd (5'-AACTTTAGCTCCAGTTGAGAAAGTACTC-3') and Hsp70Rev (5'-CATGGCTCTTTACCGTTAAAGAATTCC-3') primers are for amplifying the Hsp70 gene, with an expected product size of 144 bp. The PCR cycling annealing temperature was determined using the Integrated DNA Technologies (IDT) **Oligo Analyzer (idtdna.com)** tool, with Na^+ concentration set at 50 mM, Mg^{2+} at 2 mM, dNTPs at 0.2 mM, and oligo concentration at 0.5 μM . The PCR cycling conditions included an initial denaturation at 95°C for 2 min, followed by 35 cycles of denaturation at 95°C for 30 s, annealing at 55°C for 30 s, and extension at 72°C for 45 s, with a final extension at 72°C for 5 min. The PCR products were analyzed on 2% TAE agarose gel run at 100V for 40 minutes and visualized with UV light using DNA SYBR Safe staining.

4.6.2 qPCR Optimization with the Confirmed Targets

Quantifying sporozoites was performed using the above annealing primers (section 4.6.1) specific for the 18S rDNA and Hsp70 genes. The qPCR reaction mix included the Applied Biosystems PowerUp SYBR Green Master Mix (ThermoFischer Scientific, Eugene, USA), 0.25 μM of each forward and reverse primer, 5 μL of template DNA, and nuclease-free water to a final volume of 20 μL . The qPCR was performed on the Qiagen RotorGene Q Five-Plex RT-PCR machine (Qiagen, Germantown, USA), following the cycling conditions described in the Qiagen SYBR Green Mix manufacturer's protocol (Qiagen, Germantown, USA). The SYBR Green acquiring stage was processed on the green detection channel during the qPCR annealing step at 55°C for 30s. Standard curves were generated with eight serial dilutions of known quantities of *C. parvum* DNA (6.13-Fig. 13), and the manual detection threshold was set at $T=0.125$ (6.13-Fig.13).

4.7 Excystation and Electroporation of *C. parvum* Sporozoites

4.7.1 Purification and Preparation of Infectious Oocysts

For protocol specifics regarding oocyst purification and counting, refer to Chapter 4 Methodology, section 4.2.2 Extraction and Purification of Oocysts from Intestines.

4.7.2 Preparation of Sporozoites for Oocyst Excystation

A volume of stock oocysts $\geq 1.0 \times 10^6$ oocysts per infection well was loaded into a 1.5 mL microcentrifuge tube (6.14-Fig. 14A). The oocysts were washed with 1 mL acetate/NaCl buffer (prepared by dissolving 0.85 g NaCl, 5 mL 0.2M acetic acid, and 45 mL 0.2M sodium acetate in ddH₂O to a final volume of 100 mL, adjusting the pH to 5.5, filter-sterilizing, and storing at 4°C) by centrifuging at 10,000 x g for 5 minutes at 4°C, discarding the supernatant, and repeating the wash twice. 900 μ L acetate/NaCl buffer and 100 μ L freshly prepared 10x sodium m-periodate (prepared by dissolving 0.022 g Fischer Scientific sodium m-periodate [ThermoFisher Scientific, Eugene, USA] in 1 mL acetate/NaCl buffer, boiling to dissolve, and filter-sterilizing on the day of use) were added to the mixture and incubated on ice for 20 minutes. Next, 300 μ L 0.1% bovine serum albumin (BSA)/PBS (prepared by dissolving 0.1 g BSA in 100 mL 1X PBS, filter-sterilizing, and storing at 4°C) was added and centrifuged at 10,000 x g for 5 minutes at 4°C, discarding the supernatant and resuspending the pellet in 1 mL 0.1% BSA/PBS. This wash step was repeated twice. The pellet was then resuspended in 860 μ L supplemented Roswell Park Memorial Institute (RPMI) media. 10 μ L was used to count oocysts and determine the actual concentration. 150 μ L 10% sodium taurocholate (prepared by dissolving 0.1 g sodium taurocholate in 1 mL RPMI, filter-sterilizing, and using it fresh on the day of preparation) was added to achieve a final concentration of 1.5% to the remaining mixture. The mixture was incubated for 30 min at 37°C, and sporozoites were counted, extending the incubation if 50% excystation was not achieved.

4.7.3 Electroporation of Sporozoites with AMAXA 4D Nucleofector

The electroporation protocol was adapted from Pawlowic et al. (2018)³⁰ and Sateriale et al. (2020)¹⁸⁹. The Lonza AMAXA 4D Nucleofector X Unit was used with the small 20 μ L microcuvette strips, Lonza SF cell line buffer, and EH-100 voltage settings, starting from step 14

of the “Basic Protocol 2: Transfection of *Cryptosporidium* (AMAXA 4D Nucleofection Device)”³⁰. Successfully electroporated sporozoites were transported on ice until *in vitro* infection with previously grown confluent HCT-8 cells on 24-well tissue culture plates.

4.8 *In vitro* Infection and Verification of *C. parvum* Infection

4.8.1 Preparation of HCT-8 Cells for Infection (Days 0 – 2)

The transfectable confluent HCT-8 cells were prepared two to three days before sporozoite electroporation to ensure sufficient cell numbers to support parasite growth for 48 hours. A 175 cm² flask was filled with 24 mL RPMI supplemented with 50 mL FBS, 5 mL HEPES, 5 mL penicillin/streptomycin, and 0.5 mL gentamycin. An HCT-8 cell vial was thawed and added to the flask. Cells were checked every 2-3 days until 80-90% confluency was reached. Growth media was removed two days later, and the cell layer was washed with 20 mL HBSS without calcium. Then, 3 mL trypsin 0.25%/EDTA was added, and the flask was incubated at 37°C for 4 min. The reaction was stopped by adding an equal volume of supplemented RPMI. The cell suspension was centrifuged for 10 minutes at 400 x g, the supernatant was removed, and cells were resuspended in 10 mL supplemented RPMI. Cells were counted using a hemocytometer and diluted to 2.0 x 10⁵ cells/mL in supplemented RPMI. Finally, 1 mL of the cell suspension was added to each well of a 24-well plate and incubated at 37°C overnight. If cells were not 80% confluent the next day, they were allowed to grow for an additional day.

4.8.2 Infection of HCT-8 Cells with Electroporated Sporozoites (Day 3)

Previously stored on ice (refer to Chapter 4 Methodology, section 4.7.3 [Electroporation of Sporozoites with AMAXA 4D Nucleofector](#)), transfected sporozoites were moved into new Eppendorf tubes per cuvette and incubated at room temperature for 10 min. Pre-warmed 80 µL RPMI supplemented with 1% FBS was added to each tube, mixed gently by pipetting, and the 100 µL volume was transferred to a 15 mL conical tube containing 3 mL supplemented RPMI. This step was repeated for each cuvette. Sporozoites were distributed equally between three wells of a 24-well HCT-8 plate (~1 mL per well). The media was removed from the 24-well plate and replaced with supplemented RPMI containing sporozoites, 1 mL per well, with three wells per cuvette. The sporozoite-infected HCT-8 culture was incubated for 48 hours at 37°C with 5% CO₂.

4.8.3 Nanoluciferase Detection Quantification (Day 5)

All steps were performed with the lights off to prevent skewing the readings^{30,189}. Using the Promega Nano-Glo Luciferase Assay Detection kit (Promega, Madison, USA), the Nano-Glo substrate and lysis buffer were combined at a 1:50 ratio. Media was removed from the wells and replaced with 500 μ L of the substrate and lysis buffer mixture. 200 μ L of the mix was aliquoted into Corning® 96-well Solid White Flat Bottom Polystyrene TC-treated microplates (Corning New York, USA), ensuring each well from the 24-well plate was measured in duplicate. Luminescence was calculated using the Tecan Infinite M200 pro plate reader (Tecan, Chapel Hill, USA). The collected data was then plotted and visualized with GraphPad Prism 9.0.

4.8.4 Cell Harvesting, DNA Extraction, and PCR Verification (Day 5)

The supplemented RPMI growth media was gently removed by pipetting, and 200 μ L HBSS without calcium was slowly added to the wells. The HBSS was then gently removed without disturbing the cells. Next, 100 μ L trypsin 0.25%/EDTA was added to each well and incubated at 37°C for 4 min. The reaction was stopped by adding 100 μ L RPMI, and the contents of each well were transferred into 1.5 mL labelled microcentrifuge tubes. The tubes were kept frozen at -20°C until DNA extraction. For the exact protocols specified for *C. parvum* sporozoite DNA extraction, refer to Chapter 4, Methodology, Section 4.2.6 [DNA Extraction and Quantification](#). The nested PCR verification protocol involved using the NEB HF Phusion DNA Polymerase PCR kit (NEB, Ipswich, USA) as outlined in Chapter 4, Methodology, Section 4.3.3 [PCR Optimization Using Overlap Fusion PCR Assembly](#). The sequencing primers used for verification are listed below. The expected molecular products analyzed on TAE agarose gel electrophoresis for the CP1 and TK genes are 1355bps and 776bps long, respectively. Post verification, PCR products were sent for Sanger sequencing analysis at Genome Quebec to check for mutational or sequence misalignments.

- CP1 Fwd sequencing primer: 5'-GATGACATGACAAGATATTCAAAAAATTTGATG-3'.
- CP1 Rev sequencing primer: 5'-GTTCAATTTGAACTAAAATTATCTCTGAGAATG-3'.
- TK Fwd sequencing primer: 5'-CCATCTAACACAAAGAATTCAACAATTTACCT-3',
- TK Rev sequencing primer: 5'-CCTTGTTACCTTTTCTTGGTCTGTCTAACTTTGAC-3'.

5. Research Findings

5.1 CP1 Demonstrated Superior Immunogenicity and Antigenicity Compared to Other Antigen Candidates From T- and B-Cell Epitope Analysis

All ranking scores for each criterion, final scores for each sub-category (T cell epitope and B cell epitope), and overall scores were summarized (6.15-Table 1). The top three candidates with the highest T cell epitope scores were CP1, with a score of 45; Cpgp15/45, with a score of 42; and CSL adjacent proteins 1 and 2, each with a score of 42. For B cell epitopes, the top three candidates were CP1 with a score of 56, Cpgp23 variant 1 with a score of 55, and Cpgp15/45 with a score of 53. Combining the scores from both T cell and B cell epitope predictions, the top three candidates were CP1 with a total score of 101, Cpgp15/45 with a total score of 95, and CSL adjacent protein 2 with a total score of 88 (6.15-Table 1).

5.2 Successful Construction of Revised CP1RCFL and TKRCFL

Fragment PCR product 1 included the 5' CP1/TK UTR homologous region and a 20 bps-long part of the *C. parvum* 5' enolase promoter, resulting in 94 bps (CP1-5'FLK1) and 96 bps (TK-5'FLK1) fragments, respectively (6.5-Fig. 5 and 6.6-Fig. 6A). PCR product 2 included the *C. parvum* enolase promoter Nluc-NeoR fusion template, resulting in 1725 bps (CP1-EnoNN2) and 1730 bps (TK-EnoNN2) fragments (6.5-Fig. 5 and 6.6-Fig. 6B). PCR product 3 attached the 51 bps *C. parvum* enolase gene 3' UTR (cgd5_1960) to the donor template using complementary primers, including the first 20 bps of both the 3' Neomycin gene and CP1 or TK 3' UTR homology flank region, resulting in 124 bps (CP1-3'EnoUFLK3) and 121 bps (TK-3'EnoFLK3) fragments (6.6-Fig. 6C). All three PCR products, each containing 20 bps overlapping regions, were combined in one overlap fusion PCR using High Fidelity Phusion DNA polymerase to assemble the full-length revised repair templates at 1863 bps (CP1-RCFL) and 1862 bps (TKRC-FL) (6.6-Fig. 6D). Although not explicitly included in the figures, each round of PCR assembly and amplification underwent repeated rounds of failure, including multiple dimerization and nonspecific binding issues, failed binding attempts, and highly streaked gels. After months of revamping and retrials, each round of subsequent amplification finally succeeded. Though not fully documented here, this iterative process was crucial in achieving the final successful results. We present only the most

accurate and successful data to maintain clarity and precision. Confirmed PCR products were purified from native 2% TAE agarose gel electrophoresis (6.6-Fig. 6).

5.3 Verification and Analysis of CP1RCFL and TKRCFL Ligated Plasmids

From restriction enzyme digestion analysis, the most prominent band observed from restriction digestion was the uncleaved intact plasmid at approximately 4836 bps, which contained unique recognition and cleavage sites directly 5' and 3' of the insert site on the cloning vector (6.7-Fig. 7A). The larger cleaved plasmid fragment was the second largest observed band at ~2949 bps. The minor band at ~1888 bps was the target band containing the template repair cassette insert (6.7-Fig. 7A). High-fidelity Phusion PCR, targeting the 5' and 3' ends, confirmed the insert length in three of four plasmid clones for CP1RCFL and TKRCFL (6.7-Fig. 7B). Two additional clones with missing target products were excluded from further tests (6.7-Fig. 7B). To verify the integrity of the linearized and digested constructs, the undigested repair cassette for both CP1RCFL and TKRCFL plasmids was also analyzed and included in a separate DNA agarose gel analysis, revealing three distinct bands. The topmost band represented the relaxed, circular plasmid, the middle band corresponded to the linear plasmid, and the bottom-most band indicated the supercoiled plasmid (6.7-Fig. 7C).

5.4 *In Vitro* Characterization of Compatible CP1- and TK-sgRNA Candidates

Subsequent DNA-to-RNA *in vitro* transcription reactions from successfully amplified specific gDNA PCR templates (data not shown) showed clear bands corresponding to the expected sizes of the sgRNAs, indicating successful transcription and integrity of the sgRNAs on the 2% denaturing TBE agarose gel (6.8-Fig. 8D). Initial *in vitro* DNA cleavage assay screening for the four CP1-specific sgRNAs hybridized to activated SpCas9 revealed varying levels of enhancement in SpCas9 template DNA cleavage. Specifically, CP1sg1-205 enhanced SpCas9 template DNA cleavage by approximately 50%. In contrast, CP1sg2-1326, CP1sg3-180, and CP1sg4-1262 enhanced SpCas9 template cleavage by about 86%, 81%, and 70%, respectively (6.9-Fig. 9A). Similarly, for the four TK-specific sgRNAs, TKsg1-684 enhanced SpCas9 template DNA cleavage by approximately 47%. In contrast, TKsg2-132, TKsg3-609, and TKsg4-180 enhanced SpCas9 template cleavage by about 81%, 54%, and 84%, respectively (6.9-Fig. 9B). The darkly stained

sgRNA band visible in the third negative control well without SpCas9 addition was no longer present in the other four treatment conditions due to added RNase A digestion (6.9-Fig. 9B).

5.5 Optimizing RNP:Template Ratios and Off-Target Binding

Four different RNP:template molar ratios, ranging from 10:1 to 20:1, were tested with CP1sg2-1326 or CP1sg3-180 and TKsg2-132 or TKsg4-180. The maximum sustained *in vitro* DNA cleavage efficacy scores (saturation point) for these four sgRNAs were observed at the 15:1 molar ratio mark, with a calculated cleavage efficiency score of approximately 90% for CPsg2, 85% for CPsg3, 87% for TKsg2, and 83% for TKsg4 (6.9-Fig. 9C-D). Although a slight, insignificant increase in efficacy was observed at higher RNP molar ratios (20:1, 23:1, 26:1, and 30:1), no substantial marked increase in cleavage efficiency was noted. No off-target template effects were observed in additional off-target sgRNA controls where CP1sg2 or sg3 and TKsg2 or sg4 were mutated to contain single or multiple nucleotide polymorphisms within their 20-nt gRNA recognition site at both the 5' and 3' ends, modifying from a purine to pyrimidine base, and vice versa (6.10-Fig 10A-B). Higher cleavage specificities were consistently displayed for CP1sg2-1326 and TKsg2-132 over their target sgRNA counterparts. This high binding specificity of the sgRNA to its target sequence translates to approximately 15 μ g of SpCas9-sgRNA RNP injection for a 2×10^6 sporozoite initial *in vivo* nucleofection reaction (6.10-Fig. 10A-B).

5.6 Successful Ligation of CP1sg2-1326 and TKsg2-132 into hSpCas9 Plasmid

Sequencing flanking primers spanning the crRNA insert site confirmed non-specific sgRNA sequence integration, producing a single PCR product of ~500 bps for both the TKsg2- and CP1sg2-specific plasmid clones (6.11-Fig. 11A). The empty plasmid, used as a positive control, also produced the expected 500 bps product since the crRNA insert site contains a 20-bps inverted BbsI placeholder sequence, which is cleaved and replaced with the 20-nts sgRNA sequence. Further sgRNA-specific PCR verification yielded an expected product of ~118 bps, absent in the no-guide plasmid serving as the negative control (6.11-Fig. 11B). These two confirmed sgRNA-containing hSpCas9 plasmid clones were Sanger sequenced to confirm the absence of mutations.

5.7 High Specificity of 18S rDNA-based qPCR Curve for Sporozoite Quantification

Of the tested targets, the 18S rDNA product demonstrated a crucial trait-high specificity for positive DNA samples. This finding, validated by the absence of binding in negative controls and additional negative samples, including those with other parasitic DNA (*Borrelia*, *Babesia*, and *Ehrlichia* spp.), underscores the accuracy and reliability of our testing process (6.12-Fig. 12). In contrast, Hsp70 products had non-specific binding in regions less than 100 bps, likely due to non-specific primer binding, so we proceeded with 18S rDNA primers. Initial qPCR testing of three positive oocyst DNA samples, a negative sample, and a non-template control yielded positive Ct values within the 15–30 range for all positive DNA samples (6.12-Fig. 12). Melting curve analysis revealed a single curve for the positive DNA samples, indicating target-specific amplification, confirmed by the expected 18S rDNA product of ~178 bp on the agarose gel. An 8-point standard curve was established by qPCR, plotting Ct values against oocyst DNA concentration (6.13-Fig. 13) with an expected negative correlation. The corresponding exponential standard curve equation with a correlation coefficient of 0.98 indicates a solid inverse linear correlation between Ct values and DNA concentration.

5.8 Insignificant Reporter Detection for Preliminary *in vivo* Nucleofection

Transient sporozoite nucleofection with the full-length CP1RCFL plasmid was at various sporozoite concentrations (6.14-Fig. 14B). Nanoluciferase luminescence detection showed significant luminescence for transfection conditions A and B over a 5-minute window, with no significant difference between them. Condition C also showed significant luminescence above baseline compared to the Iowa(-) control well containing only HCT-8 cells and infection media (6.14-Fig. 14B). These results indicated that electroporating at least 2.0×10^6 sporozoites per nucleofection reaction is sufficient for detecting nanoluciferase expression and substrate cleavage. However, adding active SpCas9-RNP to the Luminex mixture resulted in no luminescence after 48 hours of *in vitro* HCT-8 infection (data not shown), indicating no parasite survival and growth. This result was consistent across three independent technical replicates.

6. Figures and Tables

6.1 Figure 1: Graphical Timeline of Project Overview

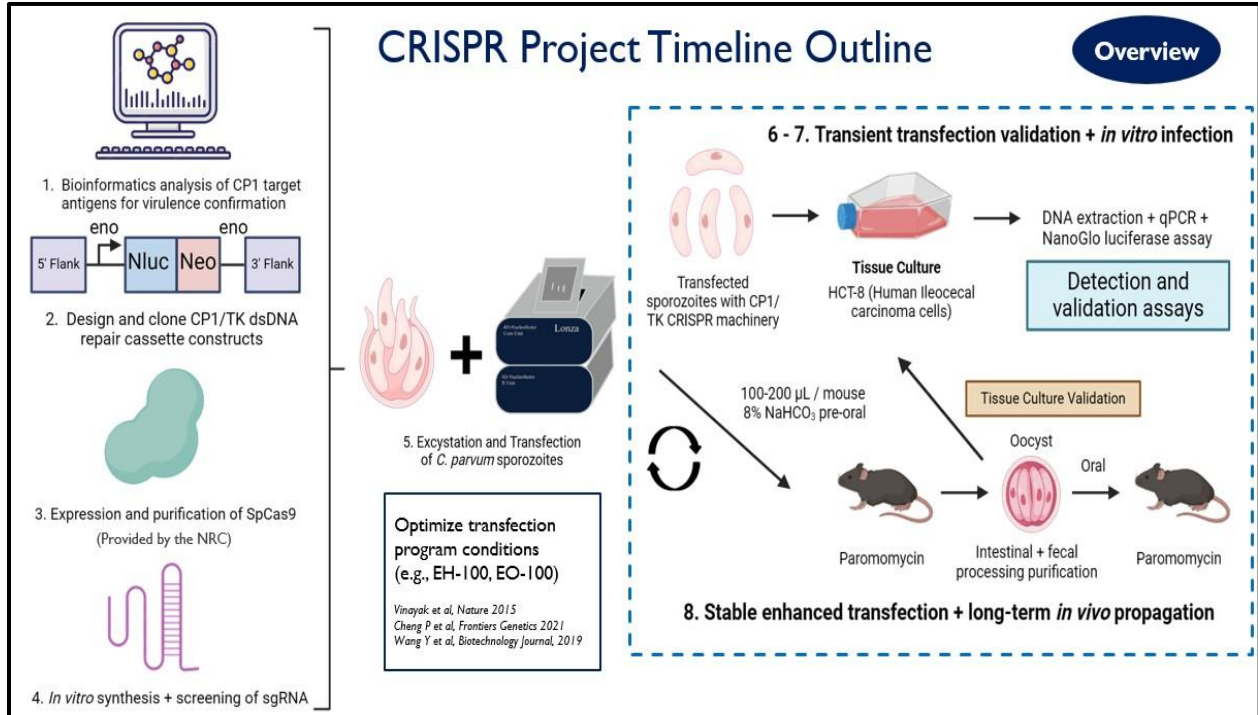


Figure 1: Comprehensive Timeline of the Pilot Initiative for CP1-KO *C. parvum* Vaccine Development. Phase 1 involved bioinformatics analysis to evaluate CP1 antigen. Phase 2 focused on designing and cloning repair cassette templates. Phases 3 and 4 included screening and synthesizing sgRNA candidates and optimizing in vitro DNA cleavage. Phase 5 developed in vivo delivery of the RNP complex using the AMAXA 4D Nucleofector. Phases 6 and 7 involved transfection and screening of KO parasites in HCT-8 cells. Phase 8 included infection of IFN γ R-KO mice and monitoring CP1-KO parasite effects. Aim three created stable transfectants, infection, and identification of transgenic oocysts.

6.2 Figure 2: Novel CRISPR-Cas9 Strategy for *C. parvum*

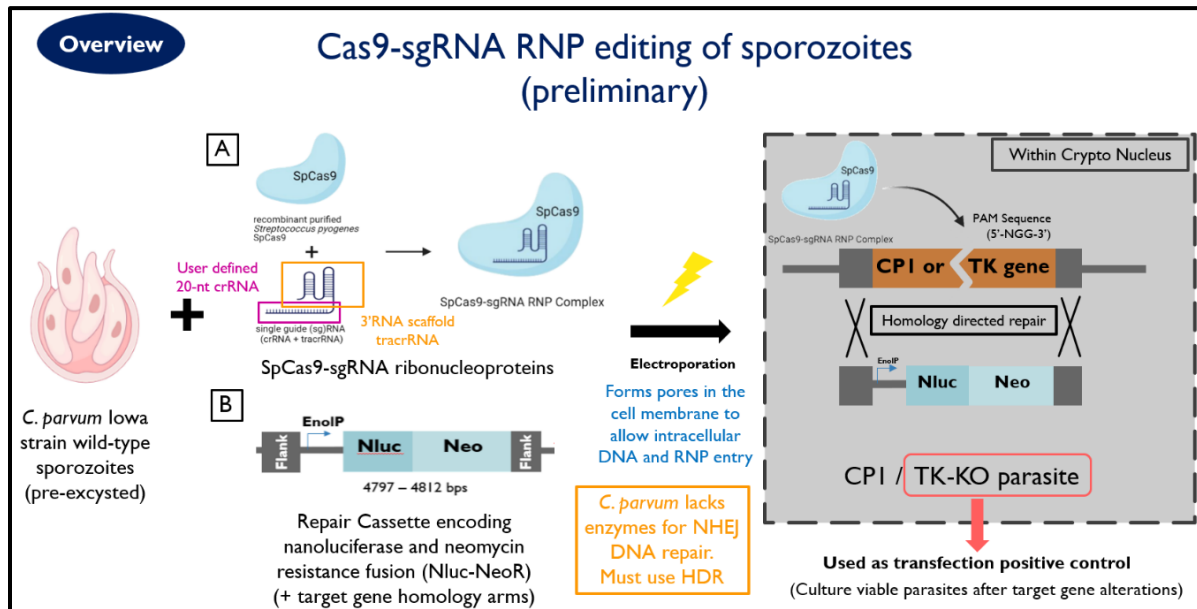


Figure 2: CRISPR-Cas9 mediated genetic knockout in excysted *C. parvum* sporozoites. Preliminary transfection protocol for the nucleolar genetic knockout in sporozoites using the SpCas9-sgRNA ribonucleoprotein complex and a DNA repair template with the Nluc-NeoR reporter gene driven by the *C. parvum* enolase gene promoter. Delivery is achieved with an AMAXA 4D nucleator^{16,30,216}. Transfected parasites are identified through Nanoluciferase luminescence and Neomycin resistance. The nonessential Thymidine Kinase (TK) gene serves as a positive control¹⁶.

6.3 Figure 3: Bioinformatics Screening of Target Antigen Candidates

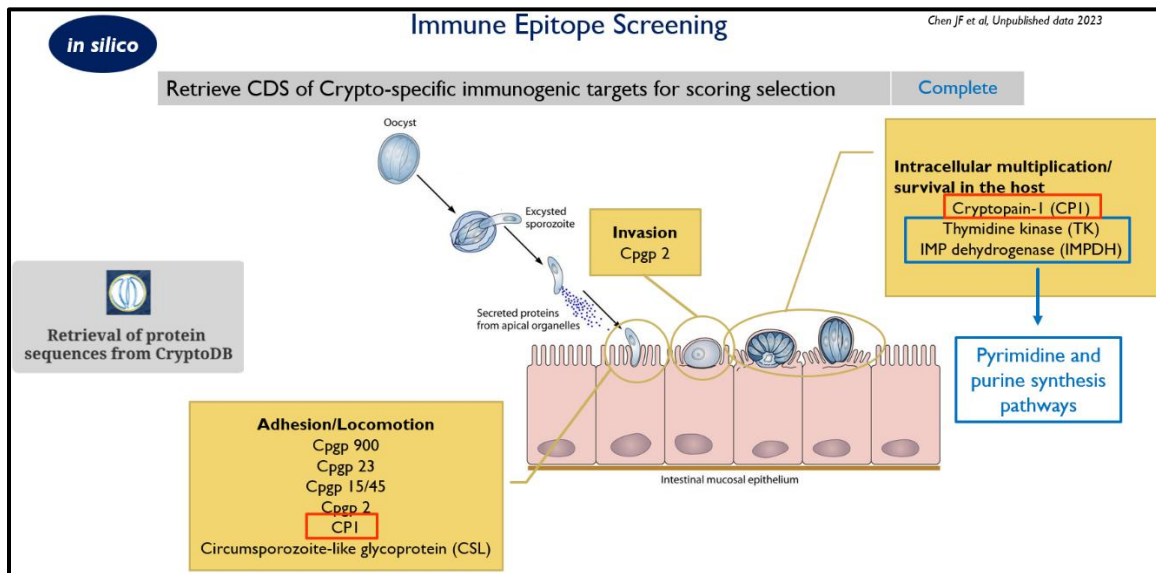


Figure 3: Immunogenicity and antigenicity of *C. parvum* surface glycoproteins and enzymes. Bioinformatics analysis of CPI and ten other highly expressed surface glycoproteins (Cpgp2, Cpgp900, Cpgp23, Cpgp15/45, and CSL) and enzymes (Thymidine kinase and IMP dehydrogenase) in *C. parvum*¹⁴⁸. These molecules are conserved across various strains, expressed during multiple life stages, and exhibit significant immunogenicity and antigenicity, making them potential vaccine targets for inclusion.

6.4 Figure 4: Immune Epitope Screening Evaluation

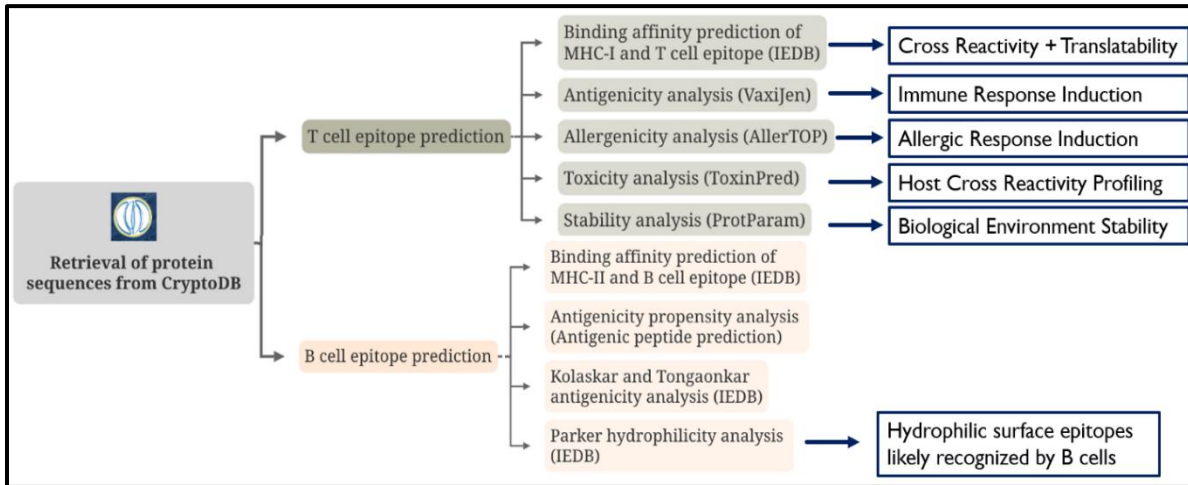


Figure 4: *In-silico* prediction and scoring of T-cell and B-cell epitopes. Epitopes were assessed for binding affinity to MHC Class I molecules using the IEDB database, followed by evaluations of antigenicity, allergenicity, toxicity, and stability using tools like VaxiJen, AllerTop, ToxiPred, and ProtParam. B cell epitopes were similarly evaluated for binding affinity to MHC Class II molecules and assessed for antigenicity and hydrophilicity.

6.5 Figure 5: Overlap Fusion PCR Process

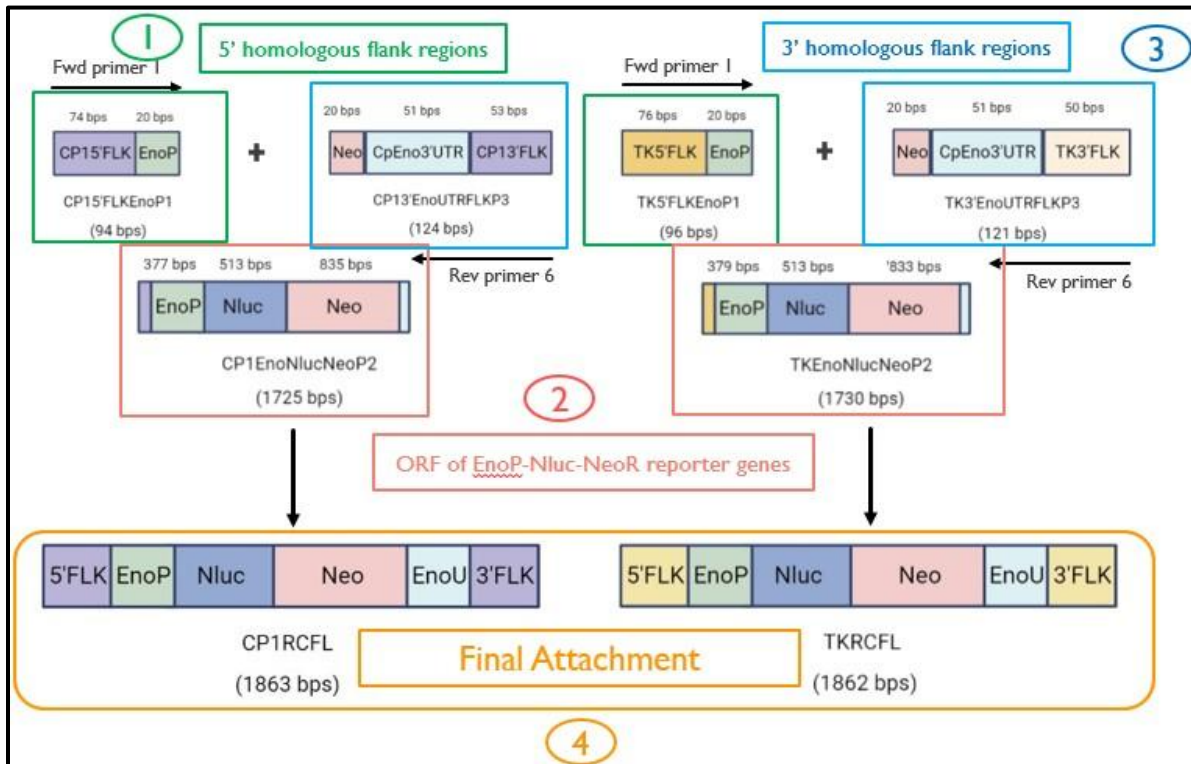


Figure 5: Overlap Fusion Assembly PCR Process for Amplifying CP1 and TK-specific Repair Cassettes. A four-step fusion PCR process streamlined the assembly of DNA fragments, including 1) the 5' untranslated region, 2) the open-reading frame containing the enolase promoter and Nluc-NeoR coding sequence, and 3) the 3' homologous untranslated region. Each PCR product contained overlapping regions, allowing attachment in one overlap PCR (4).

6.6 Figure 6: Stepwise Amplification of Repair Cassette Fragments

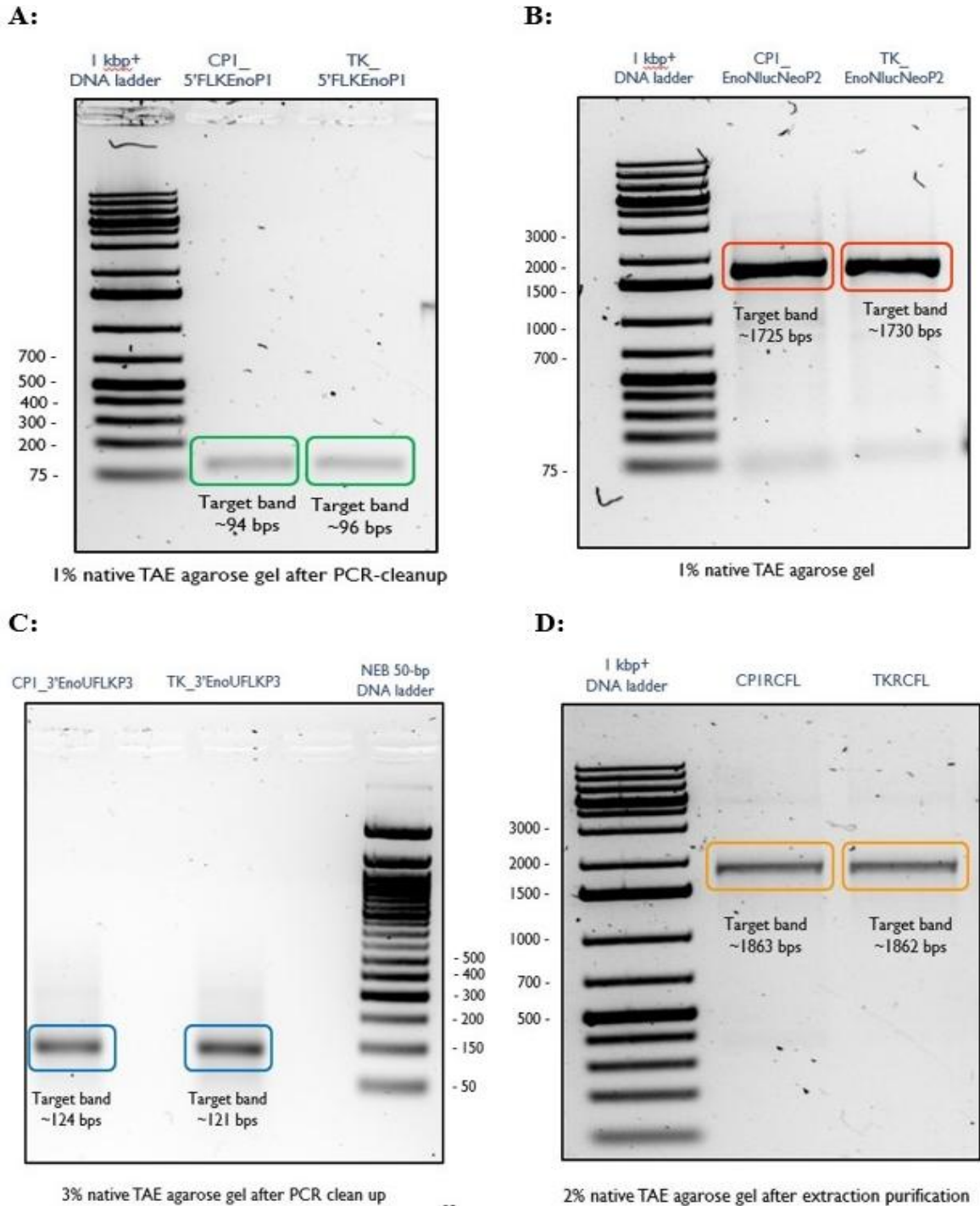
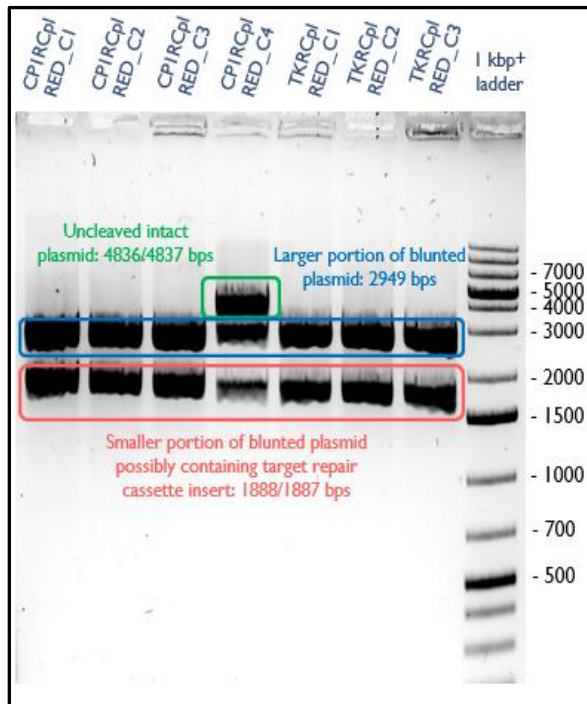


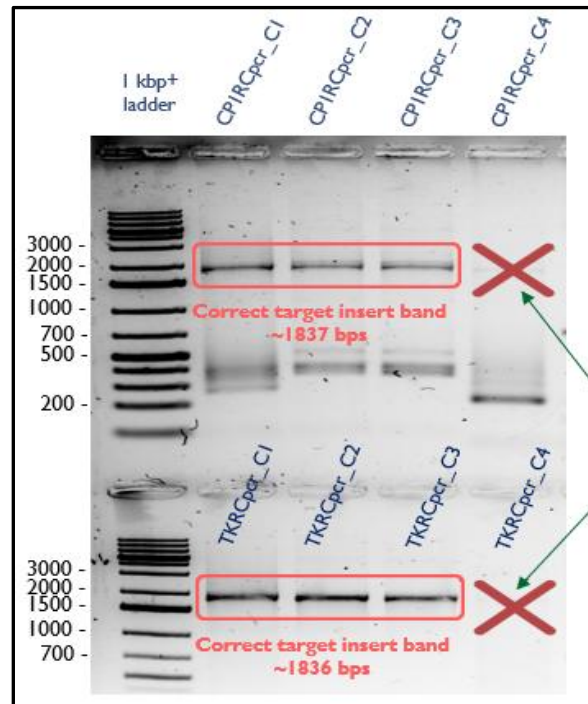
Figure 6: Successful PCR amplification of fragments and full-length repair cassette constructs. A) The 5' untranslated region, encompassing the gene-specific flanking regions for CP1 (94 bps) and TK (96 bps), was amplified and confirmed by agarose gel analysis post-PCR purification. B) The open-reading frame containing the enolase promoter and Nluc-NeoR was successfully amplified for CP1 (1725 bps) and TK (1730 bps). C) The 3' homologous untranslated region, including the *Cp* enolase gene-specific 3' UTR and the 3' CP1 (124 bps) or TK (121 bps) gene-specific flanking region, was amplified and confirmed. D) The full-length products for CP1 (1863 bps) and TK (1862 bps) were assembled using overlap fusion PCR, extracted, purified, and confirmed by agarose gel electrophoresis.

6.7 Figure 7: Restriction Enzyme Digestion Verification

A:



B:



C:

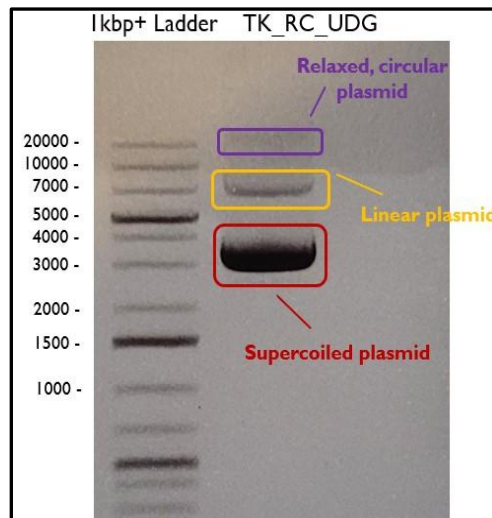


Figure 7: Verification of extracted pJet1.2 blunt cloning plasmids from transformed DH5a *E. coli* cells containing ligated CP1-/TK-repair cassettes. A) Seven different extracted plasmids were subjected to restriction digestion fragment analysis using XbaI and XhoI restriction enzymes. The digestion products were run on a 1.7% native TAE agarose gel and analyzed by DNA electrophoresis. The 1kbp+ DNA ladder was used to confirm the molecular weight of the DNA fragments. B) PCR verification was conducted on the confirmed plasmids to check for CP1- or TK-repair cassette integration. The PCR products were run on a 1.7% native TAE agarose gel and analyzed by DNA electrophoresis. The 1kbp+ DNA ladder served as a reference for DNA band sizes. C) The undigested repair cassette was also analyzed, revealing three distinct bands. The topmost band represents the relaxed, circular plasmid, the middle band corresponds to the linear plasmid, and the bottom-most band indicates the supercoiled plasmid.

6.8 Figure 8: CP1- and TK- single guide RNA Selection Process

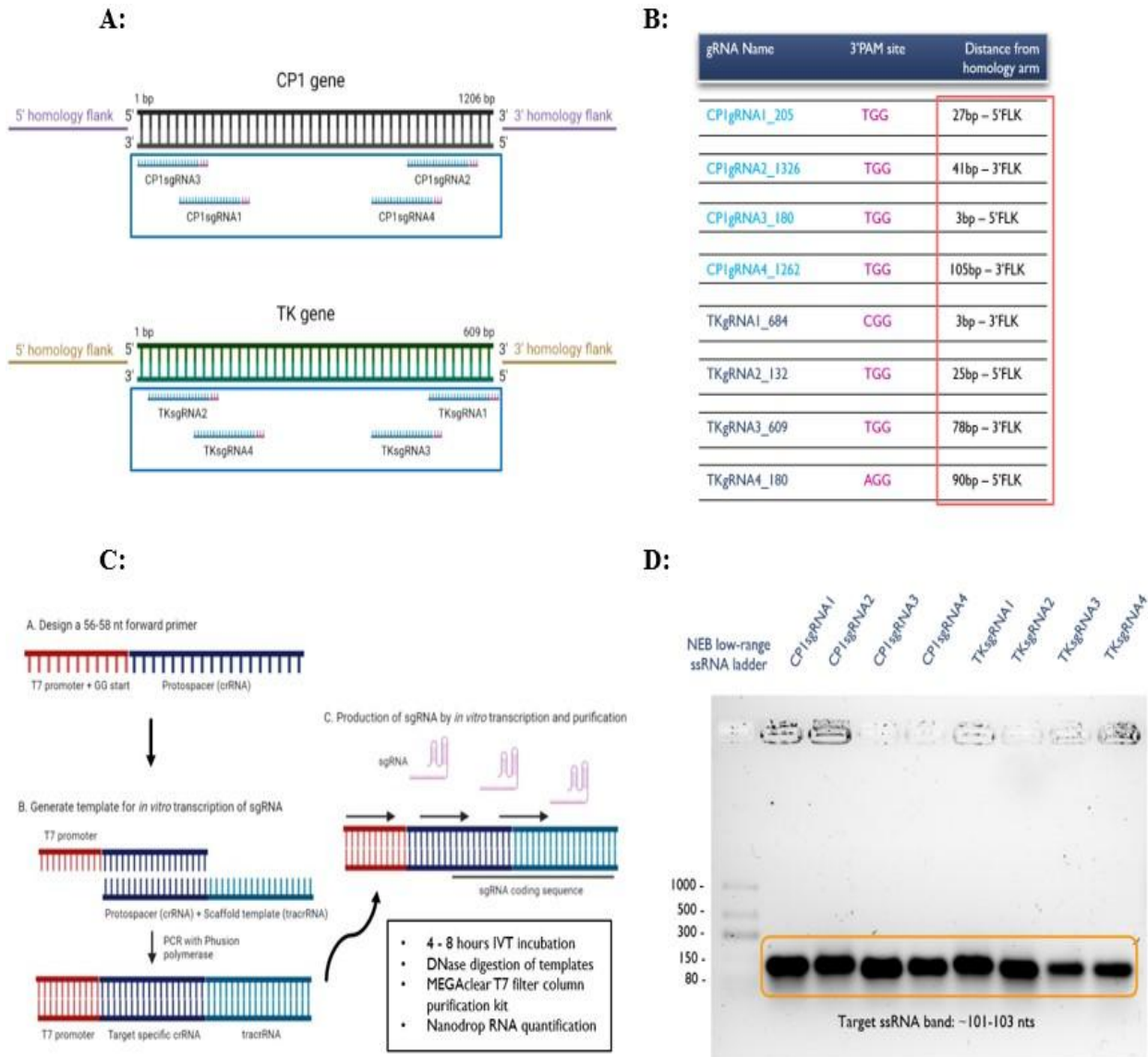


Figure 8: *In Silico* Analysis, Design, and Verification of Single Guide RNAs for CP1 and TK Gene Knockouts. A) Four guide RNA candidates were selected for each gene target using the EuPaGDT web design tool^{130,217-219}. Selection criteria included a high CRISPR cleavage score, 40-60% GC content, no off-target effects, and proximity to the 5' or 3' untranslated region to maximize RNP:genome binding and recombination efficiency^{33,34,209,214,220,221}. B) Each gRNA's coding name, respective PAM sequence, and exact proximity distance to the homology region were documented to calculate the expected cleavage fragments for the in vitro DNA cleavage assay. C) A graphical schematic illustrates the DNA product design for sgRNA PCR template amplification, agarose gel purification, and in vitro transcription steps. D) Successful transcription of all eight gRNAs was confirmed on a 2% denaturing TBE agarose gel, with the target ssRNA band observed between 101 and 103 nucleotides long, as expected.

6.9 Figure 9: Cleavage Verification of Guide RNA Candidates

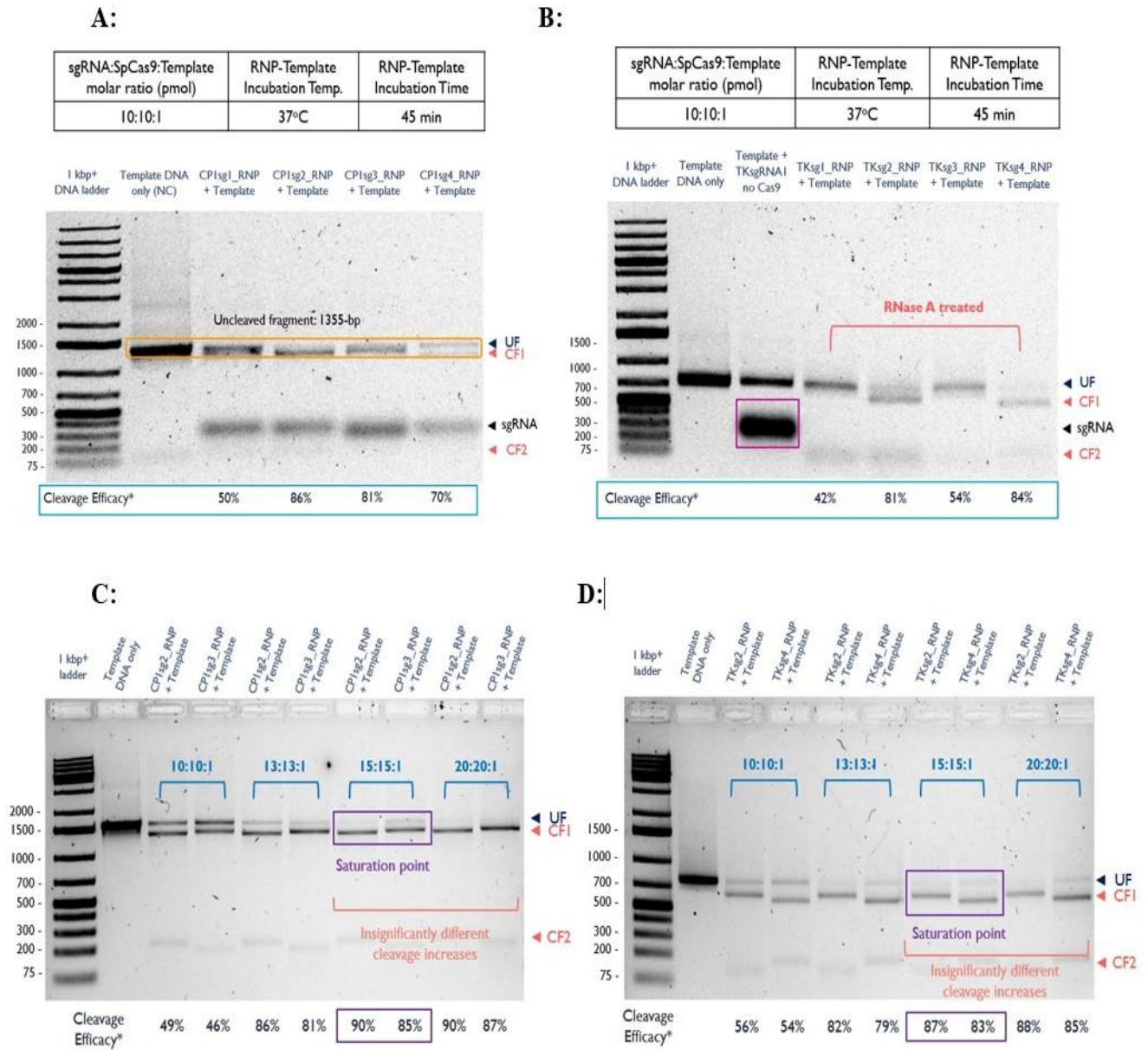
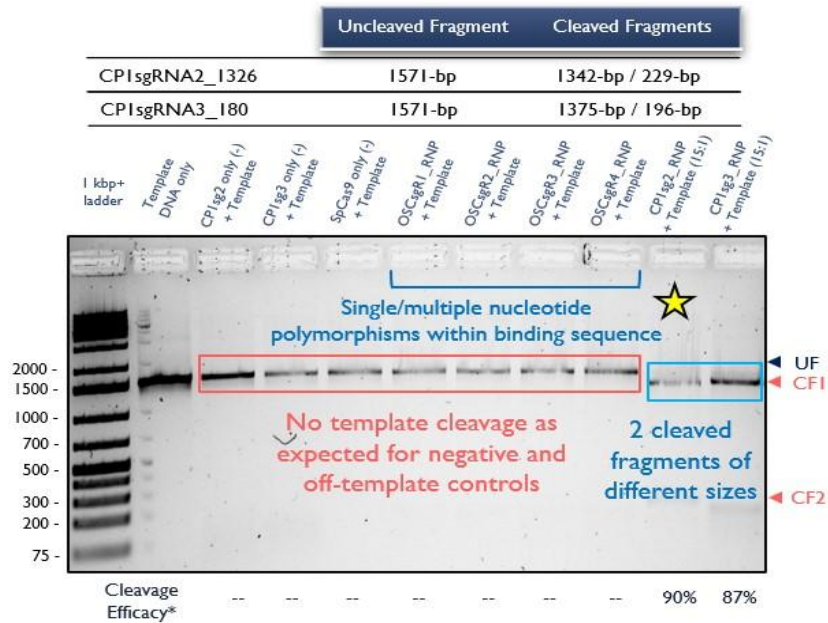


Figure 9: Selection and Optimization of sgRNA Candidates for In Vitro DNA Cleavage Efficacy. A) Initial *in vitro* DNA cleavage screening for CP1 with all four CP1-specific sgRNA candidates at a 10:1 RNP:template molar ratio. B) Initial *in vitro* DNA cleavage screening for TK with all four TK-specific sgRNA candidates at a 10:1 RNP:template molar ratio. C) Optimization of CP1 *in vitro* DNA cleavage efficacy with CP1 sgRNA 2/3 at different RNP:template ratios (10:1, 13:1, 15:1, and 20:1). Insignificant cleavage percentages were achieved past the 15:1 RNP:template ratio mark. D) Optimization of TK *in vitro* DNA cleavage efficacy with TK sgRNA 2/3 at different RNP:template ratios (10:1, 13:1, 15:1, and 20:1). Past the 15:1 RNP:template ratio mark, insignificant cleavage percentages were achieved. All SpCas9:sgRNA:DNA template *in vitro* cleavage reactions were performed at 37°C for 45 minutes, followed by Proteinase K +/- RNase A addition. Cleavage efficiency scores were based on an average of 3–4 individual technical replications and calculated using ImageJ and Microsoft Excel.

6.10 Figure 10: Off-Template Binding of CP1sg2/3 and TKsg2/3

A:



B:

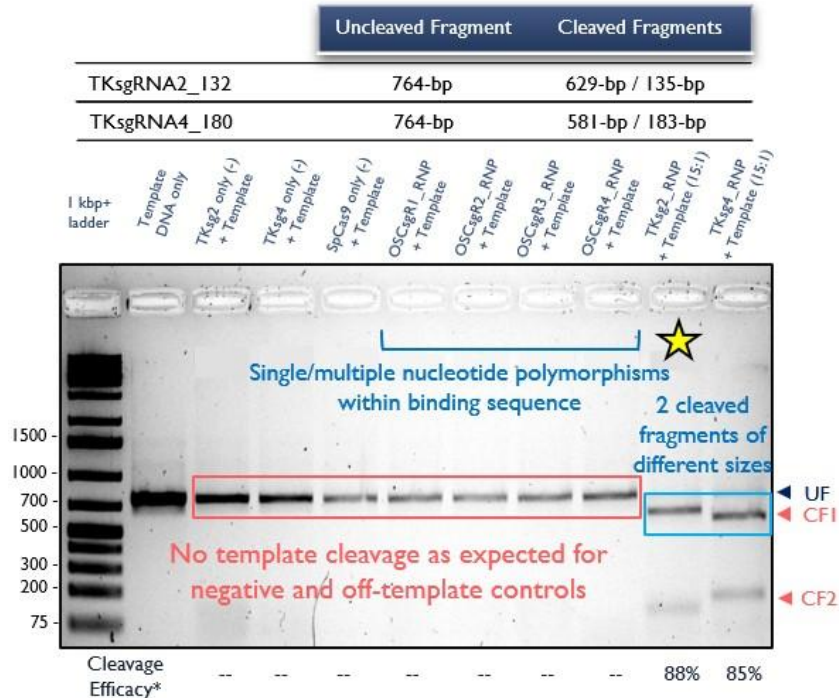
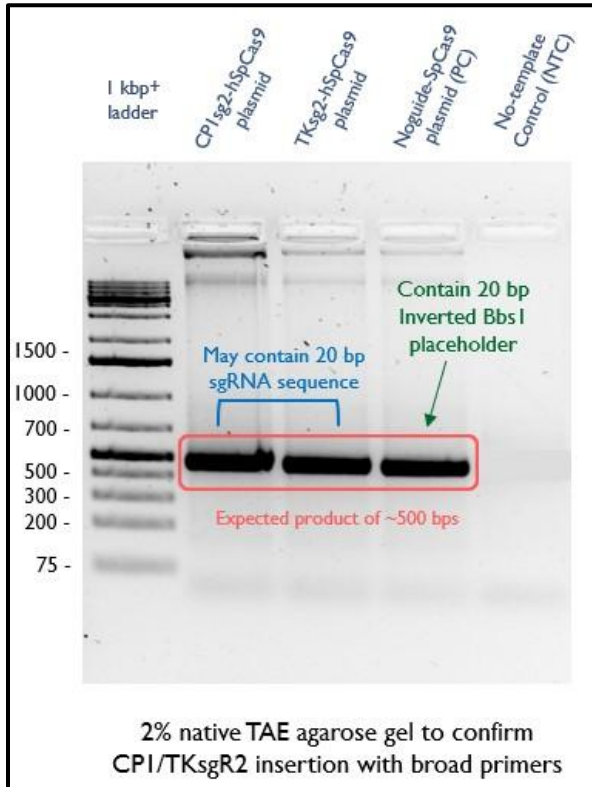


Figure 10: Verification of High Binding Specificity for CP1sg2, CP1sg3, TKsg2, and TKsg3. A) *In vitro* DNA cleavage reactions with off-template screening controls for CP1sgRNA2/3, including four different sgRNA controls containing single or multiple polymorphisms within their gRNA target sequence, yielded negative template cleavage as expected. B) *In vitro* DNA cleavage reactions with off-template screening controls for TKsgRNA2/4, including four different sgRNA controls containing single or multiple nucleotide polymorphisms within the 20-nts gRNA target sequence, also yielded negative template cleavage as expected.

6.11 Figure 11: CP1sg2 and TKsg2 Ligation Confirmation

A:



B:

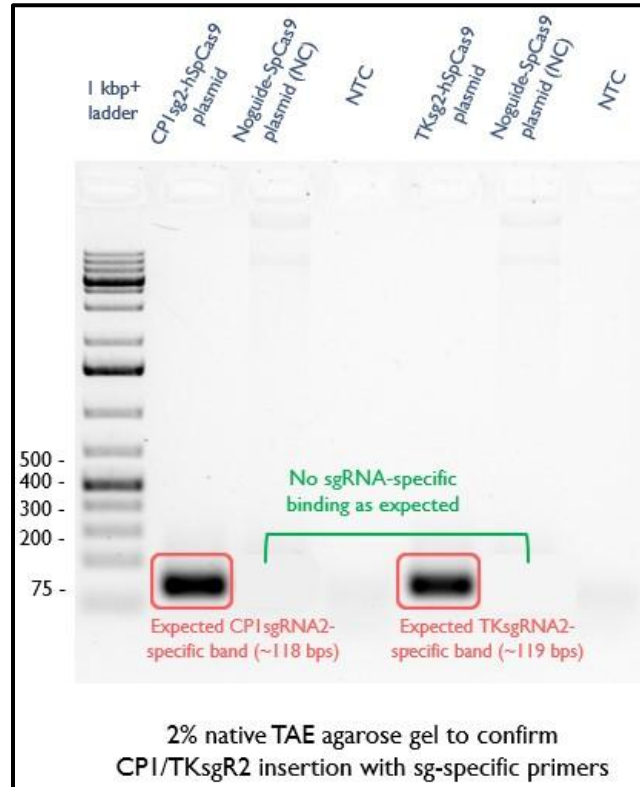


Figure 10: Verification of CP1sgRNA2-1326 and TKsgRNA2-132 Integration into hSpCas9 Plasmid via Nested PCR. A) 2% TAE agarose gel showing the insertion of CP1/TKsgRNA2 sequences into the hSpCas9 plasmid using broad, non-sgRNA specific primers. B) 2% TAE agarose gel confirming the insertion of CP1/TKsgRNA2 sequences into the hSpCas9 plasmid using a forward sgRNA-specific screening primer and a nonspecific reverse tracrRNA primer standard to all hSpCas9 plasmids.

6.12 Figure 12: Specificity Confirmation of Cp18S rDNA Target

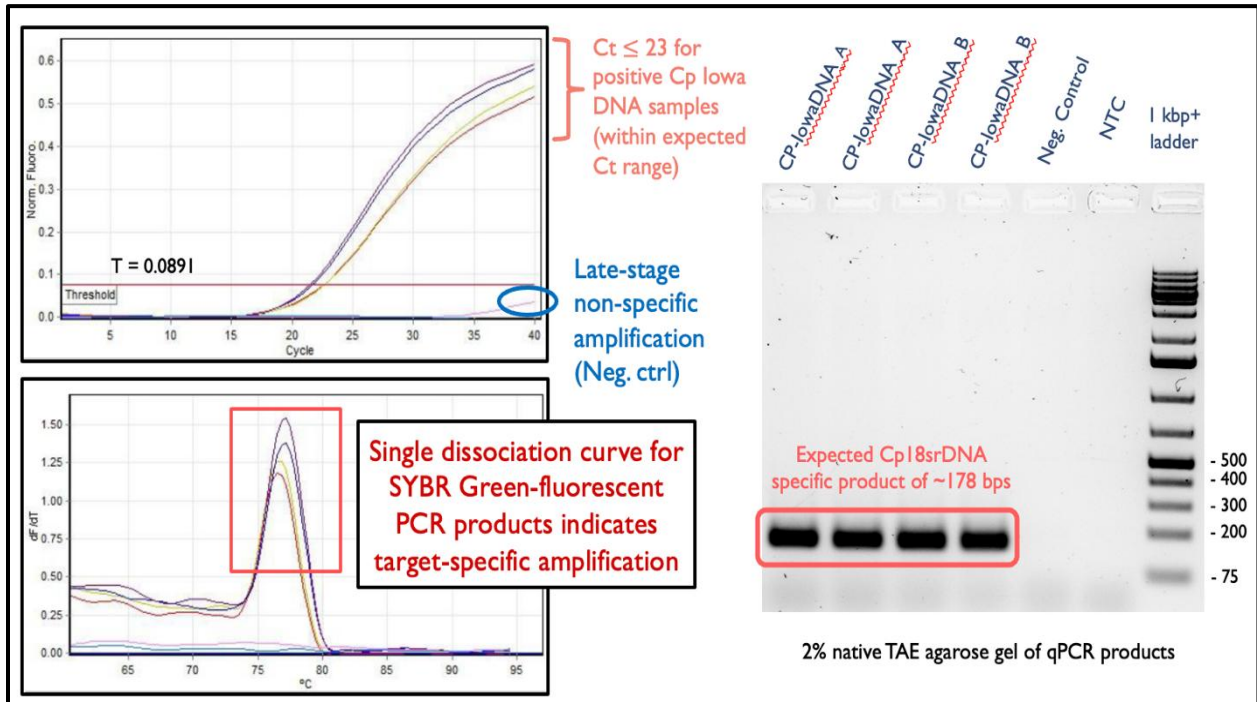


Figure 12. Validation of Cp 18S rDNA Binding to *C. parvum* IOWA DNA. **Top left:** Amplification plots show positive Ct values ≤ 23 for Cp IOWA DNA samples, within the expected range of 15-30. Non-specific amplification in the negative control was detected late in the cycles. **Bottom left:** A single dissociation curve for SYBR Green-fluorescent PCR products was observed for the four positive DNA samples between 75°C and 80°C, indicating target-specific amplification. **Right:** Agarose gel electrophoresis confirmed specific binding between Cp 18S rDNA and Cp IOWA DNA, with PCR product bands at ~178 bp.

6.13 Figure 13: Cp18S rDNA qPCR Optimization

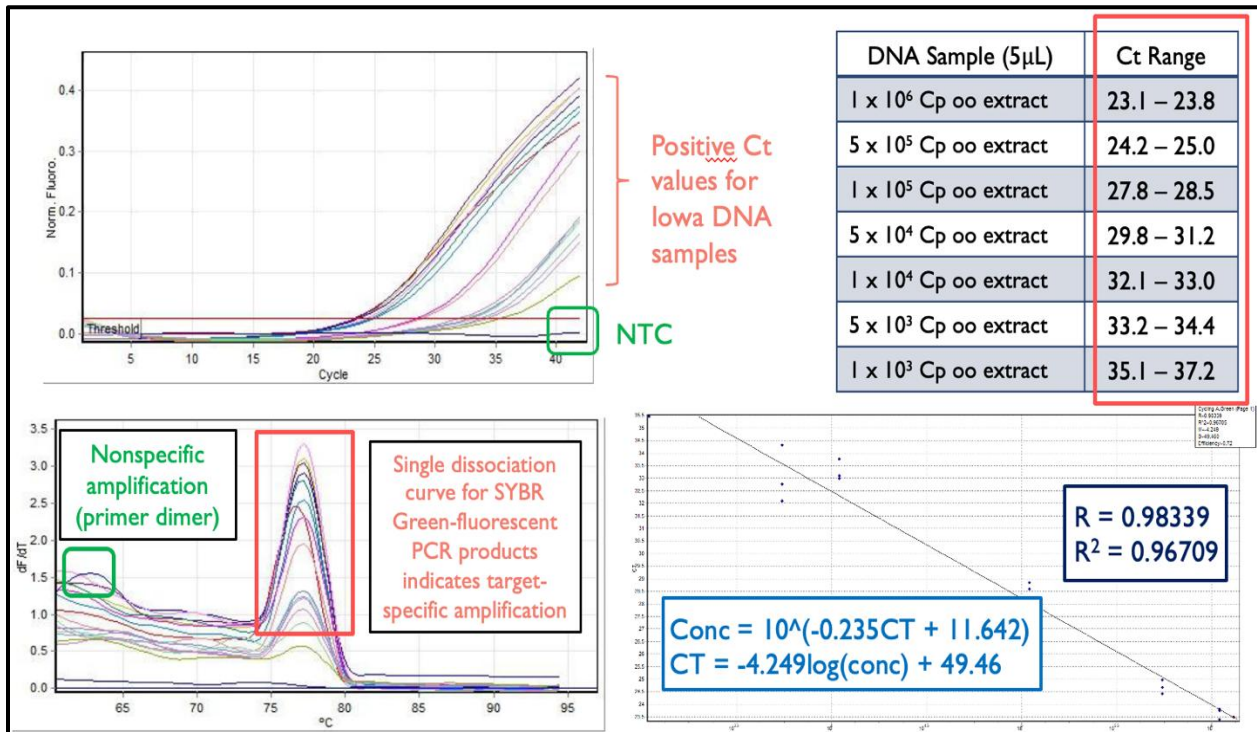
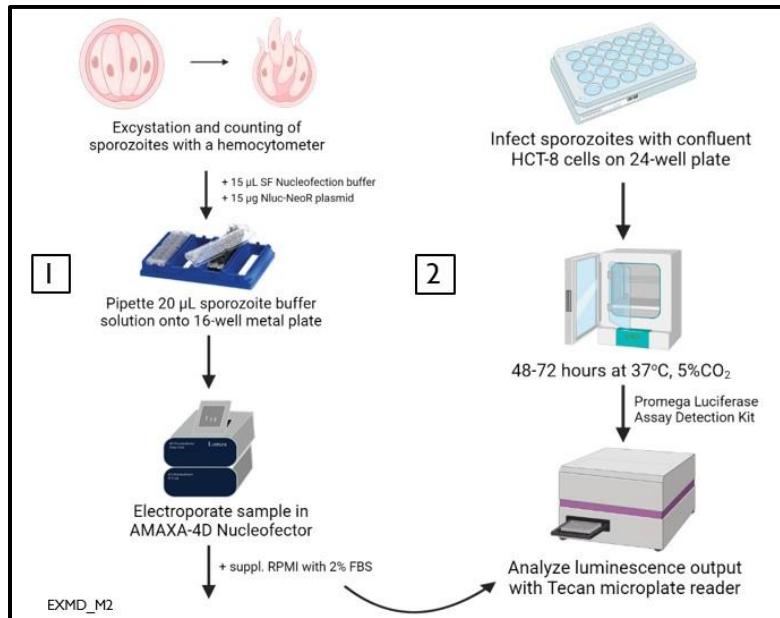


Figure 13. Quantification of *C. parvum* DNA using Cp18s rDNA qPCR standard curve. Top left and right: Amplification plots show positive Ct values for seven concentrations, from 1x10⁶ to 1x10³ *C. parvum* oocyst extracts, with Ct values ranging from 23.1 to 37.2. Non-specific amplification in the non-template control was detected late in the cycles. **Bottom left:** A single amplification curve between 75°C and 80°C indicated target-specific amplification. Minimal non-specific amplification was seen at the lowest DNA concentration, suggesting primer dimers. **Bottom right:** An exponential curve was plotted using Ct values against the log of DNA concentrations, yielding the equation: DNA concentration = 10^(-0.235×Ct + 11.642) with a coefficient of 0.98, indicating a strong negative linear relationship between Ct values and DNA concentration.

6.14 Figure 14: Preliminary *in vivo* Nucleofection Confirmation

A:



B:

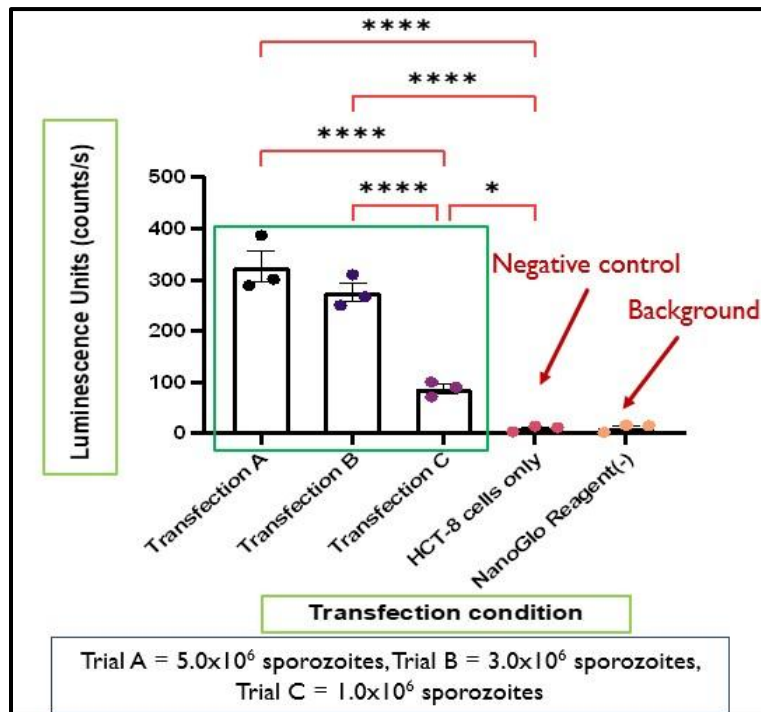


Figure 14: Optimization of Transient Sporozoite Nucleofection with Nluc-NeoR Expression Plasmid. **A)** Diagram of Nluc-NeoR plasmid expression in excysted *C. parvum* sporozoites. Electroporation with Lonza AMAXA 4D-Nucleofector and growth in HCT-8 cells. Luminescence detected using Promega Luciferase Assay. **B)** Relative luminescence units (RLU) quantified transient Nanoluciferase expression in 5.0×10^6 sporozoites (condition A), 3.0×10^6 sporozoites (condition B), and 1.0×10^6 sporozoites (condition C). NanoGlo reagent(-) control and Iowa(-) control wells served as background controls. Data are mean \pm S.E.M. from four independent technical replicates.

6.15 Table 1. Comprehensive evaluation of antigen targets. A) T-cell epitope prediction, B) B-cell epitope prediction, and C) combined scores. Points were awarded to the top two proteins in each criterion, with final scores being the sum of these points. Scores ranged from 0 to 13. The top candidates in each category are highlighted in blue, and the highest overall scores are highlighted in yellow. The most promising candidates are CP1, Cpgp15/45, and CSL adjacent protein 2.

A)

Properties Evaluated	CSL	Cpgp15	Cpgp23	Cpgp15/45	Cpgp23 Var. 1	Cpgp23 Var. 2	CSL adj. 1	CSL adj. 2	CSL+ CSL adj. 1	Cpgp2	CPI	TK	Cpgp900	IMPDH
Antigenic Propensity	10	9	2	7	4	0	13	6	12	3	8	11	1	6
Kolaskar and Tongaonkar Antigenicity	13	9	2	4	5	0	12	7	11	3	8	10	1	6
Parker Hydrophilicity	2	8	13	11	3	9	0	5	1	12	6	4	10	7
MHC-II Binding Prediction (Mouse)	0	2	9	7	13	5	4	11	4	6	10	1	12	8
MHC-II Binding Prediction (Human)	1	2	0	13	5	4	13	13	13	13	13	13	6	3
B cell epitope prediction score total	26	30	26	42	30	18	42	42	41	37	45	39	30	30

B)

Properties Evaluated	CSL	Cpgp15	Cpgp23	Cpgp15/45	Cpgp23 Var. 1	Cpgp23 Var. 2	CSL adj. 1	CSL adj. 2	CSL+ CSL adj. 1	Cpgp2	CPI	TK	Cpgp900	IMPDH
Allergenicity Prediction	13	13	0	13	13	13	13	13	0	13	13	0	0	0
Stability Prediction	9	10	0	2	5	1	7	4	6	3	11	13	12	8
Toxicity Prediction	13	0	13	13	13	0	0	0	0	0	7	8	6	13
Antigenicity Prediction	0	8	10	13	4	11	2	5	1	12	6	7	9	3
MHC-I Binding Prediction (Mouse)	0	1	11	6	7	3	10	13	10	8	12	2	4	5
MHC-I Binding Prediction (Human)	1	3	0	6	13	12	5	11	5	9	7	2	10	8
T cell epitope prediction total score	36	35	34	53	55	40	37	46	22	45	56	32	41	37

C)

Properties Evaluated	CSL	Cpgp15	Cpgp23	Cpgp15/45	Cpgp23 Var. 1	Cpgp23 Var. 2	CSL adj. 1	CSL adj. 2	CSL+ CSL adj. 1	Cpgp2	CPI	TK	Cpgp900	IMPDH
B cell epitope prediction	26	30	26	42	30	18	42	42	41	37	45	39	30	30
T cell epitope prediction	36	35	34	53	55	40	37	46	22	45	56	32	41	37
Final scores	62	65	60	95	85	58	79	88	63	82	101	71	71	67

6.16 Table 2: Features and Sequences of All Key Components Within CP1—and TK-specific Repair Cassettes. This table outlines the features, sequence lengths, and exact sequences of the components used to create the two specific repair cassettes. Each component includes specific regions necessary for homologous recombination and robust reporter gene expression, ensuring efficient and precise genetic modifications.

Key Component	Identifier	Features	Sequence Length (bps)	Exact Sequence
<i>C. parvum</i> enolase promoter	CpEnoPro	Promoter region, highly transcriptionally active, drives expression of downstream genes	363	5'- TGGGGAAACTAAATATACTGAAATTCGGTAGATTCTATATCTCACGGGAC AGCTTTTACACACACTTAGTTCATATTGCGTCATAACTTTTGTTTTTTTT TGTTGCACCTTTTTTCTCTATATTCAAGTAAGTGGTTAGATTCTCTAAG GGCGGGAATGAATTAGTGGCAATTCAAAGGATTTAAACGATCAGGCG CCTGCACACCAAACTCTAATTCGTACACAGCATGCCGAGGTTATAGATA TAGATACTGCGAAATTTTTTCAATGTTTCAGTTAAGAAATAATAAATAT TTTTATTAGTTATTTTCCAAATTTATTGAGATTTTGTATTGAAGTTTAG CCGTGCAC-3'
Nanoluciferase gene	Nluc	Coding sequence, bioluminescent reporter, allows for easy detection of gene expression	519	5'- ATGGTCTTCACTCGAAGATTTGTTGGGGACTGGCGACAGACAGCCG GCTACAACTGGACCAAGTCTTGAACGAGGAGGTGTCCAGTTTGT TCAGAATCTCGGGGTGTCGTAACTCGATCCAAGGATTGCTCAGC GGTAAAATGGGCTGAAGATCGACATCCATGTATCATCCCGTATGAAG GTCTGAGCGGCGACCAATGGGCGACATCGAAAAATTTTAAAGTGGT GTACCCCTGTGGATGATCATCTTTAAGGTGATCCTGCACTATGGCACAC TGTAATCGACGGGTTACGCCGAACATGATCGACTATTTCCGACGGCC GTATGAAGGCATCGCGTGTTCGACGGCAAAAAGATCACTGTAACAGG GACCCCTGTGAAACGGCAAAAATATCGACGAGCGCCTGATCAACCC GACGGCTCCCTGCTGTTCCGAGTAACCATCAACGGAGTGACCGGCTGG CGGCTGTGCGAACGCATTCTGGCGCTAGC-3'
Neomycin gene	NeoR	Coding sequence, confers resistance to neomycin, allows for selection of successfully transfected cells	803	5'- ATGATTGAACAAGATGGTTTACACGCTGGTCTCCCGCCGCTTGGGTGG AAAGACTTTTGGTTATGACTGGGCTCAACAAACCATCGTTGCTCTGAT GCCGCGCTCTCCGCTTTCTGCTCAAGGTCGTCTGTTCTTTTCTGTCAA GACCGACCTTTCTGGTGOCCCTAATGAACCTCAAGATGAAGCTGCCCGT CTTTCTGGCTGCCACCAACCGGTGTTCTTCCGCTGCTGCTCCTGACGT TGTCACTGAAGCCGGTAGAGACTGGCTCTTTTAGGTGAAGTCCCGGT CAAGATCTTCTTTCTTCTCACCTGCTCCTGCCGAAAAAGTTTCTATCATG GCTGATGCTATGCGTCGTCTTCATACCTGATCCCGCTACCTGCCCTT CGACCAACCAAGCCAAACATCGTATCGAACGTCCTGCTACTGATGGAA GCCCGTCTTGTGATCAAGATGATCTTGACGAAGAACATCAAGGTCTTG CCCTGCCGAACTTTTCCGACACTTAAAGCCCGTATGCCGACGGTGA AGATCTTGTGTCACCCATGGTATGCCCTGCTTACCCAATATCATGGTTG AAAAATGGTGGTTTTCTGGTTTCTGACTGTGGTGTCTTGGTGTGCC GACCGTTATCAAGATATTGCCCTAGCTACCCGTGATATTGCTGAAGAAT TGGTGGTGAATGGGCTGACCGTTTCTTGTCTTACGGTATCCCGCT CCCGATTCTCAACGATCGCCCTCTATGCTCTTCTGACGAATCTTCTGA TTAATTA-3'
CP1 5'UTR flanking homology sequence	CpCP15'UTR	Homology region, facilitates homologous recombination at the 5' end of CP1 gene	74	5'- GATGACATGACAAGATATTCAAAAAATTTGATGATTATATGTTGAAGTT AATTGAACATAAAAGTAATTAAGT-3'
CP1 3'UTR flanking homology sequence	CpCP13'UTR	Homology region, facilitates homologous recombination at the 3' end of CP1 gene	50	5'- GCATTTCAAGTGTGACTAAGTAATCTAATATATTTGAGCATTCTCAGA- 3'
TK 5'UTR flanking homology sequence	CpTK5'UTR	Homology region, facilitates homologous recombination at the 5' end of TK gene	76	5'- CCATCTAACACAAAGAATTCAACAATTTACCTAATAAATACTTTAAAGCAA TAATATCACTCATACCTACTGCAAA-3'
TK 3'UTR flanking homology sequence	CpTK3'UTR	Homology region, facilitates homologous recombination at the 3' end of TK gene	50	5'- GCAAAAATTTGGCGCAGCTATGGCGCCTCTTGAAGTGCCTAAAAAGGAG T-3'
<i>C. parvum</i> enolase 3'UTR sequence	CpEno3'UTR	3'UTR region, enhances mRNA stability and translation efficiency	51	5'- GTTCCGTGGCGTGTAGGATAGTATCGAATAAGTTTTTCTTTTATCTAATT- 3'

6.17 Table 3: Features and Sequences of PCR Fragments and Primers for CP1RCFL and TKRCFL Constructs. This table lists the critical sequence features, sequence lengths, and exact sequences of the primers used for the PCR amplification of the CP1RCFL and TKRCFL repair cassette constructs.

PCR Fragment Identifier	Key Sequence Features	Sequence Length (nt)	Forward Primer (nt)	Forward Primer	Reverse Primer (nt)	Reverse Primer Sequence
CP1RCFL Fragment 1 (CP1RC-P1)	74 bps CP1 flanking 5'UTR homology region + first 20 bps of Cp enolase promoter	94	34	5'- GATGACATGACA AGATATTCAAAAA AATTTGATG-3'	40	5'- CAGTATATTTAGTTT CCCCAACTTAATT ACTTTTTAGTTC-3'
CP1RCFL Fragment 2 (CP1RC-P2)	Last 20 bps of CP1 5'UTR flanking homology region, 357 bps Cp enolase promoter, 1320 bps Nluc-NeoR coding sequence, first 20 bps of Cp enolase 3'UTR	1725	40	5'- GAACTAAAAAGTA ATTAAGTTGGGGA AACTAAATATACT G-3'	40	5'- CTATCCTACACGC CACGAACTTAATTA ATCAGAAGAATTC- 3'
CP1RCFL Fragment 3 (CP1RC-P3)	Last 20 bps of NeoR coding sequence, 51 bps Cp enolase 3'UTR, 50 bps CP1 gene-specific 3'UTR flanking homology region	124	40	5'- GAATTCTTCTGATT AATTAAGTTCGTG GCGGTAGGATA G-3'	33	5'- ACGTCTGAGAATG CTGAAATATATTAG AATTAC-3'
TKRCFL Fragment 1 (TKRC-P1)	74 bps TK flanking 5'UTR homology region + first 20 bps of Cp enolase promoter	96	32	5'- CCATCTAACACA AAGAATTCACAA TTTACCT-3'	37	5'- CAGTATATTTAGTTT CCCCATTTGCAGT AGGTATGAG-3'
TKRCFL Fragment 2 (TKRC-P2)	Last 20 bps of TK 5'UTR flanking homology region, 357 bps Cp enolase promoter, 1320 bps Nluc-NeoR coding sequence, first 20 bps of Cp enolase 3'UTR	1722	37	5'- CTCATACTACTG CAAATGGGGAAA CTAAATATACTG- 3'	40	5'- CTATCCTACACGC CACGAACTTAATTA ATCAGAAGAATTC- 3'
TKRCFL Fragment 3 (TKRC-P3)	Last 20 bps of NeoR coding sequence, 51 bps Cp enolase 3'UTR, 50 bps TK gene-specific 3'UTR flanking homology region	121	40	5'- GAATTCTTCTGATT AATTAAGTTCGTG GCGGTAGGATA G-3'	27	5'- ACTCCTTTTAGGC ACTTTCAAGA

6.18 Table 4: Selected Guide RNA Sequences and Their Proximity to Flanking Homology Regions. The exact sequences for the eight selected guide RNA candidates for CP1 and TK genes, their identifiers, and their proximity to the UTRS are listed in detail.

Gene Target	Guide RNA Identifier	Sequence (5' to 3')	Proximity to target UTR
CP1	CP1guide#1_205	GAACATCAGGAATATATTTTC	5' UTR, 27 bps
	CP1guide#2_1326	GAAGGGAACATGTGGTATAT	3' UTR, 41 bps
	CP1guide#3_180	AATGGACATAGGAAACAACG	5' UTR, 3 bps
	CP1guide#4_1262	GAAATAGCTGGGGTGAAGCG	3' UTR, 105 bps
TK	TKguide#1_684	GTGAAGAATACAATTTCTAAGG	3' UTR, 3 bps
	TKguide#2_132	GTA CTATT CAGCAATGAATGC	5' UTR, 25 bps
	TKguide#3_609	TCTGGCGAACAAATCTTAT	3' UTR, 78 bps
	TKguide#4_180	TCATTCAACTACCAAGAAAG	5' UTR, 90 bps

6.19 Table 5: Primers Used for Amplification of Each CP1- or TK- Guide RNA Candidate.
The sequences and lengths of each primer used to amplify the eight guide RNA constructs are included.

Primer Name	Sequence (5' to 3')	Length (nts)
CP1guide#1Fwd	5'- TAATACGACTCACTATAGGAACATCAGGAATATATTTTCGTTTTAG AGCTAGAAATAG-3'	58
CP1guide#2Fwd	5'- TAATACGACTCACTATAGGAAGGGAACATGTGGTATATGTTTTAG AGCTAGAAATAG-3'	57
CP1guide#3Fwd	5'- TAATACGACTCACTATAGAATGGACATAGGAAACAACGGTTTTA GAGCTAGAAATAG-3'	57
CP1guide#4Fwd	5'- TAATACGACTCACTATAGGAAATAGCTGGGGTGAAGCGGTTTTA GAGCTAGAAATAG-3'	57
TKguide#1Fwd	5'- TAATACGACTCACTATAGGTGAAGAATACAATTTCTAAGGGTTTT AGAGCTAGAAATAG-3'	59
TKguide#2Fwd	5'- TAATACGACTCACTATAGGTACTATTCAGCAATGAATGCGTTTTA GAGCTAGAAATAG-3'	58
TKguide#3Fwd	5'- TAATACGACTCACTATAGGTCTGGCGAACAAATTCTTATGTTTTA GAGCTAGAAATAG-3'	58
TKguide#4Fwd	5'- TAATACGACTCACTATAGGTCATTCAACTACCAAGAAAGGTTTTA GAGCTAGAAATAG-3'	58
ConsTracRNARev	5'-AAAAGCACCGACTCGGTGCCACTTTTTTC-3'	28

6.20 Table 6: Precise Cleavage Bands and Molecular Sizes for the *In Vitro* DNA Cleavage Assay. The exact two cleavage bands and molecular sizes observed following the SpCas9-sgRNA *in vitro* DNA cleavage assay with the four chosen CP1- (CP1sg1_205, CP1sg2_1326, CP1sg3_180, and CP1sg4_1262) and TK guide RNA candidates (TKsg1_684, TKsg2_132, TKsg3_609, and TKsg4_180) are listed in detail.

sgRNA-RNP candidate	Uncleaved Fragment	Cleaved Fragments
CP1sgRNA1_205	1355-bp	1237-bp / 118-bp
CP1sgRNA2_1326	1355-bp	1239-bp / 116-bp
CP1sgRNA3_180	1355-bp	1262-bp / 69-bp
CP1sgRNA4_1262	1355-bp	1178-bp / 180-bp
TKsgRNA1_684	764-bp	675-bp / 89-bp
TKsgRNA2_132	764-bp	629-bp / 135-bp
TKsgRNA3_609	764-bp	600-bp / 164-bp
TKsgRNA4_180	764-bp	581-bp / 183-bp

7. Discussion

7.1 Rationale and Interpretation of Preliminary Findings

The primary objectives of this study were to validate genome editing within the compact, streamlined genome of *C. parvum* (approximately 9.1 Mbp), develop a novel investigative tool to study parasite biology, and create an attenuated strain as a live attenuated vaccine candidate for the most vulnerable populations at high risk of Crypto infection. This investigation aimed to profile the utility and necessity of cysteine proteases as potential prophylactic immunogenic targets using targeted CRISPR-Cas9 knockout with decent success. The preliminary results demonstrated significant progress in bioinformatics analysis for immunogenicity and antigenicity confirmation, successful design and optimization of repair cassette constructs and sgRNA synthesis, and *in vitro* transfection experimentation demonstrating significant reporter gene detection. However, challenges such as the lack of parasite survival *in vivo* underscore the need for further optimization.

7.1.1 Mechanistic Insights on CP1 Function

CPs are crucial enzymes in protozoan parasites, playing critical roles in various biological processes, including cell/tissue penetration, hydrolysis of host or parasite proteins, autophagy, and evasion or modulation of the host immune response. These enzymes are involved in the pathogenesis of many protozoan parasites, such as *Entamoeba histolytica*²²²⁻²²⁴, *Leishmania* spp.^{147,225,226}, *Trypanosoma brucei*^{145,227-229}, *Trypanosoma cruzi*^{153,159}, *Plasmodium* sp.^{139,154,156,230}, and *Toxoplasma gondii*^{38,97,146,231-234}. The *C. parvum* genome is highly streamlined, with greater than ~98% of its genome limited to single-copy gene families, short intergenic regions, limited introns, and the loss of many metabolic pathways¹⁴⁸⁻¹⁵⁰. Yet, it possesses an expanded multigene family of 20 clan CA papain-like cysteine proteases, the majority of which have unknown biological and biochemical functions, with CP1 being the only one previously characterized biochemically and shown to be actively transcribed and expressed in infectious sporozoites and merozoites during host mammalian infection^{36,178}. CP1 shares typical structural and biochemical properties with other cathepsin-L cysteine proteases but uniquely differs in that it does not require a prodomain for mature folding and preferentially hydrolyzes collagen and fibronectin over other common human proteins such as α -macroglobulin, albumin, hemoglobin, IgA, IgG, and IgM¹⁷⁸.

Given the critical role of CP1 in the parasite's lifecycle, its inhibition has been a focal point for therapeutic intervention. This suggests investigating this biocide class as a potential novel and urgently needed chemotherapeutic for *Crypto*^{98,145,157,235}. Despite over a century of intensive efforts, including testing hundreds of chemotherapeutic agents²³, there is still no highly effective therapy adequate for the clearance of *C. parvum* from an infected host. The development of a protective vaccine that could either prevent disease or reduce the severity of disease would be a considerable advance, especially for the protection of children or patients who have HIV or AIDS who are the most susceptible to *Crypto*^{2,3,22}.

7.1.2 Mechanistic Insights on TK Function

TK is an enzyme involved in the salvage pathway of nucleotide synthesis, playing a crucial role in DNA replication and repair¹⁹⁰. In *C. parvum*, TK is essential for parasite survival and intracellular replication¹⁶. TK catalyzes the phosphorylation of thymidine-to-thymidine monophosphate (dTMP), further phosphorylated to form thymidine triphosphate (dTTP), a building block for DNA synthesis²³⁶. This enzyme provides an alternative route for thymidine monophosphate synthesis, enabling *C. parvum* to tolerate high doses of antifolate drugs²⁸. The importance of TK in *C. parvum* has been highlighted in studies showing that its deletion impairs the parasite's ability to replicate and survive²⁸. Targeted deletion of the TK gene using CRISPR-Cas9 strategies was used to investigate its function and provides a viable tool for studying parasite biology and identifying potential therapeutics⁷⁷. Given its feasibility and importance, this gene target was included in the comprehensive epitope screening analysis and employed as a refined nucleofection optimization control group.

7.1.3 *In Silico* Findings

The bioinformatics analysis conducted in this investigation was designed to cross-reference the high immunogenicity of CP1 against other highly expressed surface antigens that have been used in previous vaccine studies with limited success for *Crypto* prevention^{100,106}. This approach aimed to identify the most promising immunogenic surface targets for vaccine development, utilizing advanced bioinformatics tools (i.e., IEDB, VaxiJen, ToxiPred, ProtParam, etc.) to predict and validate potential epitopes²¹⁹. Unlike existing studies, which focus on a limited set of antigens,

our analysis encompassed a broad range of criteria, including binding affinity to MHC Class I and II molecules, antigenicity, allergenicity, toxicity, and stability. This thorough approach ensures that the selected epitopes are highly immunogenic, safe, and stable for vaccine use, providing confidence in the results of this research.

Scoring criteria for both T- and B-cell epitope binding were designed to ensure effective MHC molecule binding and safety for selected epitopes^{237,238} (6.4-Fig. 4). Antigenicity scores identified epitopes likely to elicit strong immune responses. In contrast, allergenicity and toxicity scores ensured safety. Stability scores determined the likelihood of epitopes maintaining their structure and function in a biological context. Each criterion was scored from 0 to 13, with higher scores indicating superior performance. Non-toxic and low-toxic candidates received scores, while highly toxic targets were scored 0. B cell epitopes were similarly evaluated for binding affinity, antigenicity, and hydrophilicity. CP1 emerged as the top candidate due to its high scores across all criteria, indicating a strong potential for eliciting robust immune responses (6.15-Table 1). This was particularly significant compared to other commonly included antigens, such as Cpgp15/45 and CSL adjacent protein 2, which scored 95 and 88, respectively. Although these candidates showed high immunogenic potential, CP1's superior scores in T and B cell epitope predictions underscore its robustness as a vaccine target (6.15-Table 1).

This analysis highlighted the immunogenic potential of CP1 and provided a thorough framework for future vaccine development efforts³⁷. By systematically evaluating multiple criteria, the selected epitopes were well-suited for eliciting solid and protective immune responses¹¹⁴, ensuring that the chosen targets are effective and safe for potential vaccine use.

7.1.4 Repair Cassette Construction Refinements

The *in vitro* experiments focused on designing and testing sgRNA-SpCas9 RNPs for the targeted knockout of the CP1 gene. The high specificity and efficiency of these RNPs in cleaving the CP1 gene were confirmed through a series of assays (6.1-Fig. 1). The design and optimization of the repair cassettes were crucial steps in ensuring efficient homologous recombination. The constructs for CP1 and TK were redesigned to include the missing 3' UTR from the original donor Nluc-NeoR plasmid template that consists of the two reporter genes nanoluciferase and neomycin to facilitate the identification and selection of successfully transfected sporozoites¹⁸⁹.

Nanoluciferase is a small, bright, and stable luciferase enzyme that provides a sensitive and quantitative measure of gene expression³⁰. In contrast, the neomycin resistance gene offers complete resistance to the antibiotics neomycin and paromomycin³⁰. The redesigned framework involved a four-step fusion PCR assembly in joining small *de novo* DNA PCR fragments (6.5-Fig. 5). The final repair templates were confirmed through sequencing and restriction digestion analysis, ensuring the correct integration of the desired sequences (6.6-Fig. 6 and 6.7-Fig. 7).

In previous studies, Nluc and NeoR have been used as completely fused or cleaved proteins driven by a viral 2A peptide^{29,30,93,150}. The fused protein approach, where Nluc and NeoR are expressed as a single polypeptide, is practical in various applications. For instance, the fusion of Nluc with other proteins has been successfully used to monitor gene expression and protein interactions²³⁹. Using the P2A cleavage peptide allows the co-expression of multiple proteins from a single transcript by mediating a ribosome-skipping event that produces separate proteins^{130,240}. This method has been widely adopted in gene editing and metabolic engineering studies due to its high cleavage efficiency and ability to deliver multiple proteins from a single open reading frame²⁴¹. We used the fused Nluc-NeoR protein approach in our research for several reasons. From a technical standpoint, the fused protein design provides a straightforward and reliable means of monitoring gene editing events and selecting successfully edited cells¹¹⁸. The fusion of Nluc and NeoR ensures that both reporter functions are linked, simplifying the selection and validation process³⁰. Additionally, the donor plasmid template already provided the fused protein design, making it a more efficient and practical choice. Utilizing the existing Nluc-NeoR template allowed us to save time and resources, enabling us to focus on optimizing other aspects of the gene editing process for efficient monitoring and providing a solid foundation for future applications.

7.1.5 *In vitro* sgRNA-SpCas9 Findings

Regarding the *in vitro* DNA cleavage assays, four sgRNA candidates for CP1 (CP1sg1-205, CP1sg2-1326, CP1sg3-180, and CP1sg4-1262) and four for TK (TKsg1-684, TKsg2-132, TKsg3-609, and TKsg4-180) were synthesized and tested. CP1sg2-1326 and CP1sg3-180 exhibited the highest cleavage efficiencies, achieving approximately 90% and 85% cleavage efficiency, respectively (6.9-Fig. 9A/C). Similarly, TKsg2-132 and TKsg4-180 showed the highest cleavage efficiencies for the TK gene, achieving approximately 87% and 83% cleavage efficiency,

respectively (6.9-Fig. 9B/D). These results were obtained by incubating the transcribed sgRNAs with recombinant SpCas9 protein and a linearized, purified DNA template containing the exact target sequences, including the required PAM sequences, at different molar ratios. Cleavage products were analyzed using ImageJ and Microsoft Excel software (see Chapter 4 Methodology, section 4.4.5 *in vitro* DNA Cleavage Assay Assembly and Analysis).

In addition to the RNP-based approach, plasmid-based sgRNA candidates were also tested (6.2-Fig. 2). The sgRNA sequences for CP1sg2-1326, CP1sg3-180, TKsg2-132, and TKsg4-180 were cloned into a human codon-optimized SpCas9 plasmid and transfected into *C. parvum* sporozoites using the Lonza AMAXA 4D-Nucleofector™ (6.11-Fig. 11). The plasmid-based approach showed lower cleavage efficiency compared to the RNP-based approach, with CP1sg2-1326 achieving approximately 70% cleavage efficiency and CP1sg3-180 achieving approximately 55% cleavage efficiency (data not shown). TKsg2-132 and TKsg4-180 achieved approximately 65% and 60% cleavage efficiency for the TK gene, respectively (data not shown). These results highlight the potential advantages of using RNPs for gene editing in *C. parvum*.

7.1.6 Nucleofection Optimization and Quantification

The optimization of the nucleofection process was critical in achieving high transfection efficiency. Various parameters, including the concentration of sgRNA-SpCas9 RNPs, the number of sporozoites, and the nucleofection conditions, were refined (6.14-Fig. 14A). The optimized conditions resulted in a transfection efficiency of approximately 50% compared to the negative controls, as determined by the percentage of sporozoites expressing the nanoluciferase reporter gene (6.14-Fig. 14). Quantitative PCR was employed to quantify the efficiency of gene editing and transfection to ensure the reliability of the experimental results (6.12-Fig. 12). A standard curve was generated using serial dilutions of *C. parvum* genomic DNA, which displayed good linearity with an R² value greater than 0.96 (6.13-Fig. 13). The qPCR assays were performed more than 80% efficiently, allowing for accurate quantification of gene editing events (data not shown).

7.1.7 Off-Target Verification

Minimizing off-target effects is a critical consideration in CRISPR-Cas9 research. Our study employed thorough screening and validation processes to ensure the sgRNAs' specificity. During the *in vitro* cleavage assay analysis, off-target validation checks were performed for CP1sg2-1326,

CP1sg3-180, TKsg2-132, and TKsg4-180. Multiple polymorphism mutants in each of the crRNA recognition sites at the 5' and 3' ends were included as necessary controls to ensure the high specificity of our chosen sgRNA-SpCas9 pairing for *in vivo* work (6.10-Fig. 10). Mutations included pyrimidine to purine nucleoside modifications and vice versa. These controls are crucial for confirming that the sgRNAs specifically target the intended gene sequences without causing unintended off-target effects. The results showed no off-target cleavage, indicating that the selected sgRNAs have high specificity and are suitable for further *in vivo* applications (6.10-Fig. 10).

This finding aligns with ongoing literature, demonstrating that CRISPR-Cas9 can tolerate up to three mismatches between the sgRNA and genomic DNA without significant off-target effects^{242,243}. Moreover, recent advancements in CRISPR technology, such as high-fidelity Cas9 variants and truncated sgRNAs, have reduced the likelihood of off-target mutations^{135,243,244}. This vigilance is essential for ensuring that successfully genetically modified parasites do not acquire unintended mutations that could affect their behaviour or safety, thereby providing the long-term safety and efficacy of CRISPR-Cas9 gene editing in both primary and clinical applications²⁰⁸.

7.2 Comparison with Previous Publications

Our findings align with previous studies that have used CRISPR-Cas9 technology for genetic manipulation in *C. parvum* (6.2-Fig. 2). The pioneering work by the Striepen lab demonstrated the feasibility of using CRISPR-Cas9-driven HDR coupled with *in vivo* propagation within immunodeficient mice to create genetically modified *C. parvum* strains^{28,30,44}. Specifically, their work involved using the *C. parvum* U6 RNA promoter to drive guide RNA expression and the *Streptococcus pyogenes* cas9 gene flanked by *C. parvum* regulatory sequences targeting nonessential genes such as TK for functional genomic analyses^{16,30,189}. These methods have been advancing our understanding of *C. parvum* biology and pathogenesis, developing strategies for excystation, transfection, infection, and collection of transgenic strains. They emphasized using immunodeficient mouse models, such as IFN γ -deficient and NOD-SCID-gamma (NSG) mice, to propagate transgenic strains and validate CRISPR/Cas9 efficacy^{45,127}. However, their approach relies on the traditional plasmid-based delivery of CRISPR components, which requires transcription, translation, and post-translational modifications by host machinery before nuclear import and genome cleavage^{132,208}.

In China, a study also employed CRISPR/Cas12a (Cpf1) for on-site diagnostics of *C. parvum* IId-subtype-family from human and cattle fecal samples²⁴⁵. This approach combined recombinase polymerase amplification with the Cas12a/crRNA trans-cleavage system¹⁴⁰, directly identifying *C. parvum* subtypes without requiring highly trained operators or expensive equipment²⁴⁵.

7.2.1 Project Novel Contributions

Incorporating active RNPs for the targeted knockout of CP1 represents a novel contribution to the field. This approach offers several advantages over the plasmid-based approach. Active RNPs lower the possibility of unwanted exogenous DNA integration, reduce *in vivo* cytotoxicity, and can decrease the potential of off-target cleavage effects due to the substantially shortened half-life and nuclease activity of recombinant SpCas9^{35,131,246,247}. This alternative gene editing approach is a highly efficient novel molecular advancement that has been successful in transfecting difficult-to-transfect primary human stem cell lines^{35,135,248,249} and similar apicomplexan protozoan parasites such as *Trypanosoma cruzi*, *Plasmodium falciparum*, and *Eimeria tenella* with *Staphylococcus aureus* (Sa)Cas9²²¹, *Francisella novicida* U112 (Fn)Cas12a, *Lachnospiraceae bacterium* (Lb)Cas12a, and *Acidaminococcus* sp. (As)Cas12a nucleases^{128,213,215,216,244,250}.

These type II CRISPR-Cas nucleases are thoroughly programmable and specific, with staggered-end DNA cleavage efficacies highly comparable to the well-known SpCas9 nuclease that use modified crRNA target structures and recognize different thymidine-rich protospacer adjacent motif sequences^{215,244,251}. By integrating this advanced RNP approach, our study enhances the specificity and efficiency of gene editing in *C. parvum* and minimizes potential cytotoxicity associated with plasmid-based methods. Additionally, using bioinformatics analysis to prioritize immunogenic and safe vaccine targets in suitable mammalian hosts provides a new dimension to developing effective interventions against Crypto. By integrating computational and experimental approaches, we have created a more holistic strategy for tackling this challenging parasite.

7.3 Limitations and Drawbacks

7.3.1 Technical Challenges and *in Vitro* Validation Limits

Previous progress in creating a viable attenuated *C. parvum* strain had been significantly hindered by two principal technical challenges. Firstly, the scarce availability of the Lonza

AMAXA 4D-Nucleofector™ required for successful sporozoite transfection^{16,30}, coupled with the technical training and handling requirements for specific personnel, posed a significant challenge. This equipment is essential for the precise delivery of CRISPR-Cas9 components into the parasite²¹⁶. Secondly, the negative and insignificant luminescence results from the Promega NanoGlo luciferase assay in all three independent preliminary *in vivo* nucleofection experiments further complicated the process (data not shown).

Excysted, purified sporozoites were nucleofected with CP1/TK-specific sgRNA-hSpCas9 plasmid and CP1/TK-specific linearized repair cassette templates prepared by preceding project associates (6.7-Fig. 7). These were compared against both Iowa(-) and NanoGlo(-) background controls. The possible reasons for these findings include failed transfection due to ineffective repair cassette machinery delivery, with a reported successful transfection rate of less than 10%⁷⁷, an absence of sporozoite survival after electroporation^{45,46,189}, or technical errors in luciferase assay preparation due to numerous bubbles in the 96-well white flat-bottom plate when transferring the cellular extract and NanoGlo buffer mixture from the 24-well tissue culture plate.

The reliance on *in vitro* assays and the absence of comprehensive *in vivo* validation limit the generalizability of our findings. While the *in vitro* results are encouraging, they also highlight the value of our research. It is essential to conduct extensive *in vivo* studies to confirm the efficacy and safety of the CP1 and TK knockouts in a living organism. The absence of a proper luciferase assay positive control, due to the transgenic nanoluciferase-expressing *C. parvum* field strain no longer virulent enough, has been a challenge. However, the Striepen research group has provided the highly virulent Nluc-NeoR mCherry fluorescence-tagged *C. parvum* Iowa II strain, which can be continuously passaged in wild-type C57/BL6J mice^{27,45,46}. With intermediate levels of parasite shedding extracted from feces, we are finalizing the permit paperwork to start the shipment process.

7.3.2 Off-Target Effects and sgRNA Efficiency

Thorough *in silico* characterization and validation are essential to minimize the potential for off-target effects, but they cannot guarantee their absence. Continuous monitoring and verification are necessary to ensure the long-term safety and efficacy of gene editing^{143,252}. The older plasmid-based approach did not yield the expected positive results, as determined during sgRNA *in silico* screening. The guide RNAs for CP1 and TK initially cloned into the hSpCas9

plasmid by the previous undergraduate student working on this project were personally verified using EuPaGDT to contain several off-target effects. This experience underscores the significant limitations of the older approach and the urgent need for improved methods in our research²¹⁸. The CP1 and TK guides also had very low reported CRISPR cleavage efficiency scores. The only TK guide (TKsg1-784) included in the *in vitro* DNA cleavage assays confirmed the *in silico* findings reported by EuPaGDT, showing only an approximate 42% cleavage score, hence corroborating the findings with the pursuit of the modified protocols (6.9-Fig. 9).

7.3.3 Repair Cassette Design Issues and Nucleofector Accessibility

The absence of a functional 3' UTR in the initial repair cassette design highlights the importance of thoroughly validating and optimizing all components involved in the gene editing process^{148,206}. The plausible rationale behind impaired luminescence detection in the older assays was likely due to the absence of a functional 3' UTR in the Nluc-NeoR fusion reporter transcript when the original repair cassette templates were re-sequenced (data not shown). This absence would prevent proper protein folding and maturation after translation, leading to insufficient NanoGlo substrate cleavage^{206,253-255}. Future studies should ensure that all elements, including regulatory sequences, are correctly incorporated to avoid similar issues.

The use of the Lonza AMAXA 4D-Nucleofector™, while practical, is limited by its scarce availability and the requirement for specialized training. Developing alternative, more accessible transfection methods would be beneficial for broader applications. This limitation underscores the need to improve and validate CRISPR components continuously.

7.4 Implications for Vaccine Development

7.4.1 Live-Attenuated Vaccine Potential

CP1 knockout parasites, as a live-attenuated vaccine, aim to elicit a robust immune response that mimics natural infection without causing disease. This proposed strategy is supported by the success of live-attenuated vaccines based on other protozoan parasites, such as *Plasmodium yoelii*³⁹, *Salmonella typhimurium*⁴⁰, *Mycobacterium tuberculosis*⁴¹, and *Francisella tularensis*⁴². This can lead to the activation of macrophages, dendritic cells, and neutrophils, which recognize

and respond to the parasite through pattern recognition receptors (PRRs)^{102,110,114}. Chemokines such as CCL2 and CXCL10 are upregulated in response to infection, recruiting immune cells to the site of infection¹¹⁷. Integrins, such as LFA-1, facilitate the adhesion and migration of leukocytes to the infected tissues^{149,256}. Interleukins, including IL-12 and IL-21, play pivotal roles in differentiating and activating T cells and B cells^{105,257}.

These attenuated parasites can be delivered as a potential therapeutic via using HBC. Hyperimmune bovine colostrum, rich in antibodies against *C. parvum*, has been used to protect calves from infection by providing passive protection from the mother⁷⁶. For vulnerable, at-risk human populations, HBC can be administered orally, offering a cost-effective and scalable solution for large-scale immunization programs. This approach has shown promise in other infectious diseases, such as *Clostridium difficile* infection, providing significant protection and reducing disease severity¹²¹. The scalability and low cost of producing HBC make it a viable option for large-scale immunization programs, particularly in low- and middle-income countries²⁵⁸.

7.4.2 Future Research

Future research should focus on optimizing the nucleofection process, exploring alternative delivery methods, and conducting comprehensive *in vivo* studies to evaluate the protective efficacy of the knockout attenuated parasites. Additionally, the potential of the other highly immunogenic and antigenic *C. parvum* vaccine candidates, such as Cpgp15/45, CSL adjacent proteins 1 or 2 and Cpgp23 hypervariant protein 1, should be explored in parallel to develop a multi-target vaccine strategy (6.15-Table 1). Further studies should also investigate the genomic stability of the attenuated parasites and the broader implications for parasite biology and pathogenesis.

7.4.2.1 Exploring Alternative Delivery Methods and Virulence Reversion Mechanisms

Cryptosporidium's feeding behaviour and transporter proteins present challenges and opportunities for delivering the Cas9/12a RNP complex¹²⁹. *C. parvum* relies on the salvaging feeder system to obtain nutrients and building blocks from the host, but much is still unknown about its specific feeding behaviour and penetration mechanisms^{106,114}. Research should explore using bacteria or viruses as baits or Trojan horses to deliver the Cas9/12a RNP complex into the

parasite⁹⁸. *C. parvum* has two putative glucose transporters (CpGT1 and CpGT2) localized near the feeder organelle, which could serve as receptors for viral vectors²⁵⁹.

Cryptosporidium's immune response and killing mechanism involve NK cells and CD8+ T cells, which secrete IFN- γ and IL-33 to recruit and activate other immune cells¹¹⁷. These cells use cytotoxicity and granulysin to induce apoptosis of infected cells and trap and starve the parasite²⁵⁶. Lactoferrin, a natural antimicrobial peptide in gastric mucus, can bind to *C. parvum* and impair its infectivity, making it a potential adjuvant or delivery agent for the Cas9/12a RNP complex²⁶⁰. Granzyme B, a serine protease released by NK cells, creates pores in the membrane of target cells and could facilitate the entry of the Cas9/12a RNP complex into the parasite^{129,261}.

Investigating virulence reversion mechanisms will be crucial to ensure the stability and safety of the attenuated strains. Understanding how *C. parvum* compensates for the loss of CP1 and TK will provide insights into the parasite's biology and help refine gene editing strategies¹⁰⁶.

7.4.2.2 Optimizing Transfection Methods and Positive Controls

Electroporation using the Amaxa 4D nucleofector has shown positive results with the Nluc-NeoR plasmid but not with the SpCas9 RNPs. Alternative delivery methods for CRISPR components, such as lipid nanoparticles or viral vectors, could be explored to enhance transfection efficiency and reduce potential cytotoxicity²⁶². Other transfection methods, such as microinjection, gene gun, or polyplex, should be investigated to compare results and optimize conditions²⁶³. Positive controls, such as a fluorescent reporter plasmid or a Cas9 protein fused with a fluorescent protein, could track transfection efficiency and specificity^{135,242}. Using a Cas12a enzyme instead of Cas9 may offer more options and flexibility for gRNA design and gene targeting^{140,216}.

Alternative strategies such as short-hairpin RNA (shRNA) or liposomes could knock down or knock out CP1^{264,265}. Liposomes could be a sound delivery system, as they are biocompatible and biodegradable, protect the delivery components from degradation, and enhance cell uptake²⁶⁶. Liposomes could be modified to target specific cells or tissues, such as intestinal epithelial cells or immune cells, by using ligands or antibodies that bind to specific receptors on the cell surface²⁶⁷.

8. Final Conclusions and Summary

This study aimed to verify genome editing within *C. parvum*, develop a novel investigative tool to study parasite biology, and create an attenuated *C. parvum* strain as a live attenuated vaccine candidate. Significant progress was made from bioinformatics analysis to confirm the high immunogenicity and antigenicity of CP1, followed by refined repair cassette design, sgRNA characterization and validation, and necessary *in vitro* transfection experiments.

This investigation made significant strides in optimizing a reproducible model for studying parasite biology and host-parasite interactions (**objective 1**) by designing and optimizing repair cassettes and sgRNA synthesis that are highly specific for targeted deletion within the *C. parvum* genomic landscape (6.8-Fig. 8 and 6.9-Fig. 9). The feasibility of genetic editing in the compact genome of *C. parvum* was validated *in silico* and *in vitro* using optimal CRISPR-Cas strategies (**objective 2**), as evidenced by the DNA cleavage assays that confirmed the efficiency of sgRNA-SpCas9 RNPs in targeting the recombinant CP1 and TK gene templates (6.9-Fig. 9) without off-target effects, confirmed from multivariate crRNA-specific polymorphic mutants (6.10-Fig. 10).

However, primary challenges, such as unsuccessful *in vivo* nucleolar delivery of the sgRNA-SpCas9 RNP and sufficient parasite survival post-nucleofection with currently existing primal electroporation strategies¹⁸⁹ (6.14-Fig. 14), highlight the need for further optimization involving in-depth investigations and cross-institutional collaboration. While *in vivo* targeted disruption of critical genes necessary for parasite survival and the investigation of the immunogenicity and protectivity of utilizing CP1-KO attenuated parasites as a potential live attenuated vaccine candidate were unmet (**objectives 3 and 4**), this serves as the groundwork for downstream profiling. Further research is needed to monitor successful transfected oocyst output, explore the potential collaborative mechanisms following CP1 and TK knockout strategies, and evaluate the effectiveness of attenuated *C. parvum* as a potential vaccine candidate

The immediate next steps of this project should focus on two key experiments: quantifying CP1 mRNA expression levels *in vitro* and verifying *in vitro* expression of the CP1 protein.

Experiment A aims to map the transcriptional landscape of CP1, determining whether CP1 expression is constitutively active across different parasite life stages or only at specific time points during *in vitro* or *in vivo* infection^{36,46}. These findings will better corroborate the timing of

excystation and *in vivo* nucleofection delivery of CRISPR components for potential success^{46,189}. This experiment involves extracting and culturing infectious *C. parvum* oocysts post-infection C57/BL6 IFN γ R-KO mice (refer to Chapter 4 Methodology, sections 4.2.1 and 4.2.2), *in vitro* infection with HCT-8 cells, total RNA extraction and purification, and complementary (c)DNA synthesis via reverse transcriptase quantitative PCR (RT-qPCR). The cDNA will be amplified using Cp18S rDNA or CP1-specific primers, constructing a standard curve for 18S ribosomal cDNA to calibrate CP1 mRNA expression levels over 72 hours⁹³. Cp18S rDNA primers will serve as the baseline to measure CP1 RNA levels normalized against the 18S gene, verified for its high specificity and direct correlation with sporozoite levels (6.12-Fig. 12 and 6.13-Fig. 13).

Experiment B aims to verify the expression and immunogenicity of CP1, laying the groundwork for developing a potential vaccine candidate. This involves synthesizing and purifying CP1 and the fluorescent reporter mCherry red fluorescent protein, linked by a viral P2A cleavage peptide²⁴⁰. Since no premade primary α -CP1 IgG antibodies are available; the mCherry gene will be a reporter-tracking tool for immunoblotting detection *in vitro*²⁶⁸ after expressing transformed BL21(DE3) *E. coli* cells following IPTG stimulation. Protein expression will be purified using coated affinity columns, specifically nickel-nitrilotriacetic acid (Ni-NTA) agarose beads, to bind the Histidine (His)-tagged CP1 protein. To determine their specificity, the purified proteins will then be analyzed using SDS-PAGE and western blotting. This involves running the samples on a 12% polyacrylamide gel, transferring the proteins onto a PVDF membrane, blocking with 5% non-fat dry milk in TBST buffer, incubating with primary antibodies against mCherry, washing, incubating with horseradish peroxidase (HRP)-conjugated secondary antibodies, and visualizing using chemiluminescence reactions.

In conclusion, significant strides have been made in understanding and manipulating the genome of *C. parvum* using CRISPR-Cas9 technology. Successful verification of CP1 expression and immunogenicity *in vivo* will significantly advance our understanding of *C. parvum* biology and contribute to the development of effective prophylactic interventions. Future studies will focus on assessing the long-term stable efficacy and safety of the CP1 knockout approach, including extensive *in vivo* testing to evaluate the durability of the immune response and potential side effects. Additionally, the scalability of this approach for large-scale vaccine production and its applicability to other *Cryptosporidium* species and relevant parasites will be explored.

9. Appendix

9.1 Table 7: Comparative Analysis of MHC-I Binding Predictions for Selected Target Candidates. The analysis includes average values, peptide scores, and ranks, highlighting the antigenic properties, immunogenicity, half-life predictions, toxicity predictions, and overall activity predictions for all possible epitope sizes for all eleven candidates as visualized in raw data format.

	Additional Info.	CSL	Cpgp15	Cpgp23	Cpgp15/45	Cpgp23 Variant 1	Cpgp23 Variant 2	CSL adjacent protein 1	CSL adjacent protein 2	CSL + adj protein 1	Cpgp2
Half-life prediction (ProParam online server)	N/A	WT: 30 hours (mammalian reticulocytes, in vitro). >20 hours (yeast, in vivo). >10 hours (Escherichia coli, in vivo).	WT: 30 hours (mammalian reticulocytes, in vitro). >20 hours (yeast, in vivo). >10 hours (Escherichia coli, in vivo).	WT: 30 hours (mammalian reticulocytes, in vitro). >20 hours (yeast, in vivo). >10 hours (Escherichia coli, in vivo).	WT: 30 hours (mammalian reticulocytes, in vitro). >20 hours (yeast, in vivo). >10 hours (Escherichia coli, in vivo).	WT: 30 hours (mammalian reticulocytes, in vitro). >20 hours (yeast, in vivo). >10 hours (Escherichia coli, in vivo).	WT: 30 hours (mammalian reticulocytes, in vitro). >20 hours (yeast, in vivo). >10 hours (Escherichia coli, in vivo).	WT: 30 hours (mammalian reticulocytes, in vitro). >20 hours (yeast, in vivo). >10 hours (Escherichia coli, in vivo). Mut-1: Same with WT	WT: 30 hours (mammalian reticulocytes, in vitro). >20 hours (yeast, in vivo). >10 hours (Escherichia coli, in vivo). Mut-1: Same with WT Mut-2: Same with WT	WT: 30 hours (mammalian reticulocytes, in vitro). >20 hours (yeast, in vivo). >10 hours (Escherichia coli, in vivo). Mut-1: Same with WT Mut-2: Same with WT	WT: 30 hours (mammalian reticulocytes, in vitro). >20 hours (yeast, in vivo). >10 hours (Escherichia coli, in vivo). Mut-1: Same with WT
Toxicity Prediction (ToxinPred online server)	All peptide fragment lengths are included: 10, 15, 20, 25, 30, 35, 40, 45, 50. Using the SVM (Swiss-Port) only prediction method.	Non-toxic	10: Toxic 15: Toxic 20: Toxic 25: Toxic 30: Nontoxic 35: Toxic 40: Nontoxic 45: Nontoxic 50: Nontoxic	Non-toxic	Non-toxic	Non-toxic	Toxic	10: Toxic 15: Toxic 20: Toxic 25: Toxic 30: Toxic 35: Toxic 40: Toxic 45: Nontoxic 50: Nontoxic	10: Toxic 15: Toxic 20: Toxic 25: Toxic 30: Toxic 35: Toxic 40: Nontoxic 45: Toxic 50: Toxic Mild toxic	10: Toxic 15: Toxic 20: Toxic 25: Toxic 30: Toxic 35: Toxic 40: Toxic 45: Nontoxic 50: Nontoxic	10: Toxic 15: Toxic 20: Toxic 25: Toxic 30: Toxic 35: Toxic 40: Nontoxic 45: Nontoxic 50: Nontoxic
Antigenicity Prediction (Vaxijen v2.0)	Measure the overall protective antigen prediction values, threshold is 0.5.	WT: 0.4069 Probable non-antigen	WT: 0.6009 Probable antigen	WT: 0.7407 Probable antigen	WT: 0.8776 Probable antigen	WT: 0.4708 Probable non-antigen	WT: 0.7742 Probable antigen Mut-1: 0.7164 Probable antigen	WT: 0.4461 Probable non-antigen Mut-1: 0.4801 Probable non-antigen Mut-2: 0.4789 Probable Non-antigen	WT: 0.5289 Probable antigen	WT: 0.4348 Probable Non-antigen Mut-1: 0.4620 Probable Non-antigen Mut-2: 0.4607 Probable non-antigen	WT: 0.8514 Probable antigen Mut-1: 0.8595 Probable antigen

	Additional Info.	CSL	Cpgp15	Cpgp23	Cpgp15/45	Cpgp23 Variant 1	Cpgp23 Variant 2	CSL adjacent protein 1	CSL adjacent protein 2	CSL + adj protein 1	Cpgp2
MHC-I Binding Prediction (IEDB)	All alleles of mouse and human are included. Peptide lengths included for human alleles are: 9-10; for mouse alleles are: 8-14. Only the highest peptide scores and their percentile ranks are included in this table b/c a higher score indicates a higher affinity. (IEDB recommended 2020.09 (NetMHCpan EL4.1))	Mice: 0.777412 Rank: 0.03 Human: 0.971274 Rank: 0.01	Mice: 0.801721 Rank: 0.12 Human: 0.982859 Rank: 0.01	Mice: 0.95985 Rank: 0.01 Human: 0.901007 Rank: 0.07	Mice: 0.907102 Rank: 0.01 Human: 0.986913 Rank: 0.01	Mice: 0.911993 Rank: 0.02 Human: 0.996777 Rank: 0.01	Mice: 0.826453 Rank: 0.09 Human: 0.995087 Rank: 0.01	Mice: 0.951801 Rank: 0.01 Human: 0.984114 Rank: 0.01	Mice: 0.979353 Rank: 0.01 Human: 0.994934 Rank: 0.01	Mice: 0.951801 Rank: 0.01 Human: 0.984114 Rank: 0.01	Mice: 0.937107 Rank: 0.01 Human: 0.993429 Rank: 0.01
Allergenicity Prediction (AllerTOP v. 2.0)	Prediction of allergens based on the main physicochemical properties of proteins. AllerTOP is able to also predict the route of allergen exposure: food, inhalant, or toxin	Probable non-allergen Most similar to DET1 - Light-mediated development protein Solunum lycopersicon (Tomato) UniProtKB UniProt	Probable non-allergen Most similar to Kinetochore scaffold 1 - Homo sapiens (Human) UniProtKB UniProt	Probable allergen Most similar to latex allergen Hev b 5 [Hevea brasiliensis] https://www.ncbi.nlm.nih.gov/protein/1480457	Probable non-allergen Most similar to SLUB6 - Subtilisin-like protease 6 - Trichophyton schoenleinii UniProtKB UniProt	Probable non-allergen Most similar to CPLANE1 - Cillogenesis and planar polarity effector 1 - Homo sapiens (Human) UniProtKB UniProt	Probable non-allergen Most similar to CCDC82 - Coiled-coil domain-containing protein 82 - Homo sapiens (Human) UniProtKB UniProt	Probable non-allergen Most similar to ATP11B - Phospholipid-transporting ATPase 1F - Homo sapiens (Human) UniProtKB UniProt	Probable non-allergen Most similar to ASCC3 - Activating signal co-integrator 1 complex subunit 3 - Homo sapiens (Human) UniProtKB UniProt	Probable allergen Most similar to FE - Coagulation factor VIII - Homo sapiens (Human) UniProtKB UniProt	Probable non-allergen Most similar to ANKRD12 - Ankyrin repeat domain-containing protein 12 - Homo sapiens (Human) UniProtKB UniProt
Stability Prediction (ProParam online server)	Measure the instability index	WT: 33.36 Stable	WT: 30.06 Stable	WT: 70.11 Unstable	WT: 50.88 Unstable	WT: 40.55 Unstable	WT: 52.40 Unstable Mut-1: 50.12 Less Unstable	WT: 38.76 Stable Mut-1: 40.1 Unstable Mut-2: 42.17 Unstable	WT: 41.38 Unstable	WT: 37.81 Stable Mut-1: 38.79 Less Stable Mut-2: 40.51 Unstable	WT: 49.66 Unstable Mut-1: 49.10 Less Unstable

9.2 Table 8: Comparative Analysis of MHC-II Binding Predictions for Selected Target Candidates. The analysis includes average values, peptide scores, and ranks, highlighting all eleven candidates' antigenic and hydrophilic properties as visualized in raw data format.

MHC-II												
Protein Name	Additional Info.	CSL	Cpgp15	Cpgp23	Cpgp15/45	Cpgp900	Cpgp23 Variant 1	Cpgp23 Variant 2	CSL adjacent protein 1	CSL adjacent protein 2	CSL + adj protein 1	Cpgp2
Antigenic Propensity (http://imed.med.ucm.es/Tools/antigenic.pl)	Using method of Kolaskar and Tongaonkar (1990)	Avg: 1.0303	Avg: 1.0224	Avg: 1.0021	Avg: 1.0194	Avg: 0.9923	Avg: 1.0168	Avg: 0.9829	Avg: 1.0381	Avg: 1.0174	Avg: 1.0367	Avg: 1.0074
Kolaskar and Tongaonkar Antigenicity (of year 1990-IEDB)	Wild-Type	Avg: 1.041 Min: 0.877 Max: 1.210	Avg: 1.027 Min: 0.889 Max: 1.185	Avg: 1.002 Min: 0.911 Max: 1.110	Avg: 1.016 Min: 0.876 Max: 1.259	Avg: 0.992 Min: 0.834 Max: 1.202	Avg: 1.017 Min: 0.882 Max: 1.210	Avg: 0.981 Min: 0.852 Max: 1.162	Avg: 1.039 Min: 0.866 Max: 1.238	Avg: 1.020 Min: 0.864 Max: 1.236	Avg: 1.038 Min: 0.866 Max: 1.238	Avg: 1.007 Min: 0.855 Max: 1.240
	Mutants (After deletion of the toxic regions)	N/A	Not included	N/A	N/A	N/A	N/A	Mut-1: Avg: 0.978 Min: 0.852 Max: 1.162	Mut-1: Avg: 1.036 Min: 0.866 Max: 1.210	N/A	Mut-1: Avg: 1.035 Min: 0.866 Max: 1.210	Mut-1: Avg: 1.007 Min: 0.855 Max: 1.240
Parker Hydrophilicity (IEDB)		Avg: 0.882 Min: -5.014 Max: 6.400	Avg: 2.319 Min: -3.586 Max: 7.143	Avg: 3.921 Min: 0.729 Max: 6.200	Avg: 2.862 Min: -5.829 Max: 7.943	Avg: 2.836 Min: -4.057 Max: 8.757	Avg: 1.049 Min: -8.243 Max: 6.300	Avg: 2.428 Min: -4.857 Max: 9.057	Avg: 0.619 Min: -4.929 Max: 6.843	Avg: 1.527 Min: -5.557 Max: 6.886	Avg: 0.670 Min: -5.014 Max: 6.843	Avg: 2.917 Min: -7.586 Max: 7.643
MHC-II Binding Prediction (IEDB)	All alleles of mouse and human are included. Peptide lengths included: 12-20. Only the lowest rank values are included	Mice: 11.84	Mice: 1.94	Mice: 0.13	Mice: 0.27	Not included	Mice: 0.01	Mice: 1.15	Mice: 1.30	Mice: 0.03	Mice: 1.30	Mice: 0.71
		Human: 0.17	Human: 0.13	Human: 0.25	Human: 0.01	Not included	Human: 0.03	Human: 0.05	Human: 0.01	Human: 0.01	Human: 0.01	Human: 0.01

MHC-II	Additional Info.	Cryptopain-1	Thymidine Kinase	Cpgp900	IMP dehydrogenase
Antigenic Propensity (http://imed.med.ucm.es/Tools/antigenic.pl) Still updating...	Using method of Kolaskar and Tongaonkar (1990)	Avg: 1.0215	Avg: 1.0347	Avg: 0.9923	Avg: 1.0174
Kolaskar and Tongaonkar Antigenicity (Of year 1990-IEDB)	Wild-Type	Average: 1.022 Minimum: 0.851 Maximum: 1.263	Average: 1.036 Minimum: 0.854 Maximum: 1.199	Average: 0.992 Minimum: 0.834 Maximum: 1.202	Avg: 1.019 Min: 0.864 Max: 1.207
Parker Hydrophilicity (IEDB)	N/A	Average: 1.738 Minimum: -6.500 Maximum: 7.957	Average: 1.122 Minimum: -3.986 Maximum: 6.900	Average: 2.836 Minimum: -4.057 Maximum: 8.757	Avg: 1.799 Min: -3.329 Max: 7.271
MHC-II Binding Prediction (IEDB)	All alleles of mouse and human are included. Peptide lengths included: 12-20. Only the best peptide score and their respective percentile ranks included	Human: Peptide score: 0.99019 Rank: 0.01	Human: Peptide score: 0.972857 Rank: 0.01	Human: Peptide score: 0.9831 Rank: 0.02	Human: Peptide score: 0.9381 Rank: 0.12
		Mouse: Peptide score: 0.5979 Rank: 0.07	Mouse: Peptide score: 0.0781 Rank: 2.60	Mouse: Peptide score: 0.7946 Rank: 0.02	Mouse: Peptide score: 0.1747 Rank: 0.21

References

1. Bouzid M., Hunter P.R., Chalmers R.M., Tyler K.M. *Cryptosporidium pathogenicity and virulence*. Clin Microbiol Rev 2013;26.115-34. doi:10.1128/cmr.00076-12. PMID:PMC3553671
2. Khalil I.A., Troeger C., Rao P.C., Blacker B.F., Brown A., Brewer T.G., . . . Mokdad A.H. *Morbidity, mortality, and long-term consequences associated with diarrhoea from Cryptosporidium infection in children younger than 5 years: a meta-analysis study*. Lancet Glob Health 2018;6.e758-e68. doi:10.1016/s2214-109x(18)30283-3. PMID:PMC6005120
3. Kotloff K.L., Nataro J.P., Blackwelder W.C., Nasrin D., Farag T.H., Panchalingam S., . . . Levine M.M. *Burden and aetiology of diarrhoeal disease in infants and young children in developing countries (the Global Enteric Multicenter Study, GEMS): a prospective, case-control study*. Lancet 2013;382.209-22. doi:10.1016/s0140-6736(13)60844-2.
4. Wang R., Li J., Chen Y., Zhang L., Xiao L. *Widespread occurrence of Cryptosporidium infections in patients with HIV/AIDS: Epidemiology, clinical feature, diagnosis, and therapy*. Acta Tropica 2018;187.257-63. doi:10.1016/j.actatropica.2018.08.018.
5. Abubakar I., Aliyu S.H., Arumugam C., Hunter P.R., Usman N.K. *Prevention and treatment of cryptosporidiosis in immunocompromised patients*. Cochrane Database Syst Rev 2007;Cd004932. doi:10.1002/14651858.CD004932.pub2.
6. Smith H.V., Rose J.B. *Waterborne cryptosporidiosis: current status*. Parasitol Today 1998;14.14-22. doi:10.1016/s0169-4758(97)01150-2.
7. Addiss D.G., Pond R.S., Remshak M., Juranek D.D., Stokes S., Davis J.P. *Reduction of risk of watery diarrhea with point-of-use water filters during a massive outbreak of waterborne Cryptosporidium infection in Milwaukee, Wisconsin, 1993*. Am J Trop Med Hyg 1996;54.549-53. doi:10.4269/ajtmh.1996.54.549.
8. Chalmers R.M. *Waterborne outbreaks of cryptosporidiosis*. Ann Ist Super Sanita 2012;48.429-46. doi:10.4415/ann_12_04_10.
9. Cicirello H.G., Kehl K.S., Addiss D.G., Chusid M.J., Glass R.I., Davis J.P., . . . Havens P.L. *Cryptosporidiosis in children during a massive waterborne outbreak in Milwaukee, Wisconsin: clinical, laboratory and epidemiologic findings*. Epidemiol Infect 1997;119.53-60. doi:10.1017/s0950268897007589. PMID:PMC2808823
10. Corso P.S., Kramer M.H., Blair K.A., Addiss D.G., Davis J.P., Haddix A.C. *Cost of illness in the 1993 waterborne Cryptosporidium outbreak, Milwaukee, Wisconsin*. Emerg Infect Dis 2003;9.426-31. doi:10.3201/eid0904.020417. PMID:PMC2957981
11. Dixon B., Parrington L., Cook A., Pollari F., Farber J. *Detection of Cyclospora, Cryptosporidium, and Giardia in Ready-to-Eat Packaged Leafy Greens in Ontario, Canada*. Journal of Food Protection 2013;76.307-13. doi:10.4315/0362-028X.JFP-12-282.
12. Hutter J.A., Dion R., Irace-Cima A., Fiset M., Guy R., Dixon B., . . . Thivierge K. *Cryptosporidium spp.: Human incidence, molecular characterization and associated exposures in Québec, Canada (2016-2017)*. PLoS One 2020;15.e0228986. doi:10.1371/journal.pone.0228986. PMID:PMC7018055

13. Iqbal A., Goldfarb D.M., Slinger R., Dixon B.R. *Prevalence and molecular characterization of Cryptosporidium spp. and Giardia duodenalis in diarrhoeic patients in the Qikiqtani Region, Nunavut, Canada*. International Journal of Circumpolar Health 2015;74.27713. doi:10.3402/ijch.v74.27713.
14. Johnson K.O., P. T., B. W., Y. W., J. P., M. M. *The epidemiology of cryptosporidiosis in Ontario, Canada following the introduction of PCR testing in 2018*. Can Commun Dis Rep 2020;46.227-30. doi:10.14745/ccdr.v46i78a02.
15. Thivierge K., Iqbal A., Dixon B., Dion R., Levesque B., Cantin P., . . . Yansouni C.P. *Cryptosporidium hominis is a newly recognized pathogen in the Arctic region of Nunavik, Canada: molecular characterization of an outbreak*. PLoS Neglected Tropical Diseases 2016;10.e0004534. doi:10.1371/journal.pntd.0004534.
16. Vinayak S., Pawlowic M.C., Sateriale A., Brooks C.F., Studstill C.J., Bar-Peled Y., . . . Striepen B. *Genetic modification of the diarrhoeal pathogen Cryptosporidium parvum*. Nature 2015;523.477-80. doi:10.1038/nature14651. PMID:PMC4640681
17. Kothavade R.J. *Challenges in understanding the immunopathogenesis of Cryptosporidium infections in humans*. Eur J Clin Microbiol Infect Dis 2011;30.1461-72. doi:10.1007/s10096-011-1246-6.
18. Guerrant R.L. *Cryptosporidiosis: an emerging, highly infectious threat*. Emerg Infect Dis 1997;3.51-7. doi:10.3201/eid0301.970106. PMID:PMC2627589
19. Abraham D.R., Rabie H., Cotton M.F. *Nitazoxanide for severe cryptosporidial diarrhea in human immunodeficiency virus infected children*. Pediatr Infect Dis J 2008;27.1040-1. doi:10.1097/inf.0b013e318186257b.
20. Amadi B., Mwiya M., Sianongo S., Payne L., Watuka A., Katubulushi M., . . . Kelly P. *High dose prolonged treatment with nitazoxanide is not effective for cryptosporidiosis in HIV positive Zambian children: a randomised controlled trial*. BMC Infectious Diseases 2009;9.195. doi:10.1186/1471-2334-9-195.
21. Capparelli E.V., Syed S.S. *Nitazoxanide treatment of Cryptosporidium parvum in human immunodeficiency virus-infected children*. The Pediatric infectious disease journal 2008;27.1041-. doi:10.1097/INF.0b013e3181862ae1.
22. Kotloff K.L. *The Burden and Etiology of Diarrheal Illness in Developing Countries*. Pediatric Clinics of North America 2017;64.799-814. doi:10.1016/j.pcl.2017.03.006.
23. Checkley W., White A.C., Jr., Jaganath D., Arrowood M.J., Chalmers R.M., Chen X.M., . . . Houpt E.R. *A review of the global burden, novel diagnostics, therapeutics, and vaccine targets for cryptosporidium*. Lancet Infect Dis 2015;15.85-94. doi:10.1016/s1473-3099(14)70772-8. PMID:PMC4401121
24. Collier S.A., Deng L., Adam E.A., Benedict K.M., Beshearse E.M., Blackstock A.J., . . . Beach M.J. *Estimate of Burden and Direct Healthcare Cost of Infectious Waterborne Disease in the United States*. Emerg Infect Dis 2021;27.140-9. doi:10.3201/eid2701.190676. PMID:PMC7774540
25. Carter B.L., Chalmers R.M., Davies A.P. *Health sequelae of human cryptosporidiosis in industrialised countries: a systematic review*. Parasites & Vectors 2020;13.443. doi:10.1186/s13071-020-04308-7.

26. Chalmers R.M., Giles M. *Zoonotic cryptosporidiosis in the UK – challenges for control*. Journal of Applied Microbiology 2010;109.1487-97. doi:10.1111/j.1365-2672.2010.04764.x.
27. Gullicksrud J.A., Sateriale A., Engiles J.B., Gibson A.R., Shaw S., Hutchins Z.A., . . . Hunter C.A. *Enterocyte-innate lymphoid cell crosstalk drives early IFN- γ -mediated control of Cryptosporidium*. Mucosal Immunol 2022;15.362-72. doi:10.1038/s41385-021-00468-6. PMID:PMC8881313
28. Pawlowic M.C., Somepalli M., Sateriale A., Herbert G.T., Gibson A.R., Cuny G.D., . . . Striepen B. *Genetic ablation of purine salvage in <i>Cryptosporidium parvum</i> reveals nucleotide uptake from the host cell*. Proceedings of the National Academy of Sciences 2019;116.21160-5. doi:doi:10.1073/pnas.1908239116.
29. Wilke G., Funkhouser-Jones L.J., Wang Y., Ravindran S., Wang Q., Beatty W.L., . . . Kuhlenschmidt M.S. *A stem-cell-derived platform enables complete Cryptosporidium development in vitro and genetic tractability*. Cell Host & Microbe 2019;26.123-34. e8. doi:10.1016/j.chom.2019.05.007.
30. Pawlowic M.C., Vinayak S., Sateriale A., Brooks C.F., Striepen B. *Generating and Maintaining Transgenic Cryptosporidium parvum Parasites*. Curr Protoc Microbiol 2017;46.20b.2.1-b.2.32. doi:10.1002/cpmc.33. PMID:PMC5556942
31. Beneke T., Madden R., Makin L., Valli J., Sunter J., Gluenz E. *A CRISPR Cas9 high-throughput genome editing toolkit for kinetoplastids*. Royal Society Open Science 2017;4.170095. doi:10.1098/rsos.170095.
32. Choudhary H.H., Nava M.G., Gartlan B.E., Rose S., Vinayak S., Weiss L.M. *A Conditional Protein Degradation System To Study Essential Gene Function in Cryptosporidium parvum*. mBio 2020;11.e01231-20. doi:doi:10.1128/mBio.01231-20.
33. Karmakar S., Behera D., Baig M.J., Molla K.A. *In Vitro Cas9 Cleavage Assay to Check Guide RNA Efficiency*. In: Islam MT, Molla KA, editors. CRISPR-Cas Methods: Volume 2. New York, NY: Springer US; 2021. p 23-39. doi:10.1007/978-1-0716-1657-4_3.
34. Doudna J.A., Charpentier E. *Genome editing. The new frontier of genome engineering with CRISPR-Cas9*. Science 2014;346.1258096. doi:10.1126/science.1258096.
35. Kim S., Kim D., Cho S.W., Kim J., Kim J.S. *Highly efficient RNA-guided genome editing in human cells via delivery of purified Cas9 ribonucleoproteins*. Genome Research 2014;24.1012-9. doi:10.1101/gr.171322.113. PMID:PMC4032847
36. Ndao M., Nath-Chowdhury M., Sajid M., Marcus V., Mashiyama S.T., Sakanari J., . . . Caffrey C.R. *A cysteine protease inhibitor rescues mice from a lethal Cryptosporidium parvum infection*. Antimicrob Agents Chemother 2013;57.6063-73. doi:10.1128/aac.00734-13. PMID:PMC3837922
37. Ndao M., Beaulieu C., Black W.C., Isabel E., Vasquez-Camargo F., Nath-Chowdhury M., . . . Nicoll-Griffith D.A. *Reversible cysteine protease inhibitors show promise for a Chagas disease cure*. Antimicrob Agents Chemother 2014;58.1167-78. doi:10.1128/AAC.01855-13.
38. Siqueira-Neto J.L., Debnath A., McCall L.-I., Bernatchez J.A., Ndao M., Reed S.L., . . . Rosenthal P.J. *Cysteine proteases in protozoan parasites*. PLoS Neglected Tropical Diseases 2018;12.e0006512. doi:10.1371/journal.pntd.0006512.

39. Goswami D., Minkah N.K., Kappe S.H. *Designer parasites: genetically engineered Plasmodium as vaccines to prevent malaria infection*. The Journal of Immunology 2019;202.20-8. doi:10.4049/jimmunol.1800727.
40. Ji H.J., Jang A.-Y., Song J.Y., Ahn K.B., Han S.H., Bang S.J., . . . Seo H.S. *Development of Live Attenuated Salmonella Typhimurium Vaccine Strain Using Radiation Mutation Enhancement Technology (R-MET)*. Frontiers in Immunology 2022;13. doi:10.3389/fimmu.2022.931052.
41. Tarancón R., Domínguez-Andrés J., Uranga S., Ferreira A.V., Groh L.A., Domenech M., . . . Netea M.G. *New live attenuated tuberculosis vaccine MTBVAC induces trained immunity and confers protection against experimental lethal pneumonia*. PLOS Pathogens 2020;16.e1008404. doi:10.1371/journal.ppat.1008404.
42. Jia Q., Horwitz M.A. *Live Attenuated Tularemia Vaccines for Protection Against Respiratory Challenge With Virulent F. tularensis subsp. tularensis*. Front Cell Infect Microbiol 2018;8.154. doi:10.3389/fcimb.2018.00154. PMID:PMC5963219
43. Manjunatha U.H., Vinayak S., Zambriski J.A., Chao A.T., Sy T., Noble C.G., . . . Diagana T.T. *A Cryptosporidium PI(4)K inhibitor is a drug candidate for cryptosporidiosis*. Nature 2017;546.376-80. doi:10.1038/nature22337. PMID:PMC5473467
44. Gibson A.R., Sateriale A., Dumaine J.E., Engiles J.B., Pardy R.D., Gullicksrud J.A., . . . Striepen B. *A genetic screen identifies a protective type III interferon response to Cryptosporidium that requires TLR3 dependent recognition*. PLOS Pathogens 2022;18.e1010003. doi:10.1371/journal.ppat.1010003.
45. Sateriale A., Gullicksrud J.A., Engiles J.B., McLeod B.I., Kugler E.M., Henao-Mejia J., . . . Striepen B. *The intestinal parasite Cryptosporidium is controlled by an enterocyte intrinsic inflammasome that depends on NLRP6*. Proc Natl Acad Sci U S A 2021;118. doi:10.1073/pnas.2007807118. PMID:PMC7812745
46. Tandel J., English E.D., Sateriale A., Gullicksrud J.A., Beiting D.P., Sullivan M.C., . . . Striepen B. *Life cycle progression and sexual development of the apicomplexan parasite Cryptosporidium parvum*. Nat Microbiol 2019;4.2226-36. doi:10.1038/s41564-019-0539-x. PMID:PMC6877471
47. English E.D., Guérin A., Tandel J., Striepen B. *Live imaging of the Cryptosporidium parvum life cycle reveals direct development of male and female gametes from type I meronts*. PLoS Biol 2022;20.e3001604. doi:10.1371/journal.pbio.3001604. PMID:PMC9015140
48. Guerrant D.I., Moore S.R., Lima A.A., Patrick P.D., Schorling J.B., Guerrant R.L. *Association of early childhood diarrhea and cryptosporidiosis with impaired physical fitness and cognitive function four-seven years later in a poor urban community in northeast Brazil*. Am J Trop Med Hyg 1999;61.707-13. doi:10.4269/ajtmh.1999.61.707.
49. Ryan U., Zahedi A., Papparini A. *Cryptosporidium in humans and animals—a one health approach to prophylaxis*. Parasite Immunology 2016;38.535-47. doi:10.1111/pim.12350.
50. Armson A., Thompson R.C.A., Reynoldson J.A. *A review of chemotherapeutic approaches to the treatment of cryptosporidiosis*. Expert Review of Anti-infective Therapy 2003;1.297-305. doi:10.1586/14787210.1.2.297.

51. Benschop J., Booker C.M., Shadbolt T., Weston J.F. *A Retrospective Cohort Study of an Outbreak of Cryptosporidiosis among Veterinary Students*. *Veterinary Sciences* 2017;4:29.
52. Troeger C., Forouzanfar M., Rao P.C., Khalil I., Brown A., Reiner Jr R.C., . . . Ahmed M. *Estimates of global, regional, and national morbidity, mortality, and aetiologies of diarrhoeal diseases: a systematic analysis for the Global Burden of Disease Study 2015*. *The Lancet Infectious Diseases* 2017;17:909-48. doi:10.1016/S1473-3099(17)30276-1.
53. Abdoli A., Maspi N. *Commentary: Estimates of Global, Regional, and National Morbidity, Mortality, and Aetiologies of Diarrhoeal Diseases: A Systematic Analysis for the Global Burden of Disease Study 2015*. *Frontiers in Medicine* 2018;5. doi:10.3389/fmed.2018.00011.
54. Amadi B., Mwiya M., Musuku J., Watuka A., Sianongo S., Ayoub A., . . . Kelly P. *Effect of nitazoxanide on morbidity and mortality in Zambian children with cryptosporidiosis: a randomised controlled trial*. *The Lancet* 2002;360:1375-80. doi:10.1016/S0140-6736(02)11401-2.
55. Guarino A., Lo Vecchio A. *Faculty opinions recommendation of treatment of diarrhea caused by cryptosporidium parvum: A prospective randomized, double-blind, placebo-controlled study of nitazoxanide*. *Faculty Opinions – Post-Publication Peer Review of the Biomedical Literature* 2016doi:10.3410/f.726147430.793514608
56. Keeffe E.B., Rossignol J.F. *Treatment of chronic viral hepatitis with nitazoxanide and second generation thiazolides*. *World J Gastroenterol* 2009;15:1805-8. doi:10.3748/wjg.15.1805. PMID:PMC2670405
57. Zulu I., Kelly P., Njobvu L., Sianongo S., Kaonga K., McDonald V., . . . Pollok R. *Nitazoxanide for persistent diarrhoea in Zambian acquired immune deficiency syndrome patients: a randomized-controlled trial*. *Alimentary Pharmacology & Therapeutics* 2005;21:757-63. doi:10.1111/j.1365-2036.2005.02394.x.
58. Cacciò S.M., Putignani L. *Epidemiology of Human Cryptosporidiosis*. In: Cacciò SM, Widmer G, editors. *Cryptosporidium: parasite and disease*: Springer, Vienna; 2013. p 43-80. doi:10.1007/978-3-7091-1562-6_2.
59. Chalmers R.M., Elwin K., Thomas A.L., Guy E.C., Mason B. *Long-term Cryptosporidium typing reveals the aetiology and species-specific epidemiology of human cryptosporidiosis in England and Wales, 2000 to 2003*. *Euro Surveill* 2009;14. doi:10.2807/ese.14.02.19086-en.
60. Current W.L., Garcia L.S. *Cryptosporidiosis*. *Clinical Microbiology Reviews* 1991;4:325-58. doi:10.1128/CMR.4.3.325.
61. Korpe P.S., Haque R., Gilchrist C., Valencia C., Niu F., Lu M., . . . Petri W.A., Jr. *Natural History of Cryptosporidiosis in a Longitudinal Study of Slum-Dwelling Bangladeshi Children: Association with Severe Malnutrition*. *PLoS Negl Trop Dis* 2016;10:e0004564. doi:10.1371/journal.pntd.0004564. PMID:PMC4856361
62. Hunter P.R., Syed Q. *Community surveys of self-reported diarrhoea can dramatically overestimate the size of outbreaks of waterborne cryptosporidiosis*. *Water Science and Technology* 2001;43:27-30. doi:10.2166/wst.2001.0707.
63. Mac Kenzie W.R., Schell W.L., Blair K.A., Addiss D.G., Peterson D.E., Hoxie N.J., . . . Davis J.P. *Massive Outbreak of Waterborne Cryptosporidium Infection in Milwaukee*,

- Wisconsin: Recurrence of Illness and Risk of Secondary Transmission*. Clinical Infectious Diseases 1995;21:57-62. doi:10.1093/clinids/21.1.57.
64. Guy R.A., Yanta C.A., Muchaal P.K., Rankin M.A., Thivierge K., Lau R., . . . Boggild A.K. *Molecular characterization of Cryptosporidium isolates from humans in Ontario, Canada*. Parasit Vectors 2021;14:69. doi:10.1186/s13071-020-04546-9. PMID:PMC7821412
 65. Ong C.S., Eisler D.L., Goh S.H., Tomblin J., Awad-El-Kariem F.M., Beard C.B., . . . Isaac-Renton J.L. *Molecular epidemiology of cryptosporidiosis outbreaks and transmission in British Columbia, Canada*. The American journal of tropical medicine and hygiene 1999;61:63-9. doi:10.4269/ajtmh.1999.61.63.
 66. Stirling R., Aramini J., Ellis A., Lim G., Meyers R., Fleury M., . . . Werker D. *Waterborne cryptosporidiosis outbreak, North Battleford, Saskatchewan, Spring 2001*. Can Commun Dis Rep 2001;27:185-92.
 67. Chalmers R.M., Davies A.P. *Minireview: clinical cryptosporidiosis*. Exp Parasitol 2010;124:138-46. doi:10.1016/j.exppara.2009.02.003.
 68. Harvala H., Ögren J., Boman P., Riedel H.M., Nilsson P., Winiecka-Krusnell J., . . . Beser J. *Cryptosporidium infections in Sweden-understanding the regional differences in reported incidence*. Clin Microbiol Infect 2016;22:1012-3. doi:10.1016/j.cmi.2016.09.012.
 69. Rideout H., Cook A.J.C., Whetton A.D. *Understanding the Cryptosporidium species and their challenges to animal health and livestock species for informed development of new, specific treatment strategies*. Frontiers in Parasitology 2024;3. doi:10.3389/fpara.2024.1448076.
 70. Peake L., Inns T., Jarvis C., King G., Rabie H., Henderson J., . . . Williams C. *Preliminary investigation of a significant national Cryptosporidium exceedance in the United Kingdom, August 2023 and ongoing*. Eurosurveillance 2023;28:2300538. doi:10.2807/1560-7917.ES.2023.28.43.2300538.
 71. Peñuelas Martínez M., Carmena D., Guzmán Herrador B.R., Palau Miguel M., Saravia Campelli G., García Álvarez R.M., . . . Network w.g.f.t.N.S. *Marked increase in cryptosporidiosis cases, Spain, 2023*. Eurosurveillance 2024;29:2300733. doi:10.2807/1560-7917.ES.2024.29.28.2300733.
 72. Daniels M., Smith W., Schmidt W.-P., Clasen T., Jenkins M. *Correlates of Cryptosporidium SPP and giardia spp contamination in improved drinking water sources in rural India: Implications for universal access to improved sanitation and safe drinking water*. The Lancet Global Health 2016;4. doi:10.1016/s2214-109x(16)30017-1
 73. Janoff E.N., Mead P.S., Mead J.R., Echeverria P., Bodhidatta L., Bhaibulaya M., . . . Taylor D.N. *Endemic Cryptosporidium and Giardia lamblia infections in a Thai orphanage*. Am J Trop Med Hyg 1990;43:248-56. doi:10.4269/ajtmh.1990.43.248.
 74. Siwila J. *The Triple Food-borne Protozoan Parasites: Cryptosporidium spp., Giardia duodenalis, Cyclospora cayetanensis—Hope in Transmission Reduction*. Curr Clin Microbiol Rep 2023;10:99-107. doi:10.1007/s40588-023-00199-1.
 75. Widmer G., Carmena D., Kváč M., Chalmers R.M., Kissinger J.C., Xiao L., . . . Favenec L. *Update on Cryptosporidium spp.: highlights from the Seventh International Giardia*

- and Cryptosporidium Conference*. Parasite 2020;27.14. doi:10.1051/parasite/2020011. PMID:PMC7069357
76. Aboelsoued D., Abdel Megeed K.N. *Diagnosis and control of cryptosporidiosis in farm animals*. Journal of Parasitic Diseases 2022;46.1133-46. doi:10.1007/s12639-022-01513-2.
 77. Pinto D.J., Vinayak S. *Cryptosporidium: Host-Parasite Interactions and Pathogenesis*. Curr Clin Microbiol Rep 2021;8.62-7. doi:10.1007/s40588-021-00159-7.
 78. Craun G.F., Hubbs S.A., Frost F.J., Calderon R.L., Via S.H. *Waterborne outbreaks of cryptosporidiosis*. Journal American Water Works Association 1998;90.81-91. doi:10.1002/J.1551-8833.1998.TB08500.X.
 79. Brusseau M.L., Ramirez-Andreotta M., Pepper I.L., Maximillian J. *Chapter 26 - Environmental Impacts on Human Health and Well-Being*. In: Brusseau ML, Pepper IL, Gerba CP, editors. Environmental and Pollution Science (Third Edition): Academic Press; 2019. p 477-99. doi:10.1016/B978-0-12-814719-1.00026-4.
 80. Brankston G., Boughen C., Ng V., Fisman D.N., Sargeant J.M., Greer A.L. *Assessing the impact of environmental exposures and Cryptosporidium infection in cattle on human incidence of cryptosporidiosis in Southwestern Ontario, Canada*. PLOS ONE 2018;13.e0196573. doi:10.1371/journal.pone.0196573.
 81. Sander V.A., Sánchez López E.F., Mendoza Morales L., Ramos Duarte V.A., Corigliano M.G., Clemente M. *Use of Veterinary Vaccines for Livestock as a Strategy to Control Foodborne Parasitic Diseases*. Frontiers in Cellular and Infection Microbiology 2020;10. doi:10.3389/fcimb.2020.00288.
 82. Thomson S., Hamilton C.A., Hope J.C., Katzer F., Mabbott N.A., Morrison L.J., . . . Innes E.A. *Bovine cryptosporidiosis: impact, host-parasite interaction and control strategies*. Veterinary Research 2017;48.42. doi:10.1186/s13567-017-0447-0.
 83. Griffiths J.K. *Human cryptosporidiosis: epidemiology, transmission, clinical disease, treatment, and diagnosis*. Adv Parasitol 1998;40.37-85. doi:10.1016/s0065-308x(08)60117-7.
 84. Lumadue J.A., Manabe Y.C., Moore R.D., Belitsos P.C., Sears C.L., Clark D.P. *A clinicopathologic analysis of AIDS-related cryptosporidiosis*. Aids 1998;12.2459-66. doi:10.1097/00002030-199818000-00015.
 85. Mondal D., Minak J., Alam M., Liu Y., Dai J., Korpe P., . . . Petri W.A., Jr. *Contribution of enteric infection, altered intestinal barrier function, and maternal malnutrition to infant malnutrition in Bangladesh*. Clin Infect Dis 2012;54.185-92. doi:10.1093/cid/cir807. PMID:PMC3245731
 86. Sow S.O., Muhsen K., Nasrin D., Blackwelder W.C., Wu Y., Farag T.H., . . . Faruque A.S. *The burden of Cryptosporidium diarrheal disease among children < 24 months of age in moderate/high mortality regions of sub-Saharan Africa and South Asia, utilizing data from the Global Enteric Multicenter Study (GEMS)*. PLoS neglected tropical diseases 2016;10.e0004729. doi:10.1371/journal.pntd.0004729.
 87. Haque R., Khan O.A., Heymann D.L. *Cryptosporidiosis*. Control of Communicable Diseases Clinical Practice: American Public Health Association; 2020. doi:10.2105/ccdmc.3087.040.

88. Helmy Y.A., Hafez H.M. *Cryptosporidiosis: From Prevention to Treatment, a Narrative Review*. *Microorganisms* 2022;10.2456. doi:10.3390/microorganisms10122456.
89. Destura R.V., Cena R.B., Galarion M.J.H., Pangilinan C.M., Arevalo G.M., Alba R.O.C., . . . Sevilleja J.E.A.D. *Advancing Cryptosporidium Diagnostics from Bench to Bedside*. *Current Tropical Medicine Reports* 2015;2.150-60. doi:10.1007/s40475-015-0055-x.
90. Gökçe S. *Human cytomegalovirus infection: Biological features, transmission, symptoms, diagnosis, and treatment*. In: Thomasini RL, editor. *Human Herpesvirus Infection - Biological Features, Transmission, Symptoms, Diagnosis and Treatment* 2019. doi:10.5772/intechopen.81833
91. Miller A.D. *8 - Histopathologic diagnosis*. In: Bowman DD, editor. *Georgis' Parasitology for Veterinarians (Eleventh Edition)*. St. Louis (MO): W.B. Saunders; 2021. p 455-78.e1. doi:10.1016/B978-0-323-54396-5.00017-9.
92. Jaskiewicz J.J., Sevenler D., Swei A.A., Widmer G., Toner M., Tzipori S., . . . Sandlin R.D. *Cryopreservation of infectious Cryptosporidium parvum oocysts achieved through vitrification using high aspect ratio specimen containers*. *Sci Rep* 2020;10.11711. doi:10.1038/s41598-020-68643-6. PMID:PMC7366687
93. Xu R., Feng Y., Xiao L., Sibley L.D. *Insulinase-like Protease 1 Contributes to Macrogamont Formation in Cryptosporidium parvum*. *mBio* 2021;12. doi:10.1128/mBio.03405-20. PMID:PMC8092296
94. Namekar M., Ellis E.M., O'Connell M., Elm J., Gurary A., Park S.Y., . . . Nerurkar V.R. *Evaluation of a new commercially available immunoglobulin M capture enzyme-linked immunosorbent assay for diagnosis of dengue virus infection*. *Journal of clinical Microbiology* 2013;51.3102-6. doi:10.1128/JCM.00351-13.
95. Chalmers R.M., Alexander C. *Defining the diagnosis of cryptosporidiosis*. *The Lancet Infectious Diseases* 2021;21.589-90. doi:10.1016/S1473-3099(20)30575-2.
96. Sundar S., Piramanayagam S., Natarajan J. *A comprehensive review on human disease—causing bacterial proteases and their impeding agents*. *Archives of Microbiology* 2023;205.276. doi:10.1007/s00203-023-03618-5.
97. McKerrow J.H., Caffrey C., Kelly B., Loke P.n., Sajid M. *PROTEASES IN PARASITIC DISEASES*. *Annual Review of Pathology: Mechanisms of Disease* 2006;1.497-536. doi:10.1146/annurev.pathol.1.110304.100151.
98. A Rascon A., H McKerrow J. *Synthetic and natural protease inhibitors provide insights into parasite development, virulence and pathogenesis*. *Current Medicinal Chemistry* 2013;20.3078-102.
99. Kvale D., Aukrust P., Osnes K., Müller F., Frøland S.S. *CD4+ and CD8+ lymphocytes and HIV RNA in HIV infection: high baseline counts and in particular rapid decrease of CD8+ lymphocytes predict AIDS*. *Aids* 1999;13.195-201. doi:10.1097/00002030-199902040-00007.
100. Mead J.R. *Prospects for immunotherapy and vaccines against Cryptosporidium*. *Hum Vaccin Immunother* 2014;10.1505-13. doi:10.4161/hv.28485. PMID:PMC4185963
101. Bonafonte M.T., Smith L.M., Mead J.R. *A 23-kDa recombinant antigen of Cryptosporidium parvum induces a cellular immune response on in vitro stimulated*

- spleen and mesenteric lymph node cells from infected mice.* Exp Parasitol 2000;96:32-41. doi:10.1006/expr.2000.4545.
102. Laurent F., Lacroix-Lamadé S. *Innate immune responses play a key role in controlling infection of the intestinal epithelium by Cryptosporidium.* International Journal for Parasitology 2017;47:711-21. doi:10.1016/j.ijpara.2017.08.001.
 103. Dayao D.A., Jaskiewicz J., Lee S., Oliveira B.C., Sheoran A., Widmer G., . . . Tzipori S. *Development of Two Mouse Models for Vaccine Evaluation against Cryptosporidiosis.* Infection and Immunity 2022;90:e00127-22. doi:10.1128/iai.00127-22.
 104. Griffiths J.K., Theodos C., Paris M., Tzipori S. *The gamma interferon gene knockout mouse: a highly sensitive model for evaluation of therapeutic agents against Cryptosporidium parvum.* Journal of Clinical Microbiology 1998;36:2503-8. doi:10.1128/JCM.36.9.2503-2508.1998.
 105. Liu Y.C., Chen Q., Yang X.L., Tang Q.S., Yao K.T., Xu Y. *Generation of a new strain of NOD/SCID/IL2R γ (-/-) mice with targeted disruption of Prkdc and IL2R γ genes using CRISPR/Cas9 system.* Nan Fang Yi Ke Da Xue Xue Bao 2018;38:639-46. doi:10.3969/j.issn.1673-4254.2018.06.01. PMID:PMC6765701
 106. Cohn I.S., Henrickson S.E., Striepen B., Hunter C.A. *Immunity to Cryptosporidium: lessons from acquired and primary immunodeficiencies.* The Journal of Immunology 2022;209:2261-8. doi:10.4049/jimmunol.2200512.
 107. Crawford C.K., Kol A. *The Mucosal Innate Immune Response to Cryptosporidium parvum, a Global One Health Issue.* Frontiers in Cellular and Infection Microbiology 2021;11. doi:10.3389/fcimb.2021.689401.
 108. Ludington J.G., Ward H.D. *Systemic and Mucosal Immune Responses to Cryptosporidium-Vaccine Development.* Curr Trop Med Rep 2015;2:171-80. doi:10.1007/s40475-015-0054-y. PMID:PMC4535728
 109. Louis-Auguste J., Greenwald S., Simuyandi M., Soko R., Banda R., Kelly P. *High dose multiple micronutrient supplementation improves villous morphology in environmental enteropathy without HIV enteropathy: results from a double-blind randomised placebo controlled trial in Zambian adults.* BMC Gastroenterol 2014;14:15. doi:10.1186/1471-230x-14-15. PMID:PMC3897937
 110. Borad A., Ward H. *Human immune responses in cryptosporidiosis.* Future Microbiol 2010;5:507-19. doi:10.2217/fmb.09.128.
 111. Gilchrist C.A., Campo J.J., Pablo J.V., Ma J.Z., Teng A., Oberai A., . . . Faruque A. *Specific Cryptosporidium antigens associate with reinfection immunity and protection from cryptosporidiosis.* The Journal of clinical investigation 2023;133. doi:10.1172/JCI166814
 112. Manque Patricio A., Tenjo F., Woehlbier U., Lara Ana M., Serrano Myrna G., Xu P., . . . Buck Gregory A. *Identification and Immunological Characterization of Three Potential Vaccinogens against Cryptosporidium Species.* Clinical and Vaccine Immunology 2011;18:1796-802. doi:10.1128/CVI.05197-11.
 113. Saraav I., Sibley L.D. *Dendritic Cells and Cryptosporidium: From Recognition to Restriction.* Microorganisms 2023;11:1056. doi:10.3390/microorganisms11041056.

114. Lemieux M.W., Sonzogni-Desautels K., Ndao M. *Lessons Learned from Protective Immune Responses to Optimize Vaccines against Cryptosporidiosis*. *Pathogens* 2018;7.2. doi:10.3390/pathogens7010002.
115. Veshkini A., Dengler F., Bachmann L., Liermann W., Helm C., Ulrich R., . . . Hammon H.M. *Cryptosporidium parvum* infection alters the intestinal mucosa transcriptome in neonatal calves: implications for immune function. *Frontiers in Immunology* 2024;15. doi:10.3389/fimmu.2024.1351427.
116. Haserick J.R., Klein J.A., Costello C.E., Samuelson J. *Cryptosporidium parvum* vaccine candidates are incompletely modified with O-linked-N-acetylgalactosamine or contain N-terminal N-myristate and S-palmitate. *PLOS ONE* 2017;12.e0182395. doi:10.1371/journal.pone.0182395.
117. Bartelt L.A., Bolick D.T., Kolling G.L., Roche J.K., Zaenker E.I., Lara A.M., . . . Guerrant R.L. *Cryptosporidium* Priming Is More Effective than Vaccine for Protection against Cryptosporidiosis in a Murine Protein Malnutrition Model. *PLOS Neglected Tropical Diseases* 2016;10.e0004820. doi:10.1371/journal.pntd.0004820.
118. Liu K., Zai D., Zhang D., Wei Q., Han G., Gao H., . . . Huang B. *Divalent Cp15–23 vaccine enhances immune responses and protection against Cryptosporidium parvum* infection. *Parasite Immunology* 2010;32.335-44. doi:10.1111/j.1365-3024.2009.01191.x.
119. Wang Y., Li N., Liang G., Wang L., Zhang X., Cui Z., . . . Zhang L. *Identification of host protein ENO1 (alpha-enolase) interacting with Cryptosporidium parvum* sporozoite surface protein, *Cpgp40*. *Parasites & Vectors* 2024;17.146. doi:10.1186/s13071-024-06233-5.
120. Tomazic M.L., Rodriguez A.E., Lombardelli J., Poklepovich T., Garro C., Galarza R., . . . Schnittger L. *Identification of novel vaccine candidates against cryptosporidiosis of neonatal bovines by reverse vaccinology*. *Veterinary Parasitology* 2018;264.74-8. doi:10.1016/j.vetpar.2018.11.007.
121. Clark-Curtiss J.E., Curtiss R., 3rd. *Salmonella Vaccines: Conduits for Protective Antigens*. *J Immunol* 2018;200.39-48. doi:10.4049/jimmunol.1600608.
122. Wang L., Wang X., Bi K., Sun X., Yang J., Gu Y., . . . Zhu X. *Oral Vaccination with Attenuated Salmonella typhimurium-Delivered TsPmy DNA Vaccine Elicits Protective Immunity against Trichinella spiralis in BALB/c Mice*. *PLoS Negl Trop Dis* 2016;10.e0004952. doi:10.1371/journal.pntd.0004952. PMID:PMC5010209
123. Park S., Jung B., Kim E., Hong S.T., Yoon H., Hahn T.W. *Salmonella Typhimurium Lacking YjeK as a Candidate Live Attenuated Vaccine Against Invasive Salmonella Infection*. *Front Immunol* 2020;11.1277. doi:10.3389/fimmu.2020.01277. PMID:PMC7324483
124. Taiwo A. *Cryptosporidium* spp.: Challenges in Control and Potential Therapeutic Strategies. In: Prof. Nihal D, editor. *Intestinal Parasites - New Developments in Diagnosis, Treatment, Prevention and Future Directions*. Rijeka: IntechOpen; 2024. p Ch. 5. doi:10.5772/intechopen.1005165.
125. Hong-Xuan H., Lei C., Cheng-Min W., Kai Z., Yi T., Xi-Ming Q., . . . Ming-Xing D. *Expression of the recombinant fusion protein CP15-23 of Cryptosporidium parvum and its protective test*. *J Nanosci Nanotechnol* 2005;5.1292-6. doi:10.1166/jnn.2005.210.

126. Nie Z., Zhu S., Wu L., Sun R., Shu J., He Y., . . . Feng H. *Progress on innate immune evasion and live attenuated vaccine of pseudorabies virus*. *Frontiers in Microbiology* 2023;14. doi:10.3389/fmicb.2023.1138016.
127. Sateriale A., Šlapeta J., Baptista R., Engiles J.B., Gullicksrud J.A., Herbert G.T., . . . Striepen B. *A Genetically Tractable, Natural Mouse Model of Cryptosporidiosis Offers Insights into Host Protective Immunity*. *Cell Host & Microbe* 2019;26.135-46.e5. doi:10.1016/j.chom.2019.05.006.
128. Zetsche B., Gootenberg J.S., Abudayyeh O.O., Slaymaker I.M., Makarova K.S., Essletzbichler P., . . . Zhang F. *Cpf1 is a single RNA-guided endonuclease of a class 2 CRISPR-Cas system*. *Cell* 2015;163.759-71. doi:10.1016/j.cell.2015.09.038. PMID:PMC4638220
129. Di Cristina M., Carruthers V.B. *New and emerging uses of CRISPR/Cas9 to genetically manipulate apicomplexan parasites*. *Parasitology* 2018;145.1119-26. doi:10.1017/S003118201800001X.
130. Ran F.A., Hsu P.D., Wright J., Agarwala V., Scott D.A., Zhang F. *Genome engineering using the CRISPR-Cas9 system*. *Nat Protoc* 2013;8.2281-308. doi:10.1038/nprot.2013.143. PMID:PMC3969860
131. Vakulskas C.A., Behlke M.A. *Evaluation and Reduction of CRISPR Off-Target Cleavage Events*. *Nucleic Acid Ther* 2019;29.167-74. doi:10.1089/nat.2019.0790. PMID:PMC6686686
132. Rouet R., Thuma B.A., Roy M.D., Lintner N.G., Rubitski D.M., Finley J.E., . . . Doudna J.A. *Receptor-Mediated Delivery of CRISPR-Cas9 Endonuclease for Cell-Type-Specific Gene Editing*. *J Am Chem Soc* 2018;140.6596-603. doi:10.1021/jacs.8b01551. PMID:PMC6002863
133. Khalifa K.E. *CRISPR/Cas9 gene editing: Applications in Parasitology*. *QJM: An International Journal of Medicine* 2020;113.hcaa060.09. doi:10.1093/qjmed/hcaa060.009.
134. Bryant J.M., Baumgarten S., Glover L., Hutchinson S., Rachidi N. *CRISPR in parasitology: not exactly cut and dried!* *Trends in parasitology* 2019;35.409-22. doi:10.1016/j.pt.2019.03.0.
135. Vakulskas C.A., Dever D.P., Rettig G.R., Turk R., Jacobi A.M., Collingwood M.A., . . . Behlke M.A. *A high-fidelity Cas9 mutant delivered as a ribonucleoprotein complex enables efficient gene editing in human hematopoietic stem and progenitor cells*. *Nat Med* 2018;24.1216-24. doi:10.1038/s41591-018-0137-0. PMID:PMC6107069
136. Peng D., Kurup S.P., Yao P.Y., Minning T.A., Tarleton R.L. *CRISPR-Cas9-Mediated Single-Gene and Gene Family Disruption in Trypanosoma cruzi*. *mBio* 2015;6.e02097-14. doi:10.1128/mBio.02097-14.
137. Raj D.K., Das Mohapatra A., Jnawali A., Zuromski J., Jha A., Cham-Kpu G., . . . Kurtis J.D. *Anti-PfGARP activates programmed cell death of parasites and reduces severe malaria*. *Nature* 2020;582.104-8. doi:10.1038/s41586-020-2220-1. PMID:PMC7372601
138. Lee M.C.S., Lindner S.E., Lopez-Rubio J.-J., Llinás M. *Cutting back malaria: CRISPR/Cas9 genome editing of Plasmodium*. *Briefings in Functional Genomics* 2019;18.281-9. doi:10.1093/bfpg/elz012.

139. Sijwali P.S., Koo J., Singh N., Rosenthal P.J. *Gene disruptions demonstrate independent roles for the four falcipain cysteine proteases of Plasmodium falciparum*. Molecular and Biochemical Parasitology 2006;150:96-106. doi:10.1016/j.molbiopara.2006.06.013.
140. Collier T.C., Lee Y., Mathias D.K., Del Amo V.L. *CRISPR-Cas9 and Cas12a target site richness reflects genomic diversity in natural populations of Anopheles gambiae and Aedes aegypti mosquitoes*. BMC Genomics 2024;25:700. doi:10.1186/s12864-024-10597-4.
141. Quinn C., Anthousi A., Wondji C., Nolan T. *CRISPR-mediated knock-in of transgenes into the malaria vector Anopheles funestus*. G3 Genes|Genomes|Genetics 2021;11. doi:10.1093/g3journal/jkab201.
142. You H., Jones M.K. *Harnessing CRISPR-based molecular diagnosis in the fight against malaria*. EBioMedicine 2024;99. doi:10.1016/j.ebiom.2023.104927.
143. Pal S., Dam S. *CRISPR-Cas9: Taming protozoan parasites with bacterial scissor*. Journal of Parasitic Diseases 2022;46:1204-12. doi:10.1007/s12639-022-01534-x.
144. Chen Y.T., Brinen L.S., Kerr I.D., Hansell E., Doyle P.S., McKerrow J.H., . . . Roush W.R. *In vitro and in vivo studies of the trypanocidal properties of WRR-483 against Trypanosoma cruzi*. PLoS Negl Trop Dis 2010;4. doi:10.1371/journal.pntd.0000825. PMID:PMC2939063
145. Caffrey C.R., Lima A.-P., Steverding D. *Cysteine Peptidases of Kinetoplastid Parasites*. In: Robinson MW, Dalton JP, editors. Cysteine Proteases of Pathogenic Organisms. Boston, MA: Springer US; 2011. p 84-99. doi:10.1007/978-1-4419-8414-2_6.
146. Sajid M., McKerrow J.H. *Cysteine proteases of parasitic organisms*. Molecular and Biochemical Parasitology 2002;120:1-21. doi:10.1016/S0166-6851(01)00438-8.
147. Turk V., Stoka V., Vasiljeva O., Renko M., Sun T., Turk B., . . . Turk D. *Cysteine cathepsins: From structure, function and regulation to new frontiers*. Biochimica et Biophysica Acta (BBA) - Proteins and Proteomics 2012;1824:68-88. doi:10.1016/j.bbapap.2011.10.002.
148. Abrahamsen M.S., Templeton T.J., Enomoto S., Abrahante J.E., Zhu G., Lancto C.A., . . . Tzipori S. *Complete genome sequence of the apicomplexan, Cryptosporidium parvum*. Science 2004;304:441-5. doi:10.1126/science.1094786.
149. Rider S.D., Jr., Zhu G. *Cryptosporidium: genomic and biochemical features*. Exp Parasitol 2010;124:2-9. doi:10.1016/j.exppara.2008.12.014. PMID:PMC2819285
150. Xu Z., Guo Y., Roellig D.M., Feng Y., Xiao L. *Comparative analysis reveals conservation in genome organization among intestinal Cryptosporidium species and sequence divergence in potential secreted pathogenesis determinants among major human-infecting species*. BMC Genomics 2019;20:406. doi:10.1186/s12864-019-5788-9. PMID:PMC6532270
151. Na B.K., Kang J.M., Cheun H.I., Cho S.H., Moon S.U., Kim T.S., . . . Sohn W.M. *Cryptopain-1, a cysteine protease of Cryptosporidium parvum, does not require the pro-domain for folding*. Parasitology 2009;136:149-57. doi:10.1017/s0031182008005350.
152. Chaparro J.D., Cheng T., Tran U.P., Andrade R.M., Brenner S.B.T., Hwang G., . . . Reed S.L. *Two key cathepsins, TgCPB and TgCPL, are targeted by the vinyl sulfone inhibitor K11777 in in vitro and in vivo models of toxoplasmosis*. PLoS One 2018;13:e0193982. doi:10.1371/journal.pone.0193982. PMID:PMC5863946

153. Duschak G.V., Couto S.A. *Cruzipain, the Major Cysteine Protease of Trypanosoma cruzi: A Sulfated Glycoprotein Antigen as Relevant Candidate for Vaccine Development and Drug Target. A Review.* Current Medicinal Chemistry 2009;16:3174-202. doi:10.2174/092986709788802971.
154. Rosenthal P.J. *Falicipains and Other Cysteine Proteases of Malaria Parasites.* In: Robinson MW, Dalton JP, editors. Cysteine Proteases of Pathogenic Organisms. Boston, MA: Springer US; 2011. p 30-48. doi:10.1007/978-1-4419-8414-2_3.
155. Koussis K., Withers-Martinez C., Yeoh S., Child M., Hackett F., Knuepfer E., . . . Blackman M.J. *A multifunctional serine protease primes the malaria parasite for red blood cell invasion.* Embo j 2009;28:725-35. doi:10.1038/emboj.2009.22. PMID:PMC2647770
156. Deu E. *Proteases as antimalarial targets: strategies for genetic, chemical, and therapeutic validation.* The FEBS Journal 2017;284:2604-28. doi:10.1111/febs.14130.
157. Doyle P.S., Zhou Y.M., Hsieh I., Greenbaum D.C., McKerrow J.H., Engel J.C. *The Trypanosoma cruzi Protease Cruzain Mediates Immune Evasion.* PLOS Pathogens 2011;7:e1002139. doi:10.1371/journal.ppat.1002139.
158. Meira C.S., Guimaraes E.T., Bastos T.M., Moreira D.R., Tomassini T.C., Ribeiro I.M., . . . Soares M.B. *Physalins B and F, seco-steroids isolated from Physalis angulata L., strongly inhibit proliferation, ultrastructure and infectivity of Trypanosoma cruzi.* Parasitology 2013;140:1811-21. doi:10.1017/S0031182013001297.
159. Branquinha M., Oliveira S., Sangenito L., Sodre C., Kneipp L., d'Avila-Levy C., . . . Santos A. *Cruzipain: an update on its potential as chemotherapy target against the human pathogen Trypanosoma cruzi.* Current Medicinal Chemistry 2015;22:2225-35.
160. Kourbeli V., Chontzopoulou E., Moschovou K., Pavlos D., Mavromoustakos T., Papanastasiou I.P. *An overview on target-based drug design against kinetoplastid protozoan infections: human African trypanosomiasis, Chagas disease and leishmaniasis.* Molecules 2021;26:4629. doi:10.3390/molecules26154629.
161. Dandapani S., Germain A.R., Jewett I., le Quement S., Marie J.-C., Muncipinto G., . . . Engel J.C. *Diversity-oriented synthesis yields a new drug lead for treatment of Chagas disease.* ACS Medicinal Chemistry Letters 2014;5:149-53. doi:10.1021/ml400403u.
162. Sajid M., Robertson S.A., Brinen L.S., McKerrow J.H. *Cruzain : the path from target validation to the clinic.* Adv Exp Med Biol 2011;712:100-15. doi:10.1007/978-1-4419-8414-2_7.
163. Bowman D.D. *4 - Helminths.* In: Bowman DD, editor. Georgis' Parasitology for Veterinarians (Eleventh Edition). St. Louis (MO): W.B. Saunders; 2021. p 135-260. doi:10.1016/B978-0-323-54396-5.00013-1.
164. Grote A., Caffrey C.R., Rebello K.M., Smith D., Dalton J.P., Lustigman S. *Cysteine proteases during larval migration and development of helminths in their final host.* PLOS Neglected Tropical Diseases 2018;12:e0005919. doi:10.1371/journal.pntd.0005919.
165. Perera D.J., Koger-Pease C., Paulini K., Daoudi M., Ndao M. *Beyond schistosomiasis: unraveling co-infections and altered immunity.* Clin Microbiol Rev 2024;37:e0009823. doi:10.1128/cmr.00098-23. PMID:PMC10938899

166. 10.1371/journal.pntd.0005840 Caffrey C.R., Goupil L., Rebello K.M., Dalton J.P., Smith D. Cysteine proteases as digestive enzymes in parasitic helminths. PLoS neglected tropical diseases. Volume 122018. p e0005840.
167. Perera D.J., Hassan A.S., Jia Y., Ricciardi A., McCluskie M.J., Weeratna R.D., . . . Ndao M. *Adjuvanted Schistosoma mansoni-Cathepsin B With Sulfated Lactosyl Archaeol Archaeosomes or AddaVax™ Provides Protection in a Pre-Clinical Schistosomiasis Model*. Front Immunol 2020;11. doi:10.3389/fimmu.2020.605288.
168. Perera D.J., Hassan A.S., Liu S.S., Elahi S.M., Gadoury C., Weeratna R.D., . . . Ndao M. *A low dose adenovirus vectored vaccine expressing Schistosoma mansoni Cathepsin B protects from intestinal schistosomiasis in mice*. EBioMedicine 2022;80.104036. doi:10.1016/j.ebiom.2022.104036. PMID:PMC9065910
169. Brown G.D., Ballou E.R., Bates S., Bignell E.M., Borman A.M., Brand A.C., . . . Wilson D. *The pathobiology of human fungal infections*. Nature Reviews Microbiology 2024doi:10.1038/s41579-024-01062-w.
170. Banushree C.S., Madhusudhan N.S. *Pathogenesis of Fungal Infections*. In: Turgut M, Challa S, Akhaddar A, editors. Fungal Infections of the Central Nervous System: Pathogens, Diagnosis, and Management. Cham: Springer International Publishing; 2019. p 31-42. doi:10.1007/978-3-030-06088-6_4.
171. Zagórska A., Czopek A., Fryc M., Jończyk J. *Inhibitors of SARS-CoV-2 Main Protease (Mpro) as Anti-Coronavirus Agents*. Biomolecules 2024;14.797. doi:10.3390/biom14070797.
172. Fernandes H.S., Sousa S.F., Cerqueira N.M.F.S.A. *New insights into the catalytic mechanism of the SARS-CoV-2 main protease: an ONIOM QM/MM approach*. Molecular Diversity 2022;26.1373-81. doi:10.1007/s11030-021-10259-7.
173. Pragman A.A., Schlievert P.M. *Virulence regulation in Staphylococcus aureus: the need for in vivo analysis of virulence factor regulation*. FEMS Immunology & Medical Microbiology 2004;42.147-54. doi:10.1016/j.femsim.2004.05.005.
174. Jenul C., Horswill A.R. *Regulation of <i>Staphylococcus aureus</i> Virulence*. Microbiology Spectrum 2019;7.10.1128/microbiolspec.gpp3-0031-2018. doi:10.1128/microbiolspec.gpp3-0031-2018.
175. Armson A., Meloni B.P., Reynoldson J.A., Thompson R.C.A. *Assessment of drugs against Cryptosporidium parvum using a simple in vitro screening method*. FEMS Microbiology Letters 1999;178.227-33. doi:10.1111/j.1574-6968.1999.tb08681.x.
176. Heiges M., Wang H., Robinson E., Aurrecoechea C., Gao X., Kaluskar N., . . . Su Y. *CryptoDB: a Cryptosporidium bioinformatics resource update*. Nucleic Acids Research 2006;34.D419-D22. doi:10.1093/nar/gkj078.
177. Funkhouser-Jones Lisa J., Ravindran S., Sibley L.D. *Defining Stage-Specific Activity of Potent New Inhibitors of Cryptosporidium parvum Growth In Vitro*. mBio 2020;11.10.1128/mbio.00052-20. doi:10.1128/mbio.00052-20.
178. Na B.-K., Kang J.-M., Cheun H.-I., Cho S.-H., Moon S.-U., Kim T.-S., . . . Sohn W.-M. *Cryptopain-I, a cysteine protease of Cryptosporidium parvum, does not require the pro-domain for folding*. Parasitology 2009;136.149-57. doi:10.1017/S0031182008005350.
179. Askari N., Shayan P., Mokhber-Dezfouli M.R., Ebrahimzadeh E., Lotfollahzadeh S., Rostami A., . . . Ragh M.J. *Evaluation of recombinant P23 protein as a vaccine for*

- passive immunization of newborn calves against Cryptosporidium parvum*. Parasite Immunology 2016;38.282-9. doi:10.1111/pim.12317.
180. Wang X., Liu C., Rcheulishvili N., Papukashvili D., Xie F., Zhao J., . . . He Y. *Strong immune responses and protection of PcrV and OprF-I mRNA vaccine candidates against Pseudomonas aeruginosa*. npj Vaccines 2023;8.76. doi:10.1038/s41541-023-00672-4.
 181. Li X., Yin J., Wang D., Gao X., Zhang Y., Wu M., . . . Zhu G. *The mucin-like, secretory type-I transmembrane glycoprotein GP900 in the apicomplexan Cryptosporidium parvum is cleaved in the secretory pathway and likely plays a lubrication role*. Parasites & Vectors 2022;15.170. doi:10.1186/s13071-022-05286-8.
 182. Dayao D.A.E., Jaskiewicz J.J., Sheoran A.S., Widmer G., Tzipori S. *A highly antigenic fragment within the zoonotic Cryptosporidium parvum Gp900 glycoprotein (Domain 3) is absent in human restricted Cryptosporidium species*. PLOS ONE 2023;18.e0287997. doi:10.1371/journal.pone.0287997.
 183. Wanyiri J.W., O'Connor R., Allison G., Kim K., Kane A., Qiu J., . . . Ward H.D. *Proteolytic processing of the Cryptosporidium glycoprotein gp40/15 by human furin and by a parasite-derived furin-like protease activity*. Infect Immun 2007;75.184-92. doi:10.1128/iai.00944-06. PMID:PMC1828422
 184. Strong W. B., Gut J., Nelson Richard G. *Cloning and Sequence Analysis of a Highly Polymorphic Cryptosporidium parvum Gene Encoding a 60-Kilodalton Glycoprotein and Characterization of Its 15- and 45-Kilodalton Zoite Surface Antigen Products*. Infect Immun 2000;68.4117-34. doi:10.1128/iai.68.7.4117-4134.2000.
 185. Li M., Sun X., Chen H., Li N., Feng Y., Xiao L., . . . Guo Y. *Stable expression of mucin glycoproteins GP40 and GP15 of Cryptosporidium parvum in Toxoplasma gondii*. Parasites & Vectors 2024;17.65. doi:10.1186/s13071-024-06159-y.
 186. Coppi A., Pinzon-Ortiz C., Hutter C., Sinnis P. *The Plasmodium circumsporozoite protein is proteolytically processed during cell invasion*. Journal of Experimental Medicine 2005;201.27-33. doi:10.1084/jem.20040989.
 187. Riggs M.W., Cama V.A., Leary H.L., Sterling C.R. *Bovine antibody against Cryptosporidium parvum elicits a circumsporozoite precipitate-like reaction and has immunotherapeutic effect against persistent cryptosporidiosis in SCID mice*. Infection and Immunity 1994;62.1927-39. doi:10.1128/iai.62.5.1927-1939.1994.
 188. Riggs M.W., Stone A.L., Yount P.A., Langer R.C., Arrowood M.J., Bentley D.L. *Protective monoclonal antibody defines a circumsporozoite-like glycoprotein exoantigen of Cryptosporidium parvum sporozoites and merozoites*. The Journal of Immunology 1997;158.1787-95. doi:10.4049/jimmunol.158.4.1787.
 189. Sateriale A., Pawlowic M.C., Vinayak S., Brooks C.F., Striepen B. *Genetic Manipulation of Cryptosporidium parvum with CRISPR/Cas9*. In: Mead J., M. A, editors. Cryptosporidium Methods in Molecular Biology,. Humana, New York, NY: Springer Protocols; 2020. doi:10.1007/978-1-4939-9748-0_13.
 190. Bitter E.E., Townsend M.H., Erickson R., Allen C., O'Neill K.L. *Thymidine kinase 1 through the ages: a comprehensive review*. Cell & Bioscience 2020;10.138. doi:10.1186/s13578-020-00493-1.

191. Nava Maria G., Calderón F., Fernández E., Ballell L., Bamborough P., Vinayak S. *Tyrosine Kinase Inhibitors Display Potent Activity against Cryptosporidium parvum*. *Microbiology Spectrum* 2022;11.e03874-22. doi:10.1128/spectrum.03874-22.
192. Choi R., Hulverson M.A., Huang W., Vidadala R.S.R., Whitman G.R., Barrett L.K., . . . Van Voorhis W.C. *Bumped Kinase Inhibitors as therapy for apicomplexan parasitic diseases: lessons learned*. *Int J Parasitol* 2020;50.413-22. doi:10.1016/j.ijpara.2020.01.006. PMID:PMC8565993
193. Arnold S.L.M., Choi R., Hulverson M.A., Schaefer D.A., Vinayak S., Vidadala R.S.R., . . . Van Voorhis W.C. *Necessity of Bumped Kinase Inhibitor Gastrointestinal Exposure in Treating Cryptosporidium Infection*. *The Journal of Infectious Diseases* 2017;216.55-63. doi:10.1093/infdis/jix247.
194. Keppeke G.D., Chang C.C., Peng M., Chen L.-Y., Lin W.-C., Pai L.-M., . . . Liu J.-L. *IMP/GTP balance modulates cytoophidium assembly and IMPDH activity*. *Cell Division* 2018;13.5. doi:10.1186/s13008-018-0038-0.
195. Kim Y., Makowska-Grzyska M., Gorla S.K., Gollapalli D.R., Cuny G.D., Joachimiak A., . . . Hedstrom L. *Structure of Cryptosporidium IMP dehydrogenase bound to an inhibitor with in vivo antiparasitic activity*. *Acta Crystallographica Section F: Structural Biology Communications* 2015;71.531-8. doi:10.1107/S2053230X15000187.
196. Jefferies R., Yang R., Woh C.K., Weldt T., Milech N., Estcourt A., . . . Ryan U.M. *Target validation of the inosine monophosphate dehydrogenase (IMPDH) gene in Cryptosporidium using Phylomer® peptides*. *Experimental Parasitology* 2015;148.40-8. doi:10.1016/j.exppara.2014.11.003.
197. Gorla Suresh K., McNair Nina N., Yang G., Gao S., Hu M., Jala Venkatakrishna R., . . . Hedstrom L. *Validation of IMP Dehydrogenase Inhibitors in a Mouse Model of Cryptosporidiosis*. *Antimicrobial Agents and Chemotherapy* 2014;58.1603-14. doi:10.1128/aac.02075-13.
198. Doytchinova I.A., Flower D.R. *VaxiJen: a server for prediction of protective antigens, tumour antigens and subunit vaccines*. *BMC Bioinformatics* 2007;8.4. doi:10.1186/1471-2105-8-4. PMID:PMC1780059
199. Dimitrov I., Bangov I., Flower D.R., Doytchinova I. *AllerTOP v.2--a server for in silico prediction of allergens*. *J Mol Model* 2014;20.2278. doi:10.1007/s00894-014-2278-5.
200. Sharma N., Naorem L.D., Jain S., Raghava G.P.S. *ToxinPred2: an improved method for predicting toxicity of proteins*. *Brief Bioinform* 2022;23. doi:10.1093/bib/bbac174.
201. Garg V.K., Avashthi H., Tiwari A., Jain P.A., Ramkete P.W., Kayastha A.M., . . . Singh V.K. *MFPPI - Multi FASTA ProtParam Interface*. *Bioinformatics* 2016;12.74-7. doi:10.6026/97320630012074. PMID:PMC5237651
202. Balbin C.A., Nunez-Castilla J., Stebliankin V., Baral P., Sobhan M., Cickovski T., . . . Mathee K. *Epitopedia: identifying molecular mimicry between pathogens and known immune epitopes*. *ImmunoInformatics* 2023;9.100023. doi:10.1016/j.immuno.2023.100023.
203. Sonzogni-D. K., Mead J.R., Ndao M. *Mouse Models for Use in Cryptosporidium Infection Studies and Quantification of Parasite Burden Using Flow Cytometry, qPCR, and Histopathology*. *Methods Mol Biol* 2020;2052.229-51. doi:10.1007/978-1-4939-9748-0_14.

204. Sonzogni-Desautels K., Renteria A.E., Camargo F.V., Di Lenardo T.Z., Mikhail A., Arrowood M.J., . . . Ndao M. *Oleylphosphocholine (OIPC) arrests Cryptosporidium parvum growth in vitro and prevents lethal infection in interferon gamma receptor knock-out mice*. *Frontiers in Microbiology* 2015;6:973. doi:10.3389/fmicb.2015.00973.
205. Sonzogni-Desautels K., Di Lenardo T.Z., Renteria A.E., Gascon M.-A., Geary T.G., Ndao M. *A protocol to count Cryptosporidium oocysts by flow cytometry without antibody staining*. *PLOS Neglected Tropical Diseases* 2019;13:e0007259. doi:10.1371/journal.pntd.0007259.
206. Cheng L.C., Zheng D., Zhang Q., Guvenek A., Cheng H., Tian B. *Alternative 3' UTRs play a widespread role in translation-independent mRNA association with the endoplasmic reticulum*. *Cell Reports* 2021;36:109407. doi:10.1016/j.celrep.2021.109407.
207. Schultz J.C., Cao M., Zhao H. *Development of a CRISPR/Cas9 system for high efficiency multiplexed gene deletion in Rhodosporidium toruloides*. *Biotechnol Bioeng* 2019;116:2103-9. doi:10.1002/bit.27001.
208. Liang Z., Chen K., Li T., Zhang Y., Wang Y., Zhao Q., . . . Gao C. *Efficient DNA-free genome editing of bread wheat using CRISPR/Cas9 ribonucleoprotein complexes*. *Nat Commun* 2017;8:14261. doi:10.1038/ncomms14261. PMID:PMC5253684
209. Ramakrishna S., Kwaku Dad A.B., Beloor J., Gopalappa R., Lee S.K., Kim H. *Gene disruption by cell-penetrating peptide-mediated delivery of Cas9 protein and guide RNA*. *Genome Res* 2014;24:1020-7. doi:10.1101/gr.171264.113. PMID:PMC4032848
210. Zhang T., Gao Y., Wang R., Zhao Y. *Production of Guide RNAs in vitro and in vivo for CRISPR Using Ribozymes and RNA Polymerase II Promoters*. *Bio Protoc* 2017;7. doi:10.21769/BioProtoc.2148. PMID:PMC5463609
211. Karmakar S., Behera D., Baig M.J., Molla K.A. *In Vitro Cas9 Cleavage Assay to Check Guide RNA Efficiency*. In: Islam MT, Molla KA, editors. *CRISPR-Cas Methods: Volume 2*. New York, NY: Springer US; 2021. p 23-39. doi:10.1007/978-1-0716-1657-4_3.
212. Zetsche B., Volz S.E., Zhang F. *A split-Cas9 architecture for inducible genome editing and transcription modulation*. *Nat Biotechnol* 2015;33:139-42. doi:10.1038/nbt.3149. PMID:PMC4503468
213. Zhao Y., Wang F., Wang C., Zhang X., Jiang C., Ding F., . . . Zhang Q. *Optimization of CRISPR/Cas System for Improving Genome Editing Efficiency in Plasmodium falciparum*. *Frontiers in Microbiology* 2021;11. doi:10.3389/fmicb.2020.625862.
214. Crawford E.D., Quan J., Horst J.A., Ebert D., Wu W., DeRisi J.L. *Plasmid-free CRISPR/Cas9 genome editing in Plasmodium falciparum confirms mutations conferring resistance to the dihydroisoquinolone clinical candidate SJ733*. *PLOS ONE* 2017;12:e0178163. doi:10.1371/journal.pone.0178163.
215. Tu M., Lin L., Cheng Y., He X., Sun H., Xie H., . . . Gu F. *A 'new lease of life': FnCpfI possesses DNA cleavage activity for genome editing in human cells*. *Nucleic Acids Research* 2017;45:11295-304. doi:10.1093/nar/gkx783.
216. Cheng P., Zhang Z., Yang F., Cai S., Wang L., Wang C., . . . Gu F. *FnCas12a/crRNA-Mediated Genome Editing in Eimeria tenella*. *Frontiers in Genetics* 2021;12. doi:10.3389/fgene.2021.738746.

217. Chauvier A., St-Pierre P., Nadon J.F., Hien E.D.M., Pérez-González C., Eschbach S.H., . . . Lafontaine D.A. *Monitoring RNA dynamics in native transcriptional complexes*. Proc Natl Acad Sci U S A 2021;118. doi:10.1073/pnas.2106564118. PMID:PMC8609307
218. Peng D., Tarleton R. *EuPaGDT: a web tool tailored to design CRISPR guide RNAs for eukaryotic pathogens*. Microb Genom 2015;1.e000033. doi:10.1099/mgen.0.000033. PMID:PMC5320623
219. Goodswen S.J., Kennedy P.J., Ellis J.T. *A state-of-the-art methodology for high-throughput in silico vaccine discovery against protozoan parasites and exemplified with discovered candidates for Toxoplasma gondii*. Scientific Reports 2023;13.8243. doi:10.1038/s41598-023-34863-9.
220. Medeiros L.C.S., South L., Peng D., Bustamante J.M., Wang W., Bunkofske M., . . . Tarleton R.L. *Rapid, Selection-Free, High-Efficiency Genome Editing in Protozoan Parasites Using CRISPR-Cas9 Ribonucleoproteins*. mBio 2017;8.e01788-17. doi:10.1128/mBio.01788-17.
221. Wang Y., Wang B., Xie H., Ren Q., Liu X., Li F., . . . Gu F. *Efficient Human Genome Editing Using SaCas9 Ribonucleoprotein Complexes*. Biotechnology Journal 2019;14.1800689. doi:10.1002/biot.201800689.
222. Moncada D., Keller K., Chadee K. *Entamoeba histolytica Cysteine Proteinases Disrupt the Polymeric Structure of Colonic Mucin and Alter Its Protective Function*. Infection and Immunity 2003;71.838-44. doi:10.1128/IAI.71.2.838-844.2003.
223. Lauwaet T., Oliveira M.J., Callewaert B., De Bruyne G., Saelens X., Ankri S., . . . Leroy A. *Proteolysis of Enteric Cell Villin by Entamoeba histolytica Cysteine Proteinases **. Journal of Biological Chemistry 2003;278.22650-6. doi:10.1074/jbc.M300142200.
224. Que X., Kim S.-H., Sajid M., Eckmann L., Dinarello C.A., McKerrow J.H., . . . Reed S.L. *A Surface Amebic Cysteine Proteinase Inactivates Interleukin-18*. Infection and Immunity 2003;71.1274-80. doi:10.1128/IAI.71.3.1274-1280.2003.
225. Mottram J.C., Coombs G.H., Alexander J. *Cysteine peptidases as virulence factors of Leishmania*. Current Opinion in Microbiology 2004;7.375-81. doi:10.1016/j.mib.2004.06.010.
226. Mottram J.C., Frame M.J., Brooks D.R., Tetley L., Hutchison J.E., Souza A.E., . . . Coombs G.H. *The Multiple cpb Cysteine Proteinase Genes of Leishmania mexicana Encode Isoenzymes That Differ in Their Stage Regulation and Substrate Preferences **. Journal of Biological Chemistry 1997;272.14285-93. doi:10.1074/jbc.272.22.14285.
227. Nikolskaia O.V., de A. Lima A.P.C., Kim Y.V., Lonsdale-Eccles J.D., Fukuma T., Scharfstein J., . . . Grab D.J. *Blood-brain barrier traversal by African trypanosomes requires calcium signaling induced by parasite cysteine protease*. The Journal of Clinical Investigation 2006;116.2739-47. doi:10.1172/JCI27798.
228. Santos C.C., Coombs G.H., Lima A.P.C.A., Mottram J.C. *Role of the Trypanosoma brucei natural cysteine peptidase inhibitor ICP in differentiation and virulence*. Molecular Microbiology 2007;66.991-1002. doi:10.1111/j.1365-2958.2007.05970.x.
229. Alsford S., Currier R.B., Guerra-Assunção J.A., Clark T.G., Horn D. *Cathepsin-L Can Resist Lysis by Human Serum in Trypanosoma brucei brucei*. PLOS Pathogens 2014;10.e1004130. doi:10.1371/journal.ppat.1004130.

230. Sijwali P.S., Rosenthal P.J. *Gene disruption confirms a critical role for the cysteine protease falcipain-2 in hemoglobin hydrolysis by Plasmodium falciparum*. Proceedings of the National Academy of Sciences 2004;101.4384-9. doi:10.1073/pnas.0307720101.
231. Larson E.T., Parussini F., Huynh M.-H., Giebel J.D., Kelley A.M., Zhang L., . . . Carruthers V.B. *Toxoplasma gondii Cathepsin L Is the Primary Target of the Invasion-inhibitory Compound Morpholinurea-leucyl-homophenyl-vinyl Sulfone Phenyl **. Journal of Biological Chemistry 2009;284.26839-50. doi:10.1074/jbc.M109.003780.
232. Teo Chin F., Zhou Xing W., Bogoyo M., Carruthers Vern B. *Cysteine Protease Inhibitors Block Toxoplasma gondii Microneme Secretion and Cell Invasion*. Antimicrobial Agents and Chemotherapy 2007;51.679-88. doi:10.1128/AAC.01059-06.
233. Que X., Ngô H., Lawton J., Gray M., Liu Q., Engel J., . . . Reed S.L. *The Cathepsin B of Toxoplasma gondii, Toxopain-1, Is Critical for Parasite Invasion and Rhoptyr Protein Processing **. Journal of Biological Chemistry 2002;277.25791-7. doi:10.1074/jbc.M202659200.
234. Huang R., Que X., Hirata K., Brinen L.S., Lee J.H., Hansell E., . . . Reed S. *The cathepsin L of Toxoplasma gondii (TgCPL) and its endogenous macromolecular inhibitor, toxostatin*. Molecular and Biochemical Parasitology 2009;164.86-94. doi:10.1016/j.molbiopara.2008.11.012.
235. McKerrow J.H., Rosenthal P.J., Swenerton R., Doyle P. *Development of protease inhibitors for protozoan infections*. Curr Opin Infect Dis 2008;21.668-72. doi:10.1097/QCO.0b013e328315cca9. PMID:PMC2732359
236. Nava M.G., Calderón F., Fernández E., Ballell L., Bamborough P., Vinayak S. *Tyrosine Kinase Inhibitors Display Potent Activity against Cryptosporidium parvum*. Microbiology Spectrum 2023;11.e03874-22. doi:doi:10.1128/spectrum.03874-22.
237. Li D., Zhang Y., Li S., Zheng B. *A novel Toxoplasma gondii TGGT1_316290 mRNA-LNP vaccine elicits protective immune response against toxoplasmosis in mice*. Front Microbiol 2023;14.1145114. doi:10.3389/fmicb.2023.1145114. PMID:PMC10070739
238. Rawlings N.D., Barrett A.J., Bateman A. *MEROPS: the database of proteolytic enzymes, their substrates and inhibitors*. Nucleic Acids Res 2012;40.D343-50. doi:10.1093/nar/gkr987. PMID:PMC3245014
239. He X., Tan C., Wang F., Wang Y., Zhou R., Cui D., . . . Feng B. *Knock-in of large reporter genes in human cells via CRISPR/Cas9-induced homology-dependent and independent DNA repair*. Nucleic Acids Research 2016;44.e85-e. doi:10.1093/nar/gkw064.
240. Liu Z., Chen O., Wall J.B.J., Zheng M., Zhou Y., Wang L., . . . Liu J. *Systematic comparison of 2A peptides for cloning multi-genes in a polycistronic vector*. Scientific Reports 2017;7.2193. doi:10.1038/s41598-017-02460-2.
241. White C.W., Vanyai H.K., See H.B., Johnstone E.K., Pflieger K.D. *Using nanoBRET and CRISPR/Cas9 to monitor proximity to a genome-edited protein in real-time*. Scientific Reports 2017;7.3187. doi:10.1038/s41598-017-03486-2.
242. Liu H., Robinson D.S., Wu Z.-Y., Kuo R., Yoshikuni Y., Blaby I.K., . . . Cheng J.-F. *Bacterial genome editing by coupling Cre-lox and CRISPR-Cas9 systems*. PLOS ONE 2020;15.e0241867. doi:10.1371/journal.pone.0241867.

243. Kim H.-M., Zhang X. *Design of Repair Templates for CRISPR-Cas9-Triggered Homologous Recombination in Caenorhabditis elegans*. In: Islam MT, Molla KA, editors. *CRISPR-Cas Methods: Volume 2*. New York, NY: Springer US; 2021. p 357-70. doi:10.1007/978-1-0716-1657-4_24.
244. Lin L., He X., Zhao T., Gu L., Liu Y., Liu X., . . . Gu F. *Engineering the Direct Repeat Sequence of crRNA for Optimization of FnCpf1-Mediated Genome Editing in Human Cells*. *Molecular Therapy* 2018;26:2650-7. doi:10.1016/j.ymthe.2018.08.021.
245. Yu F., Zhang K., Wang Y., Li D., Cui Z., Huang J., . . . Zhang L. *CRISPR/Cas12a-based on-site diagnostics of Cryptosporidium parvum IId-subtype-family from human and cattle fecal samples*. *Parasites & Vectors* 2021;14:208. doi:10.1186/s13071-021-04709-2.
246. Chakraborty S. *Sequencing data from Massachusetts General Hospital shows Cas9 integration into the genome, highlighting a serious hazard in gene-editing therapeutics [version 1; peer review: 1 approved with reservations]*. 2019;8. doi:10.12688/f1000research.20744.1.
247. Mout R., Ray M., Yesilbag Tonga G., Lee Y.W., Tay T., Sasaki K., . . . Rotello V.M. *Direct Cytosolic Delivery of CRISPR/Cas9-Ribonucleoprotein for Efficient Gene Editing*. *ACS Nano* 2017;11:2452-8. doi:10.1021/acsnano.6b07600. PMID:PMC5848212
248. Adams B., Xiao Q., Xu Q. *Stem Cell Therapy for Vascular Disease*. *Trends in Cardiovascular Medicine* 2007;17:246-51. doi:10.1016/j.tcm.2007.08.005.
249. Yu C., Liu Y., Ma T., Liu K., Xu S., Zhang Y., . . . Qi Lei S. *Small Molecules Enhance CRISPR Genome Editing in Pluripotent Stem Cells*. *Cell Stem Cell* 2015;16:142-7. doi:10.1016/j.stem.2015.01.003.
250. Nessel T., Beck J.M., Rayatpisheh S., Jami-Alahmadi Y., Wohlschlegel J.A., Goldberg D.E., . . . Beck J.R. *EXP1 is required for organisation of EXP2 in the intraerythrocytic malaria parasite vacuole*. *Cellular Microbiology* 2020;22:e13168. doi:10.1111/cmi.13168.
251. Kim D., Kim J., Hur J.K., Been K.W., Yoon S.-h., Kim J.-S. *Genome-wide analysis reveals specificities of Cpf1 endonucleases in human cells*. *Nature Biotechnology* 2016;34:863-8. doi:10.1038/nbt.3609.
252. Jinek M., Chylinski K., Fonfara I., Hauer M., Doudna J.A., Charpentier E. *A Programmable Dual-RNA-Guided DNA Endonuclease in Adaptive Bacterial Immunity*. *Science* 2012;337:816-21. doi:doi:10.1126/science.1225829.
253. Ribeiro D.M., Prod'homme A., Teixeira A., Zanzoni A., Brun C. *The role of 3'UTR-protein complexes in the regulation of protein multifunctionality and subcellular localization*. *Nucleic Acids Research* 2020;48:6491-502. doi:10.1093/nar/gkaa462.
254. Mayr C. *3' UTRs Regulate Protein Functions by Providing a Nurturing Niche during Protein Synthesis*. *Cold Spring Harb Symp Quant Biol* 2019;84:95-104. doi:10.1101/sqb.2019.84.039206. PMID:PMC7351046
255. Menendez-Gil P., Toledo-Arana A. *Bacterial 3'UTRs: A Useful Resource in Post-transcriptional Regulation*. *Frontiers in Molecular Biosciences* 2021;7. doi:10.3389/fmolb.2020.617633.
256. Li T., Liu H., Jiang N., Wang Y., Wang Y., Zhang J., . . . Cao J. *Comparative proteomics reveals Cryptosporidium parvum manipulation of the host cell molecular expression and*

- immune response*. PLOS Neglected Tropical Diseases 2021;15.e0009949. doi:10.1371/journal.pntd.0009949.
257. McDonald S.A.C., O'Grady J.E., Bajaj-Elliott M., Notley C.A., Alexander J., Brombacher F., . . . McDonald V. *Protection against the Early Acute Phase of Cryptosporidium parvum Infection Conferred by Interleukin-4-Induced Expression of T Helper 1 Cytokines*. The Journal of Infectious Diseases 2004;190.1019-25. doi:10.1086/422761.
 258. Ledford H. *Vaccine made of live malaria parasites shows early success*. Nature 2021doi:10.1038/d41586-021-01806-1.
 259. Dumaine J.E., Sateriale A., Gibson A.R., Reddy A.G., Gullicksrud J.A., Hunter E.N., . . . Striepen B. *The enteric pathogen Cryptosporidium parvum exports proteins into the cytosol of the infected host cell*. eLife 2021;10.e70451. doi:10.7554/eLife.70451.
 260. Kell D.B., Heyden E.L., Pretorius E. *The Biology of Lactoferrin, an Iron-Binding Protein That Can Help Defend Against Viruses and Bacteria*. Frontiers in Immunology 2020;11. doi:10.3389/fimmu.2020.01221.
 261. Bykonya A.G., Lavrov A.V., Smirnikhina S.A. *Methods for CRISPR-Cas as Ribonucleoprotein Complex Delivery In Vivo*. Molecular Biotechnology 2023;65.181-95. doi:10.1007/s12033-022-00479-z.
 262. Bok K., Sitar S., Graham B.S., Mascola J.R. *Accelerated COVID-19 vaccine development: milestones, lessons, and prospects*. Immunity 2021;54.1636-51. doi:10.1016/j.immuni.2021.07.017. PMID:PMC8328682
 263. McKee A.S., MacLeod M.K.L., Kappler J.W., Marrack P. *Immune mechanisms of protection: can adjuvants rise to the challenge?* BMC Biology 2010;8.37. doi:10.1186/1741-7007-8-37.
 264. Taxman D.J., Livingstone L.R., Zhang J., Conti B.J., Iocca H.A., Williams K.L., . . . Reed W. *Criteria for effective design, construction, and gene knockdown by shRNA vectors*. BMC Biotechnology 2006;6.7. doi:10.1186/1472-6750-6-7.
 265. Jamal A., Usman S., Teh M.-T., Waseem A. *Preparation and Use of shRNA for Knocking Down Specific Genes*. In: Turksen K, editor. Skin Stem Cells: Methods and Protocols. New York, NY: Springer US; 2024. p 55-72. doi:10.1007/7651_2024_515.
 266. Wang S., Chen Y., Guo J., Huang Q. *Liposomes for Tumor Targeted Therapy: A Review*. International Journal of Molecular Sciences 2023;24.2643.
 267. Nisini R., Poerio N., Mariotti S., De Santis F., Fraziano M. *The Multirole of Liposomes in Therapy and Prevention of Infectious Diseases*. Frontiers in Immunology 2018;9. doi:10.3389/fimmu.2018.00155.
 268. Van Zyl W.F., Van Staden A.D., Dicks L.M.T., Trindade M. *Use of the mCherry fluorescent protein to optimize the expression of class I lanthipeptides in Escherichia coli*. Microbial Cell Factories 2023;22.149. doi:10.1186/s12934-023-02162-7.